

General Disclaimer

One or more of the Following Statements may affect this Document

- This document has been reproduced from the best copy furnished by the organizational source. It is being released in the interest of making available as much information as possible.
- This document may contain data, which exceeds the sheet parameters. It was furnished in this condition by the organizational source and is the best copy available.
- This document may contain tone-on-tone or color graphs, charts and/or pictures, which have been reproduced in black and white.
- This document is paginated as submitted by the original source.
- Portions of this document are not fully legible due to the historical nature of some of the material. However, it is the best reproduction available from the original submission.

02

NASA TECHNICAL
MEMORANDUM

NASA TM X-72712

NASA TM X-72712

AERODYNAMIC CHARACTERISTICS OF
A 14-PERCENT-THICK NASA
SUPERCRITICAL AIRFOIL DESIGNED
FOR A NORMAL-FORCE COEFFICIENT OF 0.7

By Charles D. Harris



(NASA-TM-X-72712) AERODYNAMIC
CHARACTERISTICS OF A 14-PERCENT-THICK NASA
SUPERCRITICAL AIRFOIL DESIGNED FOR A
NORMAL-FORCE COEFFICIENT OF 0.7 (NASA)
101 p HC A05/MF A01

N83-11077

CSCL 01A G3/02

Unclassified
32181

10261

1. Report No. NASA TM X-72712	2. Government Accession No.	3. Recipient's Catalog No.	
4. Title and Subtitle Aerodynamic Characteristics of a 14-Percent-Thick NASA Supercritical Airfoil Designed for a Normal-Force Coefficient of 0.7 (U)		5. Report Date July 1975	
6. Performing Organization Code		7. Author(s) Charles D. Harris	
		8. Performing Organization Report No.	
9. Performing Organization Name and Address NASA-Langley Research Center Hampton, Virginia 23665		10. Work Unit No. 505-06-31-02	
		11. Contract or Grant No.	
		13. Type of Report and Period Covered NASA Technical Memorandum	
12. Sponsoring Agency Name and Address National Aeronautics and Space Administration Washington, D. C. 20546		14. Sponsoring Agency Code	
15. Supplementary Notes Interim release of NASA supercritical airfoil data.			
16. Abstract This report documents the experimental aerodynamic characteristics of a 14-percent-thick supercritical airfoil based on an off-design sonic-pressure plateau criterion. The design normal-force coefficient was 0.7. The results are compared with those of the family related 10-percent-thick supercritical airfoil 33. Comparisons are also made between experimental and theoretical characteristics and composite drag rise characteristics derived for a full scale Reynolds number of 40 million.			
ORIGINAL PAGE IS OF POOR QUALITY			
17. Key Words (Suggested by Author(s)) (STAR category under) <u>Aerodynamics</u> Supercritical Airfoils Transonic Aerodynamics			
18. Security Classif. (of this report) Conf. [REDACTED]	20. Security Classif. (of this page) Unclassified	21. No. of Pages 99	22. Price* STIF

[REDACTED]

AERODYNAMIC CHARACTERISTICS OF
A 14-PERCENT-THICK NASA
SUPERCRITICAL AIRFOIL DESIGNED
FOR A NORMAL-FORCE COEFFICIENT OF 0.7

By Charles D. Harris

Langley Research Center

SUMMARY

A 14-percent-thick supercritical airfoil based on an off-design sonic-pressure plateau criterion has been developed and experimental aerodynamic characteristics measured. The design normal-force coefficient was 0.7. Results show the airfoil to have good drag rise characteristics over a wide range of normal force coefficients with no measurable shock losses up to the Mach numbers at which drag divergence occurred for normal-force coefficients up to 0.7. Comparisons of experimental and theoretical characteristics were made and composite drag rise characteristics were derived for normal-force coefficients of 0.5 and 0.7 and a Reynolds number of 40 million.

INTRODUCTION

Continued development of supercritical airfoil technology has resulted in recognition of design criteria which permit the design of family related supercritical airfoils. Based on these criteria, two supercritical airfoils have been designed - the 14-percent-thick airfoil reported herein and the 10-percent-thick airfoil 33 reported in reference 1. The design normal-force coefficient was 0.7 for both airfoils.

[REDACTED]

SYMBOLS

Values are given in both SI and U.S. Customary Units. Measurements and calculations are made in U.S. Customary Units.

C_p	pressure coefficient, $\frac{P_1 - P_\infty}{q_\infty}$
$C_{p,sonic}$	pressure coefficient corresponding to local Mach number of 1.0
c	chord of airfoil, 63.5 centimeters (25.0 inches)
c_d	section drag coefficient
$\Delta c_{d,s}$	drag increment due to shock wave losses
c_l	section lift coefficient
c_m	section pitching-moment coefficient about the quarter-chord point
c_n	section normal-force coefficient
K	surface curvature, reciprocal of local radius of curvature
M	Mach number
m	surface slope, dy/dx
p	static pressure, newtons per meter ² (pounds per foot ²)
Δp_t	total-pressure loss, newtons per meter ² (pounds per foot ²)
q	dynamic pressure, newtons per meter ² (pounds per foot ²)
R	Reynolds number based on airfoil chord
x	ordinate along airfoil reference line measured from airfoil leading edge, centimeters (inches)
y	ordinate normal to airfoil reference line, centimeters (inches)
z	vertical distance in wake profile measured from bottom of rake, centimeters (inches)
α	geometric angle of attack of airfoil reference line, degrees

Subscripts:

- l local point on airfoil
- ∞ undisturbed stream

Abbreviations:

- l airfoil lower surface
- u airfoil upper surface
- B.L. boundary layer

APPARATUS AND TECHNIQUES

Model Configuration

The supercritical airfoil basic concept and detailed design philosophy are discussed in reference 2.

Background.-- The design criteria consist essentially of three principal guidelines which may be used in designing supercritical airfoils to have the best drag characteristics over a wide range of lift coefficients. There are several additional, more detailed, design guidelines (treatment of leading and trailing edges, and local minimum thickness constraints, for example) which are beyond the intended scope of this report and will be discussed in a later report.

The first principal guideline, referred to as the off-design sonic-plateau criterion, is that at some incremental normal-force coefficient below the design normal-force coefficient the pressure distribution on the upper and lower surfaces be flat with the upper surface pressures just below the sonic value. The increment is a function of the design normal-force coefficient and appears to be about -0.25 to -0.30 for a design normal-force coefficient of 0.7.

On the upper surface the plateau extends from near the leading edge to the start of the aft pressure recovery and on the lower surface from near the

[REDACTED]

leading edge to the recompression region entering into the cusp. The rearward extent of the upper surface plateau is determined by the second principal design guideline which requires that the gradient of the aft pressure recovery be gradual enough to avoid separation problems for lift coefficients and Mach numbers up to the design values. Consequently, the rearward extent of the upper surface plateau would depend on thickness ratio since the thicker the airfoil, the higher the induced velocities from which the flow must recover and, therefore, the further forward the aft pressure recovery must begin. The upper surface plateau extends from approximately 3- to 80-percent chord on the 10-percent-thick airfoil of reference 1 and from approximately 5- to 66-percent chord on the 14-percent-thick airfoil herein.

The third principal guideline requires that the airfoil have sufficient aft camber so that at design conditions the angle of attack be about zero. This prevents a too-forward location of the upper surface crest with the negative pressure coefficients over the mid-chord region acting over a rearward facing surface. Both experimental and theoretical analyses (ref. 3) have indicated that an increase in angle of attack to positive values results in an abrupt increase in wave drag.

Based on these criteria two supercritical airfoils were designed - a 10-percent-thick airfoil (airfoil 33) reported in reference 1 and the 14-percent-thick airfoil reported herein. The design normal-force coefficient was 0.7 for both airfoils. An iterative design process was used which consisted of altering the airfoil coordinates until the viscous, airfoil analysis program of reference 3 indicated that the aforementioned design criteria had been satisfied.

Since the best drag characteristics are often obtained on airfoils with a small amount of upper surface trailing edge separation and since theoretical

treatments of the flow at trailing edge regions are generally unreliable, theoretically-predicted flow separation at the 97-percent chord location was accepted during the design process. Attempts to achieve a more rearward location of theoretical separation by reducing the aft pressure recovery gradient would have forced the rear terminus of the sonic plateau forward, resulting in higher induced velocities in the plateau region and a probable reduction in drag rise Mach number.

Wind tunnel models.- Geometric characteristics of the experimental 14-percent-thick airfoil are presented in figures 1 and 2 and compared with those of the 10-percent-thick airfoil 33 of reference 1. Measured section coordinates are presented in table I. The coordinates of the experimental airfoil deviated slightly from the design profile (not presented). These small deviations, nowhere greater than $\Delta y/c = 0.0002$ and generally less than 0.0001, should not significantly affect the results.

Irregularities in the curvature distributions (fig. 2) are due to small surface irregularities that become greatly exaggerated when examined from the standpoint of local curvature. Such irregularities are not as apparent in the slope distributions (fig. 2). Both airfoils included a trailing-edge cavity (see the insert in fig. 1 and the photographs of fig. 3) which had a favorable effect on the wake as discussed in reference 4.

The wind-tunnel models, mounted in an inverted position, spanned the width of the tunnel with a span-chord ratio of 3.43. They were constructed with metal leading and trailing edges and a metal core around which plastic fill was used to form the contours of the model. Angle of attack was changed manually by rotating the model about pivots in the tunnel side walls. A photograph and a drawing of a typical airfoil model installed in the tunnel are shown in figures 3 and 4, respectively.

Wind Tunnel

The investigation was conducted in the Langley 8-foot transonic pressure tunnel (ref. 5). This tunnel is a continuous flow, variable-pressure wind tunnel with controls that permit the independent variation of Mach number, stagnation pressure and temperature, and dewpoint. It has a 2.16-meter-square (85.2-inch-square) test section with filleted corners so that the total cross-sectional area is equivalent to that of a 2.44-meter-diameter (8-foot-diameter) circle. The upper and lower test-section walls are axially slotted to permit testing through the transonic speed range. The total slot width at the position of the model averaged about 5 percent of the width of the upper and lower walls.

The solid side walls and slotted upper and lower walls make this tunnel well suited to the investigation of two-dimensional models since the side walls act as end plates and the slots permit development of the flow field in the vertical direction.

Boundary-Layer Transition

Based on the technique discussed in reference 6, boundary-layer transition was fixed along the 28-percent chord line on the upper and lower surfaces of the models in an attempt to simulate full-scale Reynolds numbers by providing the same relative trailing-edge boundary-layer-displacement thickness at model scale as would exist at full-scale flight conditions. The simulation technique, which requires that laminar flow be maintained ahead of the transition trip, is limited to those test conditions in which shock waves or steep adverse pressure gradients occur behind the point of fixed transition so that the flow is not tripped prematurely. The transition trips consisted of 0.25-cm-wide (0.10 in.) bands of No. 90 Carborundum grains.

[REDACTED]

Analysis of theoretically computed (ref. 3) drag and boundary-layer-displacement thickness at the trailing edge indicated that the simulated full scale Reynolds number was around 40 million rather than the 20 to 30 million quoted for earlier supercritical airfoil investigations (ref. 4, for example).

Measurements

Surface-pressure measurements.— Normal force and pitching moments acting on the airfoils were determined from surface static-pressure measurements. The surface-pressure measurements were obtained from a chordwise row of orifices located approximately $0.32c$ from the tunnel center line. Orifices were more concentrated near the leading and trailing edges of the airfoil to define the pressure gradients in these regions. In addition, a rearward facing orifice was included in the cavity at the trailing edge (identified at an upper surface x/c location of 1.00). The transducers used in the differential pressure scanning valves to measure the static pressure at the airfoil surface had a range of $\pm 68.9 \text{ kN/m}^2$ ($\pm 10 \text{ lb/in}^2$).

Wake measurements.— Drag forces were determined from vertical variations of the total and static pressures measured across the wake with the profile drag rake shown in figure 4(b). The profiles, schematically illustrated in figure 5, represent the momentum losses as indicated by stagnation-pressure deficits across the wake. The middle section of these profiles reflects viscous and separation losses in the boundary layer, whereas the "wings" of the profile reflect direct losses in stagnation pressure across the shock waves.

The rake was positioned in the vertical center-line plane of the tunnel, approximately 1 chord length rearward of the trailing edge of the airfoil. The total-pressure tubes were flattened horizontally and closely spaced vertically

(0.36 percent of the airfoil chord) in the region of the wake associated with skin-friction boundary-layer losses. Outside this region, the tube vertical spacing progressively widened until in the region above the wing where only shock losses were anticipated, the total-pressure tubes were spaced apart about 7.2 percent of the chord. Static-pressure tubes were distributed as shown in figure 4(b). Each static pressure measured was used over a section of the rake to determine local flow conditions in the vicinity of the static-pressure tube rather than using an average of all the static pressures measured. The rake was attached to the conventional center-line sting mount of the tunnel; this arrangement permitted it to be moved vertically to center the close concentration of tubes in the boundary-layer wake. The transducer in the differential-pressure scanning valve connected to total-pressure tubes intended to measure boundary-layer losses had a range of $\pm 17.2 \text{ kN/m}^2$ (2.5 lb/in^2), and the transducers in the valves for measuring shock losses and static pressure had a range of $\pm 6.8 \text{ kN/m}^2$ (1 lb/in^2).

Reduction of Data

Calculation of c_n and c_m . - Section normal-force and pitching-moment coefficients were obtained by numerical integration (based on the trapezoidal method) of the local surface-pressure coefficient measured at each orifice multiplied by an appropriate weighting factor (incremental area).

Calculation of c_d . - To obtain section drag coefficients, point drag coefficients were computed for each total-pressure measurement in the wake by using the procedure of reference 7. These point drag coefficients were then summed by numerical integration across the wake, again based on the trapezoidal method. Drag increments due to shock wave losses ($\Delta c_{d,s}$) were determined from integration of the drag measured across the wings (fig. 5) of the wake profile.

Wind-Tunnel-Wall Effects

Because of the uncertainty in lift-induced interference effects and solid and wake blockage effects (particularly in the presence of local supercritical flow) no corrections for wall effects have been applied to the basic experimental data. Adjustments for blockage were applied to the composite drag rise data and are explained in the DISCUSSION section.

TEST CONDITIONS

Tests were conducted at Mach numbers from 0.50 to 0.78 for a stagnation pressure of 0.1013 MN/m^2 (1 atm). The stagnation temperature of the tunnel air was automatically controlled at approximately 322 K (120°F) and the air was dried until the dewpoint in the test section was reduced sufficiently to avoid condensation effects. Resultant test Reynolds numbers based on the airfoil chord length were as shown in figure 6.

PRESENTATION OF RESULTS

The experimental data reported herein are presented in the following figures:

	Figure
Force and moment characteristics.	7
Variation of measured section drag coefficient with Mach number	8
Drag increment due to shock-wave losses	9
Composite drag-rise curve	10
Chordwise pressure distributions at -	
$M = 0.50$	11
$M = 0.60$	12
$M = 0.65$	13
$M = 0.70$	14

[REDACTED]
Figure

M = 0.72	15
M = 0.73	16
M = 0.74	17
M = 0.75	18
M = 0.76	19
M = 0.77	20
M = 0.78	21

Comparisons of theoretical and experimental characteristics at -

M = 0.720, $c_n = 0.425$	22
M = 0.750, $c_n = 0.509$	23
M = 0.730, $c_n = 0.691$	24

Complete surface pressure distributions for the 10-percent-thick supercritical airfoil 33 are presented in reference 1.

DISCUSSION

Measured Aerodynamic Characteristics

Sonic plateau.- Figures 15(b) and 15(c) indicate how close the experimental airfoil came to satisfying the off-design sonic plateau criterion. If an experimental pressure distribution had been obtained for a normal-force coefficient between these two conditions ($c_n \approx 0.44$), upper and lower surface pressure plateaus would have been achieved with the upper surface pressures just under the sonic value. Irregularities in the plateau pressures are due to small surface imperfections which become greatly exaggerated when the flow is right on the verge of sonic velocity. As discussed previously, the rearward extent of the upper surface plateau was reduced when compared to the 10-percent-thick airfoil of reference 1.

The characteristic supercritical airfoil pressure distribution near design conditions (slightly decelerating upper surface velocities terminated by a very weak recompression near the midchord and followed by a near-sonic pressure plateau before entering the final trailing-edge pressure recovery) for an angle of attack near 0° (fig. 24) fell between figures 16(e), 16(f), and 17(e) at $M \approx 0.735$ and $c_n \approx 0.72$. The increment between normal-force coefficients at design and off-design sonic plateau conditions was, therefore, about -0.25 to -0.30 as suggested.

Measured drag characteristics.- Figures 8 and 9 show good drag rise characteristics for the 14- and 10-percent-thick airfoils over a wide range of normal-force coefficients with no measurable shock losses up to the Mach numbers at which drag-divergence occurred for normal-force coefficients up to 0.7. Generally, the drag rise characteristics for the two airfoils with different thickness ratios are similar except for the approximately 0.04 difference in drag rise Mach number which has been accounted for by a shift in the Mach number scale at the bottom of figure 8.

The apparent dips in the drag-rise curves for the 14-percent-thick airfoil (fig. 8) should not be interpreted as single point shockless conditions. At $c_n = 0.7$, for example, there is a dip at $M = 0.73$ but there were no shock losses evident (fig. 9) at $c_n = 0.7$ for Mach numbers below 0.74. In an attempt to simulate full scale Reynolds numbers for the design Mach number, boundary-layer transition trips were fixed at 28-percent chord. At $M = 0.70$, the pressure distribution for $c_n = 0.7$ (fig. 14) was such that laminar flow could not be maintained back to the trip. The higher drag level preceding $M = 0.73$ was, therefore, due to premature boundary-layer transition with greater skin friction drag than there would have been if laminar flow could have been

[REDACTED]

maintained back to the trip at 28-percent chord. Higher drag levels preceding the dip are not associated with increased form drag due to separation effects since no losses in trailing-edge pressure recovery were evident. The apparent dips in the drag rise curves for the 10-percent-thick airfoil (fig. 8) may be explained in a similar manner.

Measured pitching-moment characteristics.- At design conditions ($M \approx 0.74$) and $c_n = 0.7$ for the 14-percent-thick airfoil (fig. 7), and $M \approx 0.78$ and $c_n = 0.7$ for the 10-percent-thick airfoil (ref. 1) pitching-moment coefficients were practically the same for the two airfoils.

Comparison With Theory

Correlation was established between experimental and theoretically-predicted data using the viscous, analysis program of reference 3. Representative results are presented in figures 22 to 24. Since the viscous, analysis program was known to overpredict trailing-edge pressure recovery, Mach number was varied to achieve the best matches of the theoretical and experimental pressure distributions over the forward regions of the airfoil and shock wave locations for given normal-force coefficients. The results indicate the Mach number and angle-of-attack adjustments needed to correct for tunnel wall interference effects.

When the flow over the model is subcritical (fig. 22, for example) the blockage or Mach number correction required to match the experimental and theoretical pressure distributions over the forward region of the airfoil are small and tend to agree with what would be predicted by subcritical theory (ref. 8, for example). When substantial amounts of supercritical flow begin to appear over the airfoil blockage corrections become significant as indicated by figures 23 and 24.

Attention must be called to two important points in the correlations shown in figures 22 to 24. The total theoretical drag calculated by the viscous, analysis program of reference 3 is calculated in two parts; profile drag, consisting of skin friction and form or pressure drag, and the contribution of wave drag which exists in supersonic flow. Experience has indicated that because of overprediction of wave losses the total theoretical drag tends to become too large as soon as supercritical flow appears on the airfoil. Consequently, the theoretical drag shown in figures 22 to 24 is that drag associated with only profile drag and agrees well with the experimental drag. If the wave losses as calculated by the method of reference 3 were taken into account, the theoretical drag would be greater than the experimental drag by 0.0008 and 0.0010 for figures 23 and 24 respectively.

The second point which must be made concerning the correlation figures pertains to the position of boundary-layer transition specified for the theoretical data. Reference 3 neglects the laminar portion of the flow ahead of the transition point. Because of the lengthy run of laminar flow (28-percent) and its effect on the turbulent boundary-layer development on the present model, the neglected laminar boundary layer had to be taken into account. This was accomplished by moving the transition point forward of 28-percent chord in the theoretical calculations until the theoretical and experimental drag agreed for flow conditions with no supercritical flow (zero wave losses) and where the experimental transition occurred at 28 percent. Specifying transition around 22-percent chord in the theoretical calculations seemed to yield good agreement and the theoretical characteristics shown in figures 22 to 24 were calculated for tunnel Reynolds numbers with transition fixed at 22-percent chord.

Composite Drag and Angle-of-Attack Characteristics

Drag.- A combination of experimental and theoretical drag characteristics is shown in figure 10 in order to synthesize a realistic drag-rise curve for a full-scale Reynolds number. Theoretical drag values (solid line) based on 40 million Reynolds number and boundary-layer transition at 3-percent chord are used for Mach numbers up to the Mach number at which shock losses become evident in the experimental data. Because of the inaccuracy of the theoretical wave losses, experimental drag values (dashed line) are used beyond that point. The experimental and theoretical drag agree at the junction of the solid and dashed lines. The nominal Mach numbers for the experimental data were reduced by the increments indicated by figures 23 and 24 to be required to account for blockage effects.

The gradual increase in drag with Mach number up to drag divergence for both airfoils is associated with increased profile drag due to the effect of Mach number on the induced velocities. As noted in an earlier section there were no measurable shock losses up to the Mach numbers at which drag divergence occurred. The higher drag levels for the 14-percent-thick airfoil are, of course, due to the higher induced velocities over the thicker airfoil.

Angle of attack.- Theoretical angles of attack required to obtain the desired section lift coefficients are nearly the same for the two airfoils after the 0.04 shift in design Mach number is taken into account and are zero near the design or cruise Mach numbers. The difference in angle of attack for $c_n = 0.5$ and 0.7 provides an indication of the lift-curve slope in this lift range.

CONCLUDING REMARKS

A 14-percent-thick supercritical airfoil based on an off-design sonic pressure plateau criterion has been developed and experimental aerodynamic characteristics measured. The airfoil had good drag rise characteristics over a wide range of normal force coefficients with no measurable shock losses up to the Mach numbers at which drag divergence occurred for normal-force coefficients up to 0.7. Comparisons of experimental and theoretical characteristics were made and composite drag rise characteristics were derived for normal-force coefficients of 0.5 and 0.7 and a Reynolds number of 40 million.

REFERENCES

1. Harris, Charles D.: Aerodynamic Characteristics of the 10-Percent-Thick NASA Supercritical Airfoil 33 Designed for a Normal-Force Coefficient of C.7. NASA TM X-72711, 1975.
2. Whitcomb, Richard T.: Review of NASA Supercritical Airfoils. ICAS Paper No. 74-10, Aug. 1974.
3. Bauer, F.; Garabedian, P.; Korn, D.; and Jameson, A.: Supercritical Wing Sections II. Lecture Notes in Economics and Mathematical Systems, M Beckmann and H. P. Lünzi, eds., Springer-Verlag, c. 1975.
4. Harris, Charles D.: Wind-Tunnel Investigation of Effects of Trailing-Edge Geometry on a NASA Supercritical Airfoil Section. NASA TM X-2336, 1971.
5. Schaefer, William T., Jr.: Characteristics of Major Active Wind Tunnels at the Langley Research Center. NASA TM X-1130, 1965.
6. Blackwell, James A., Jr.: Preliminary Study of Effects of Reynolds Number and Boundary-Layer Transition Location on Shock-Induced Separation. NASA TN D-5003, 1969.
7. Baals, Donald D.; and Mourhess, Mary J.: Numerical Evaluation of the Wake-Survey Equations for Subsonic Flow Including the Effect of Energy Addition. NACA WR L-5, 1945, (Formerly NACA ARR L5H27.)
8. Davis, Don D., Jr.; and Moore, Dewey: Analytical Study of Blockage- and Lift-Interference Corrections for Slotted Tunnels Obtained by the Substitution of an Equivalent Homogeneous Boundary for the Discrete Slots. NACA RM L53E07b, 1953.

ORIGINAL PAGE IS
OF POOR QUALITY

TABLE I.- SECTION COORDINATES FOR

14-PERCENT-THICK SUPERCRITICAL AIRFOIL

[$c = 63.5$ cm (25 in.); leading-edge radius = $0.030c$]

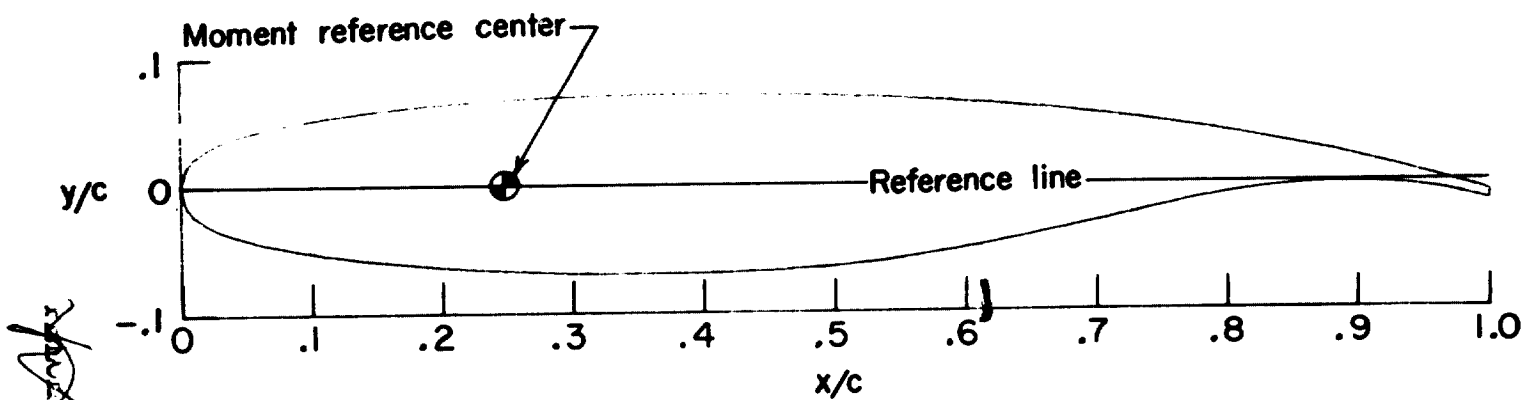
x/c	$(y/c)_u$	$(y/c)_l$	x/c	$(y/c)_u$	$(y/c)_l$
0.0	0.0	0.0	.240	.0659	-.0661
.002	.0108	-.0108	.250	.0665	-.0667
.005	.0167	-.0165	.260	.0670	-.0672
.010	.0225	-.0223	.270	.0675	-.0677
.020	.0297	-.0295	.280	.0679	-.0681
.030	.0346	-.0343	.290	.0683	-.0685
.040	.0383	-.0381	.300	.0686	-.0688
.050	.0414	-.0411	.310	.0689	-.0691
.060	.0440	-.0438	.320	.0692	-.0693
.070	.0463	-.0461	.330	.0694	-.0695
.080	.0484	-.0481	.340	.0696	-.0696
.090	.0502	-.0500	.350	.0698	-.0697
.100	.0519	-.0517	.360	.0699	-.0697
.110	.0535	-.0533	.370	.0700	-.0697
.120	.0549	-.0547	.380	.0700	-.0696
.130	.0562	-.0561	.390	.0700	-.0695
.140	.0574	-.0574	.400	.0700	-.0693
.150	.0585	-.0585	.410	.0699	-.0691
.160	.0596	-.0596	.420	.0698	-.0689
.170	.0606	-.0606	.430	.0697	-.0686
.180	.0615	-.0616	.440	.0696	-.0682
.190	.0624	-.0625	.450	.0694	-.0678
.200	.0632	-.0633	.460	.0692	-.0673
.210	.0640	-.0641	.470	.0689	-.0667
.220	.0647	-.0648	.480	.0686	-.0661
.230	.0653	-.0655	.490	.0683	-.0654

ORIGINAL PAGE IS
OF POOR QUALITY

TABLE I.- SECTION COORDINATES FOR
14-PERCENT-THICK SUPERCRITICAL AIRFOIL - Concluded

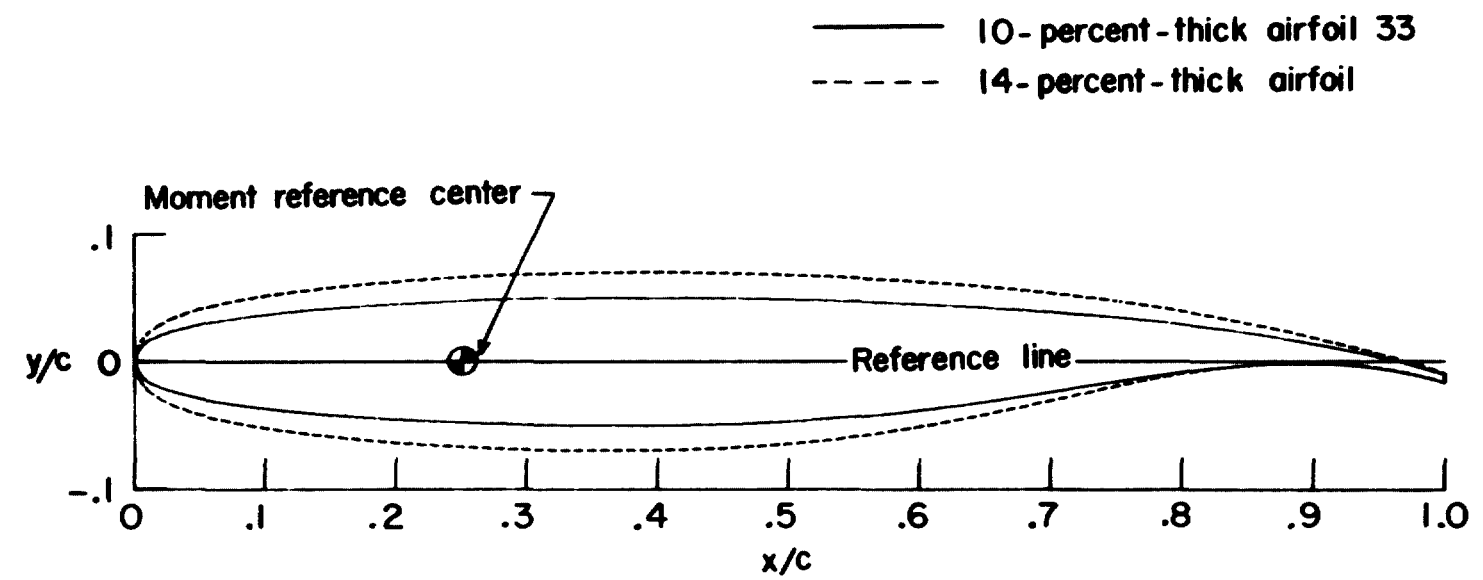
x/c	(y/c) _u	(y/c) ₁	x/c	(y/c) _u	(y/c) ₁
.500	.0680	-.0646	.760	.0457	-.0173
.510	.0676	-.0637	.770	.0442	-.0152
.520	.0672	-.0627	.780	.0426	-.0132
.530	.0668	-.0616	.790	.0409	-.0113
.540	.0663	-.0604	.800	.0392	-.0095
.550	.0658	-.0591	.810	.0374	-.0079
.560	.0652	-.0577	.820	.0356	-.0064
.570	.0646	-.0562	.830	.0337	-.0050
.580	.0640	-.0546	.840	.0317	-.0038
.590	.0634	-.0529	.850	.0297	-.0028
.600	.0627	-.0511	.860	.0276	-.0020
.610	.0620	-.0493	.870	.0255	-.0014
.620	.0613	-.0474	.880	.0233	-.0010
.630	.0605	-.0454	.890	.0210	-.0008
.640	.0596	-.0434	.900	.0186	-.0008
.650	.0587	-.0413	.910	.0162	-.0011
.660	.0578	-.0392	.920	.0137	-.0016
.670	.0568	-.0371	.930	.0111	-.0024
.680	.0558	-.0349	.940	.0084	-.0035
.690	.0547	-.0327	.950	.0057	-.0049
.700	.0536	-.0305	.960	.0029	-.0066
.710	.0524	-.0283	.970	0.0	-.0086
.720	.0512	-.0261	.980	-.0030	-.0109
.730	.0499	-.0239	.990	-.0062	-.0136
.740	.0486	-.0217	1.000	-----	-.0165
.750	.0472	-.0195			

Sketch of trailing edge at expanded scale



(a) 14-percent-thick supercritical airfoil.

Figure 1.- Airfoil sketches.

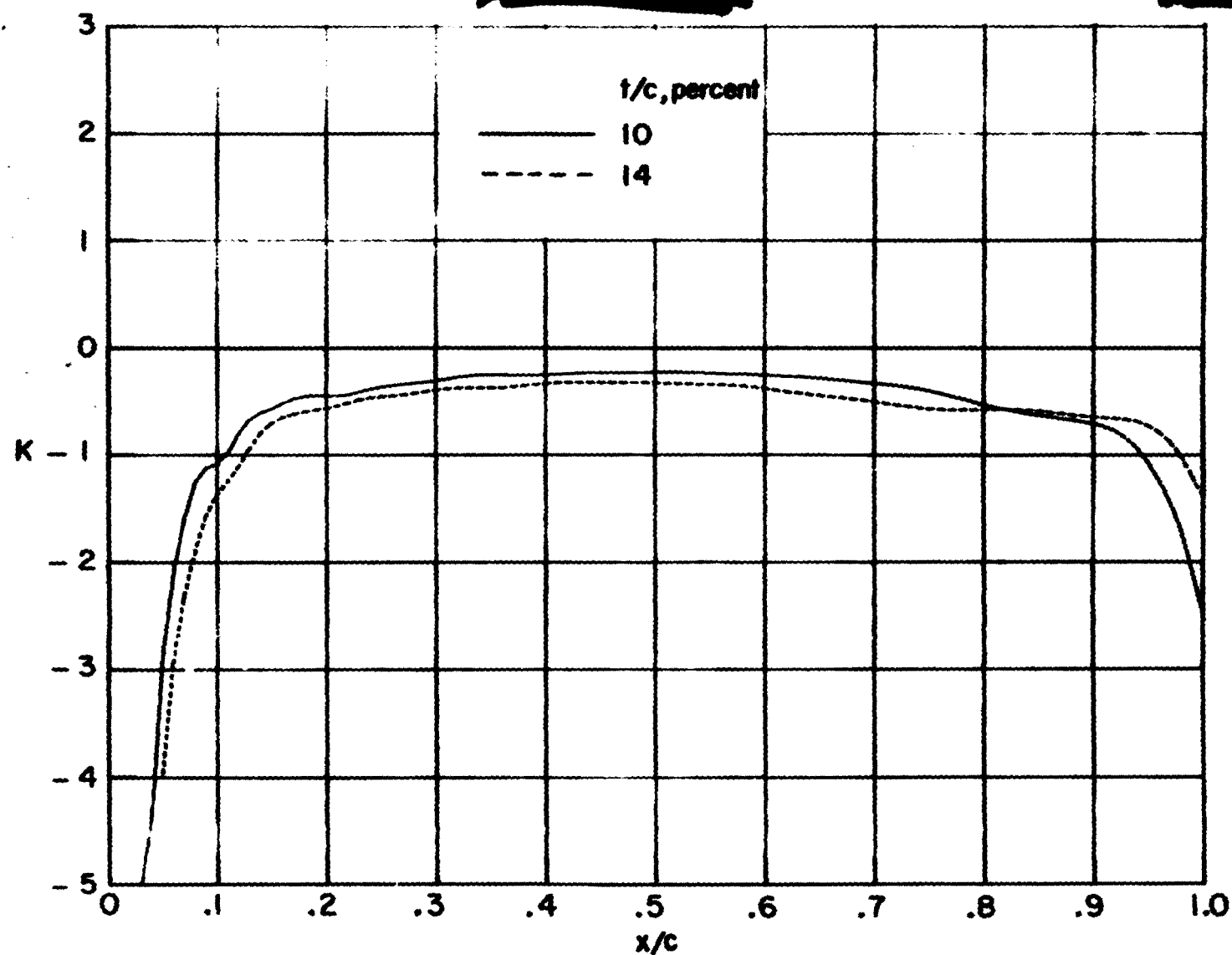


(b) Comparison of 14-percent-thick airfoil with 10-percent-thick airfoil 33.

Figure I. - Concluded.

ORIGINAL FACE IS
OF POOR QUALITY

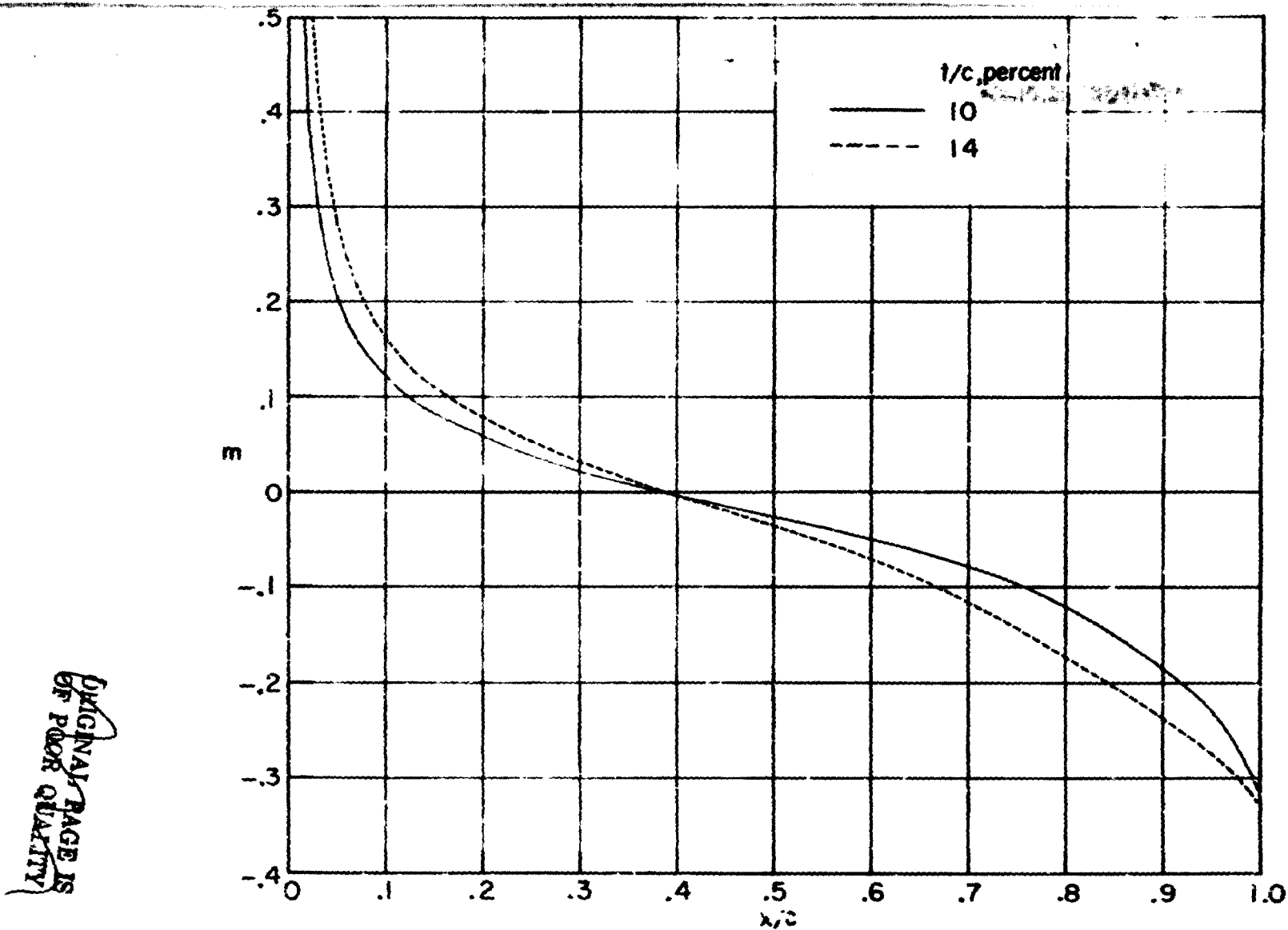
ORIGINAL PAGE IS
OF POOR QUALITY



(a) Upper surface. Concluded.

Figure 2. - Continued.

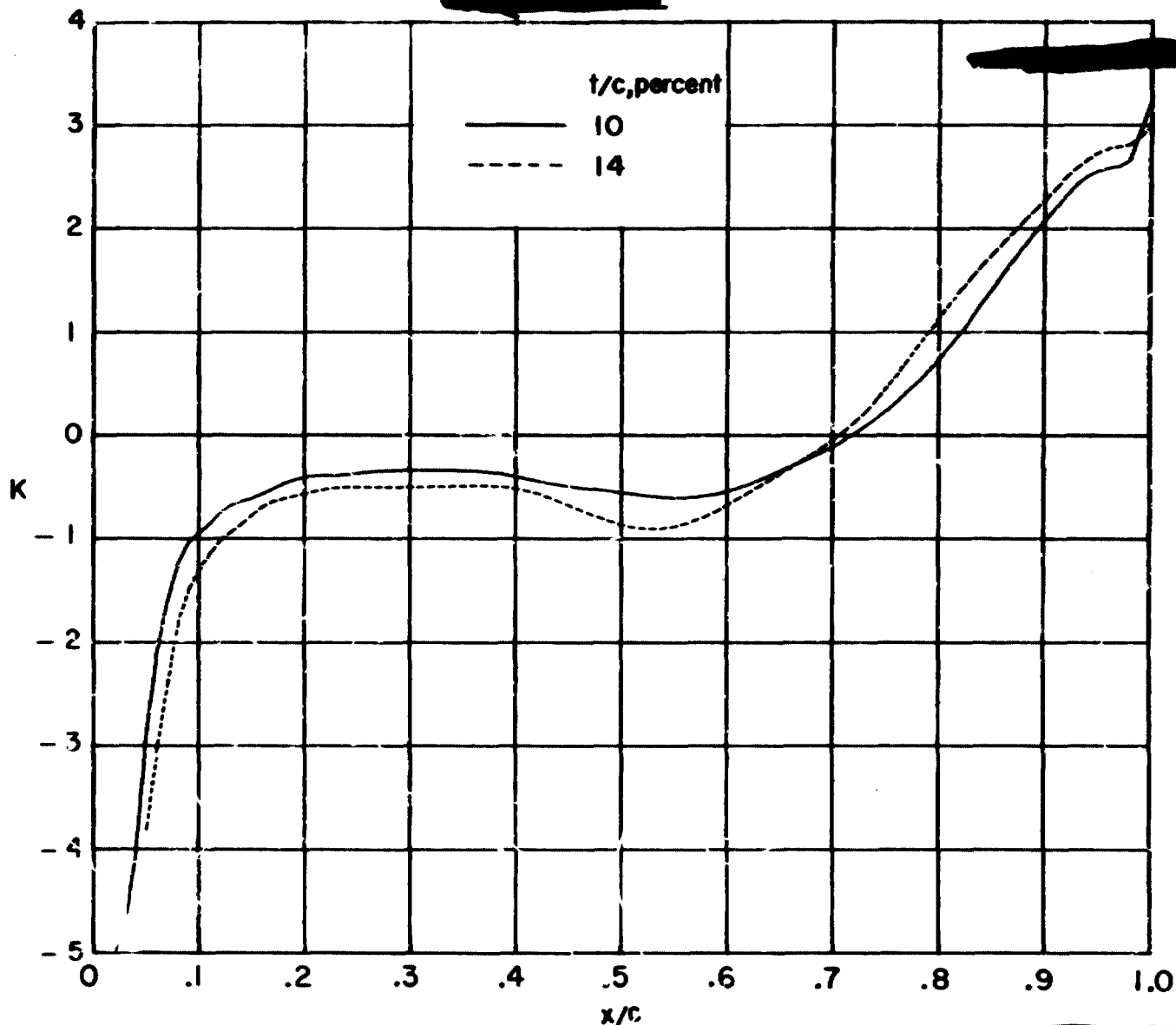
ORIGINAL PAGE IS
OF POOR QUALITY



(a) Upper surface.

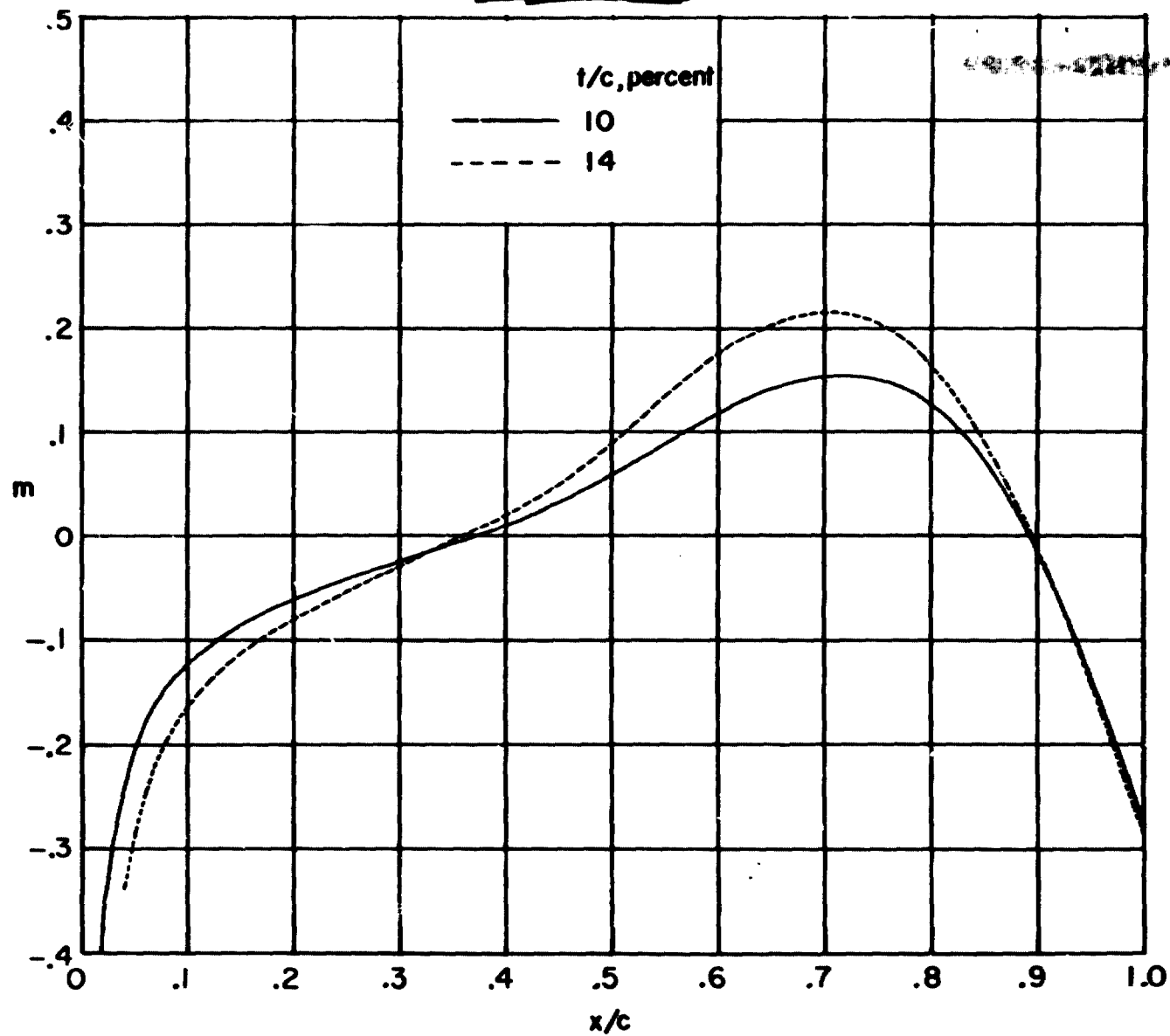
Figure [redacted] shows the variation of airfoil surface slopes and curvature.

ORIGINAL PAGE IS
OF POOR QUALITY



(b) Lower surface. Concluded.

ORIGINAL PAGE IS
OF POOR
QUALITY

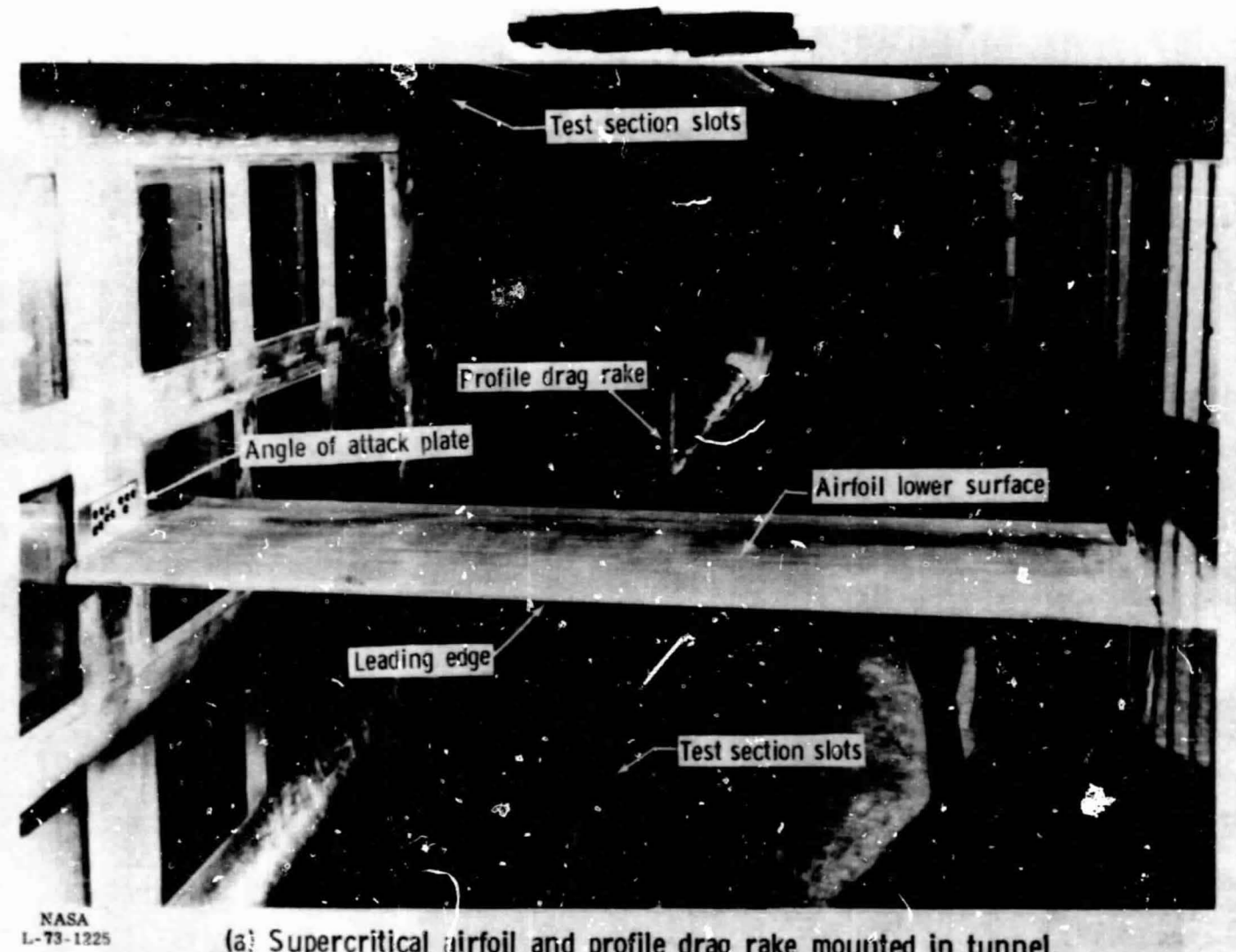


(b) Lower surface.

Figure 2-4 Continued.

ORIGINAL PAGE IS
OF POOR QUALITY

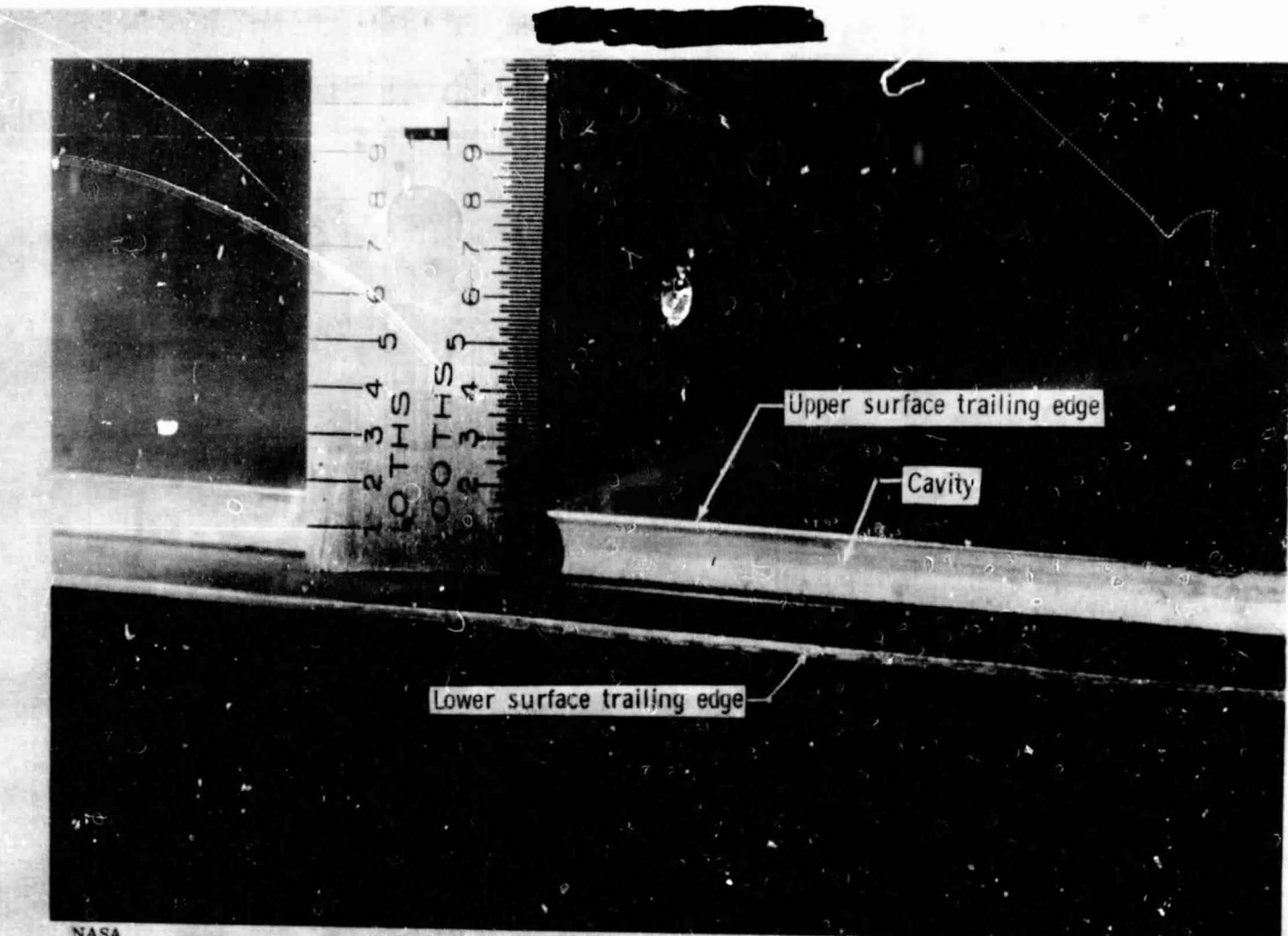
ORIGINAL PAGE IS
OF POOR QUALITY



(a) Supercritical airfoil and profile drag rake mounted in tunnel.

Figure 3. - Photographs of typical airfoil model in tunnel.

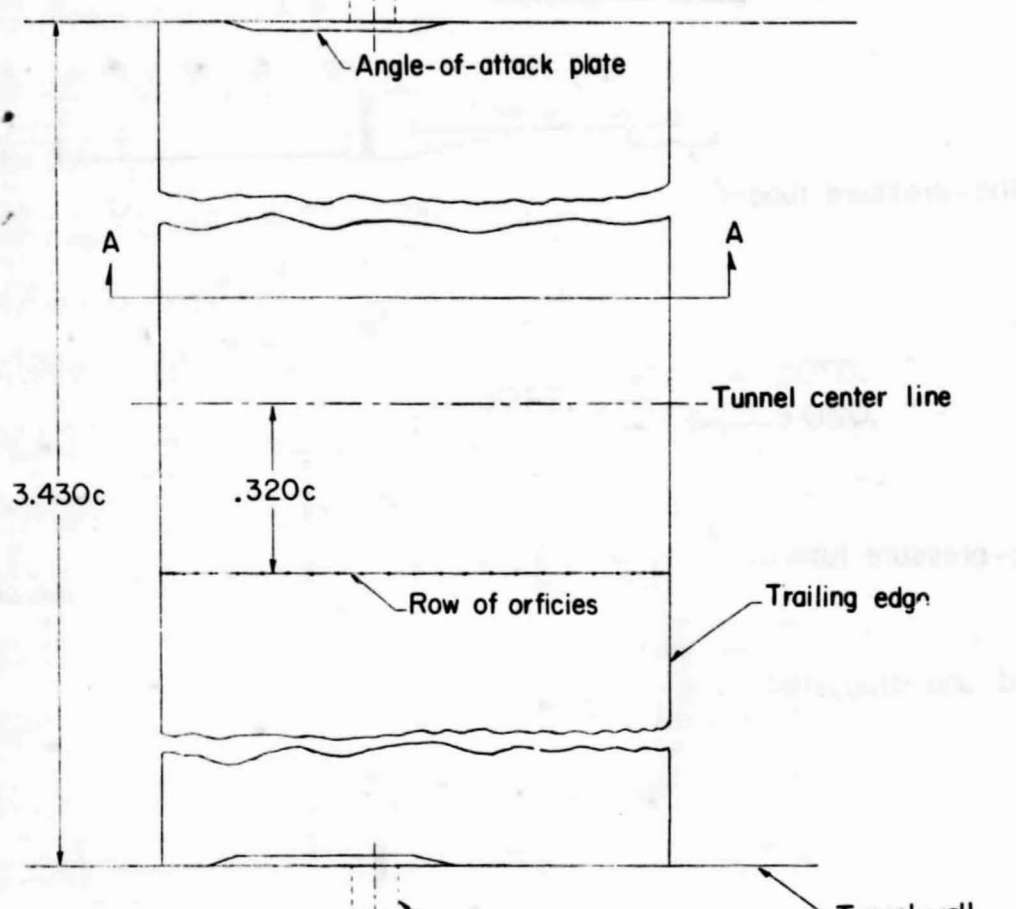
ORIGINAL FROM N
OF PRODUCTION



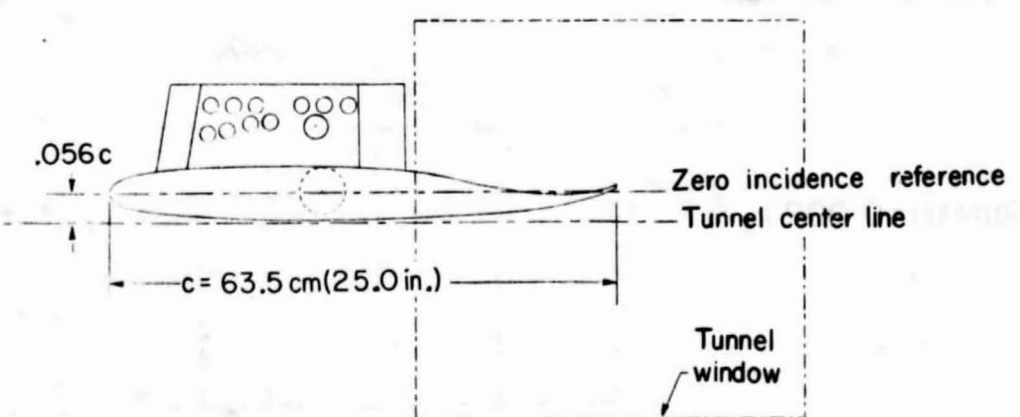
(b) Trailing-edge cavity.

Figure 3.- Concluded.

ORIGINAL PAGE IS
OF POOR QUALITY



Top view

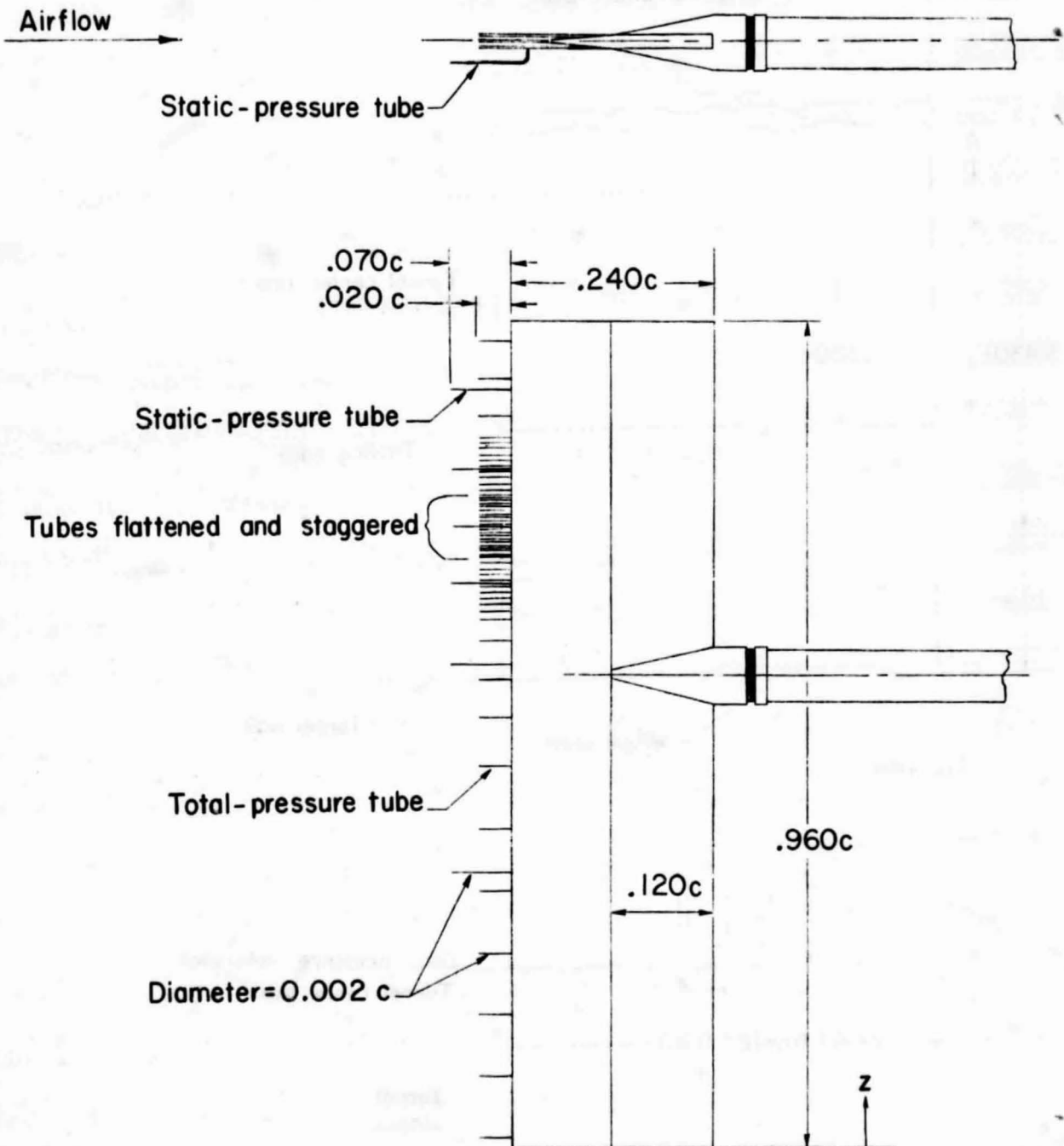


End view, section A-A

(a) Airfoil mounted in tunnel.

Figure 4.- Apparatus dimensions in terms of chord. $c = 63.5 \text{ cm} (25.0 \text{ in.})$.

ORIGINAL PAGE IS
OF POOR QUALITY



(b) Profile drag rake.

Figure 4. - Concluded.

ORIGINAL PAGE IS
OF POOR QUALITY

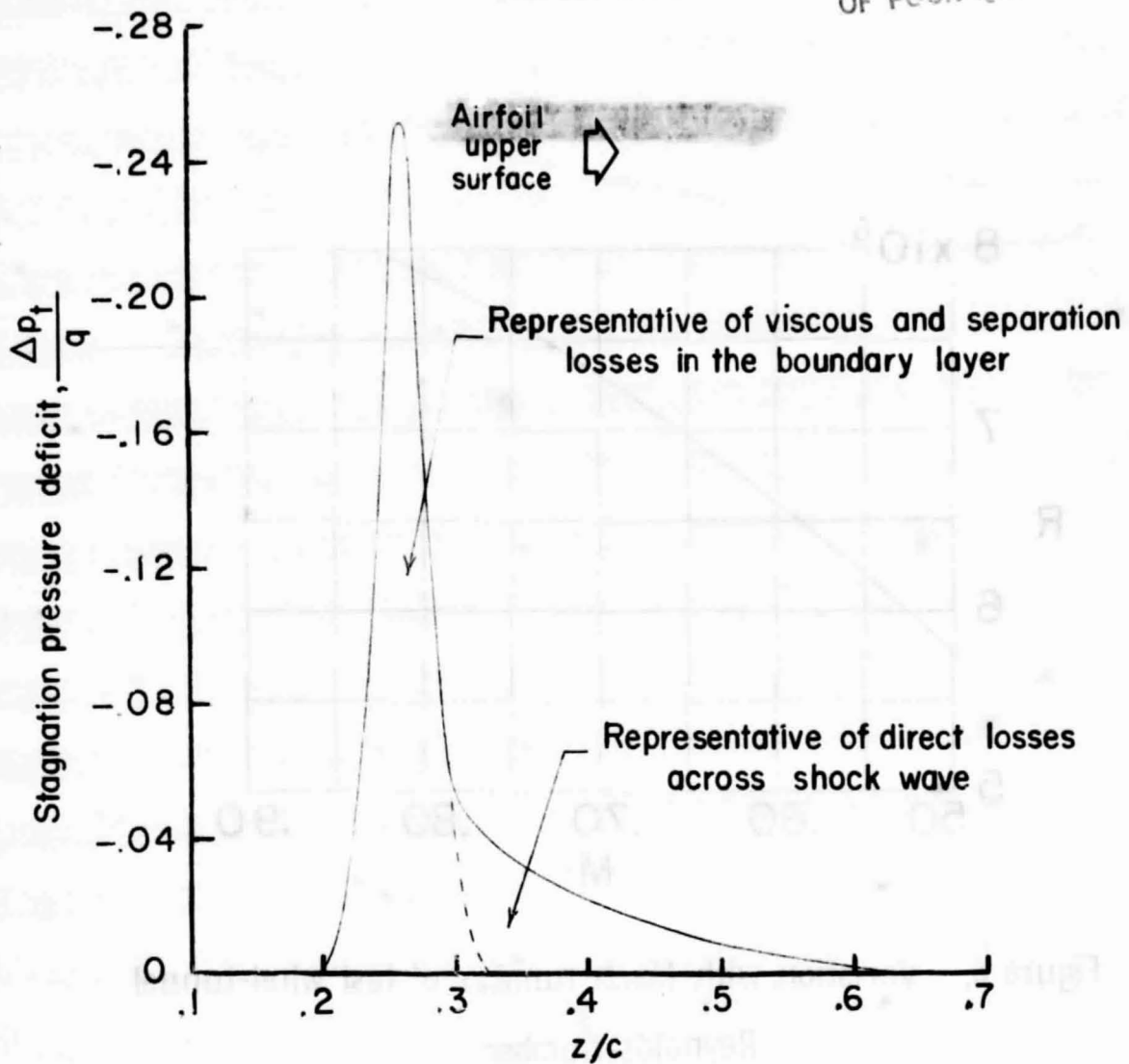


Figure 5. - Schematic of wake profiles.

ORIGINAL PAGE IS
OF POOR QUALITY

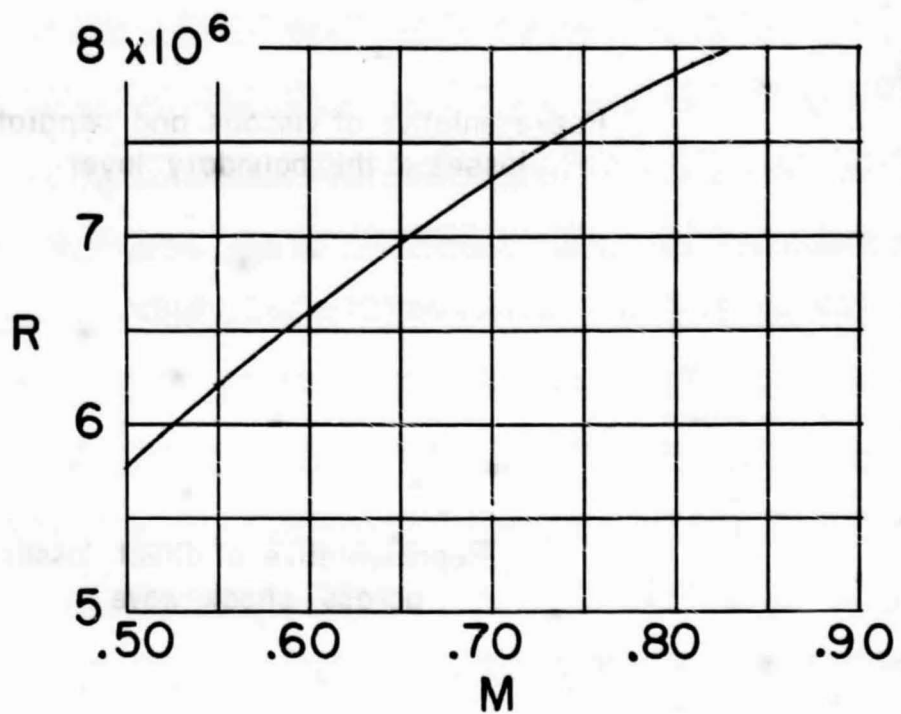
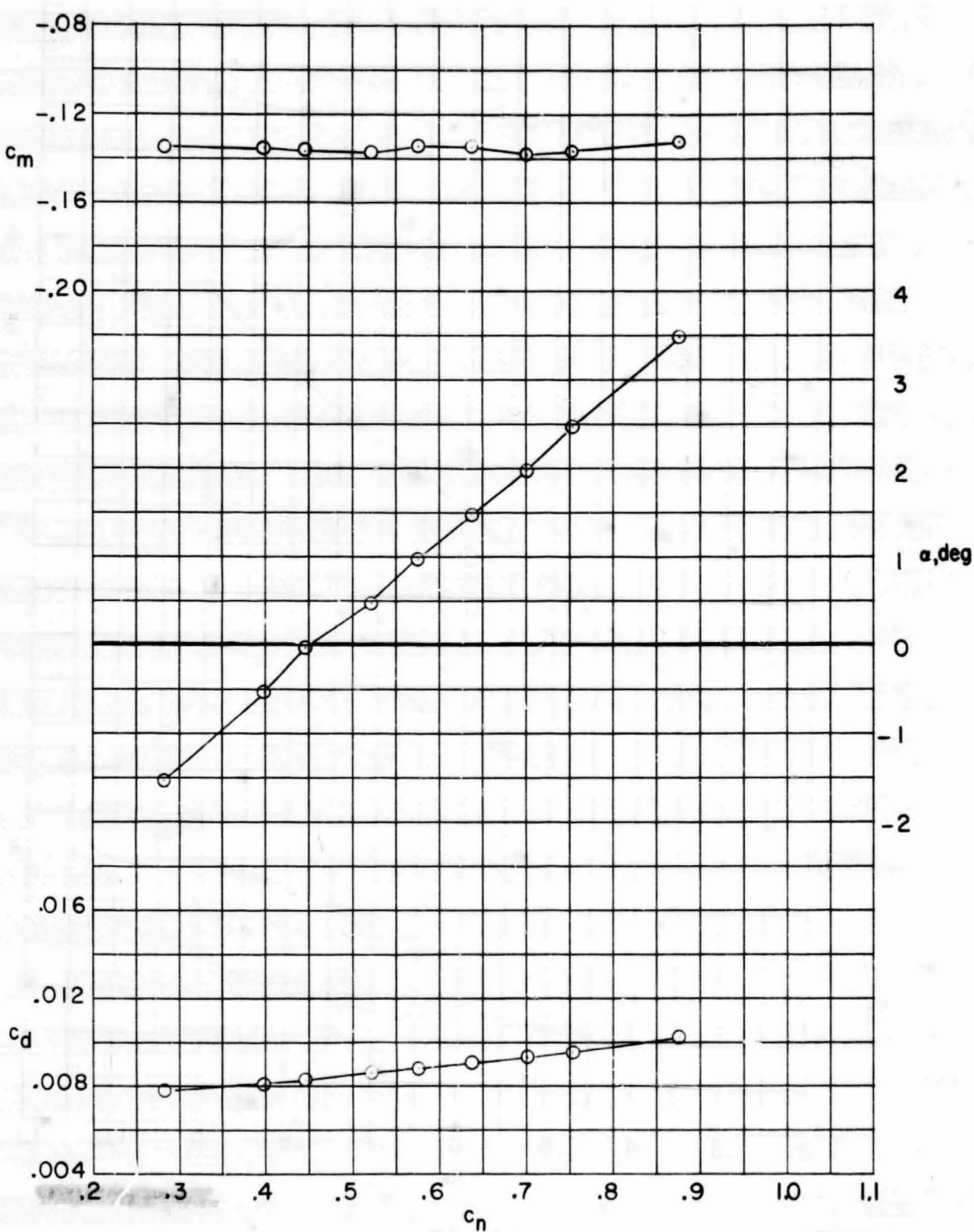


Figure 6. - Variation with Mach number of test wind-tunnel
Reynolds number.

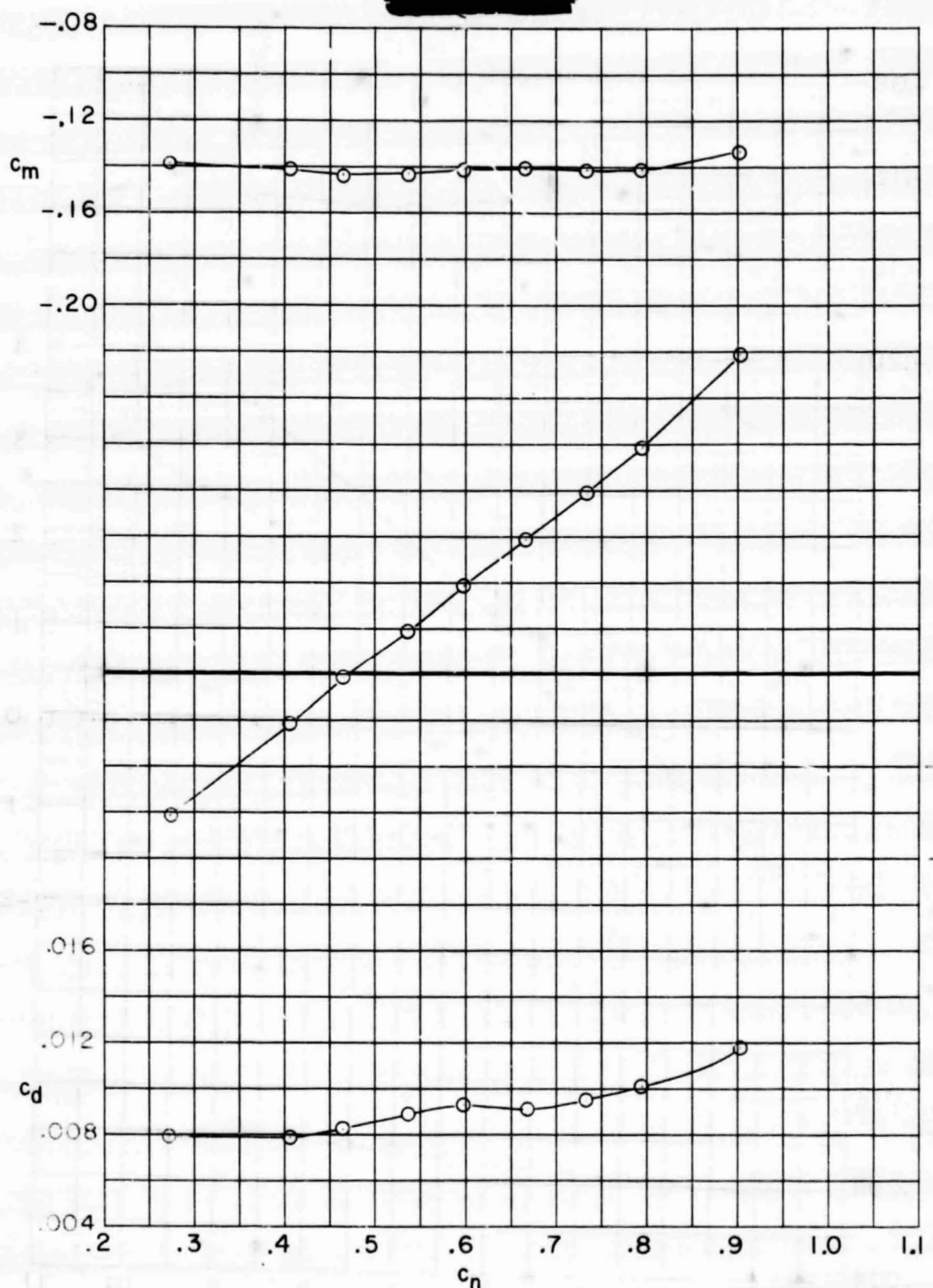
ORIGINAL PAGE IS
OF POOR QUALITY.



(a) $M = 0.50$.

Figure 7.- Force and moment characteristics of 14-percent-thick supercritical airfoil.

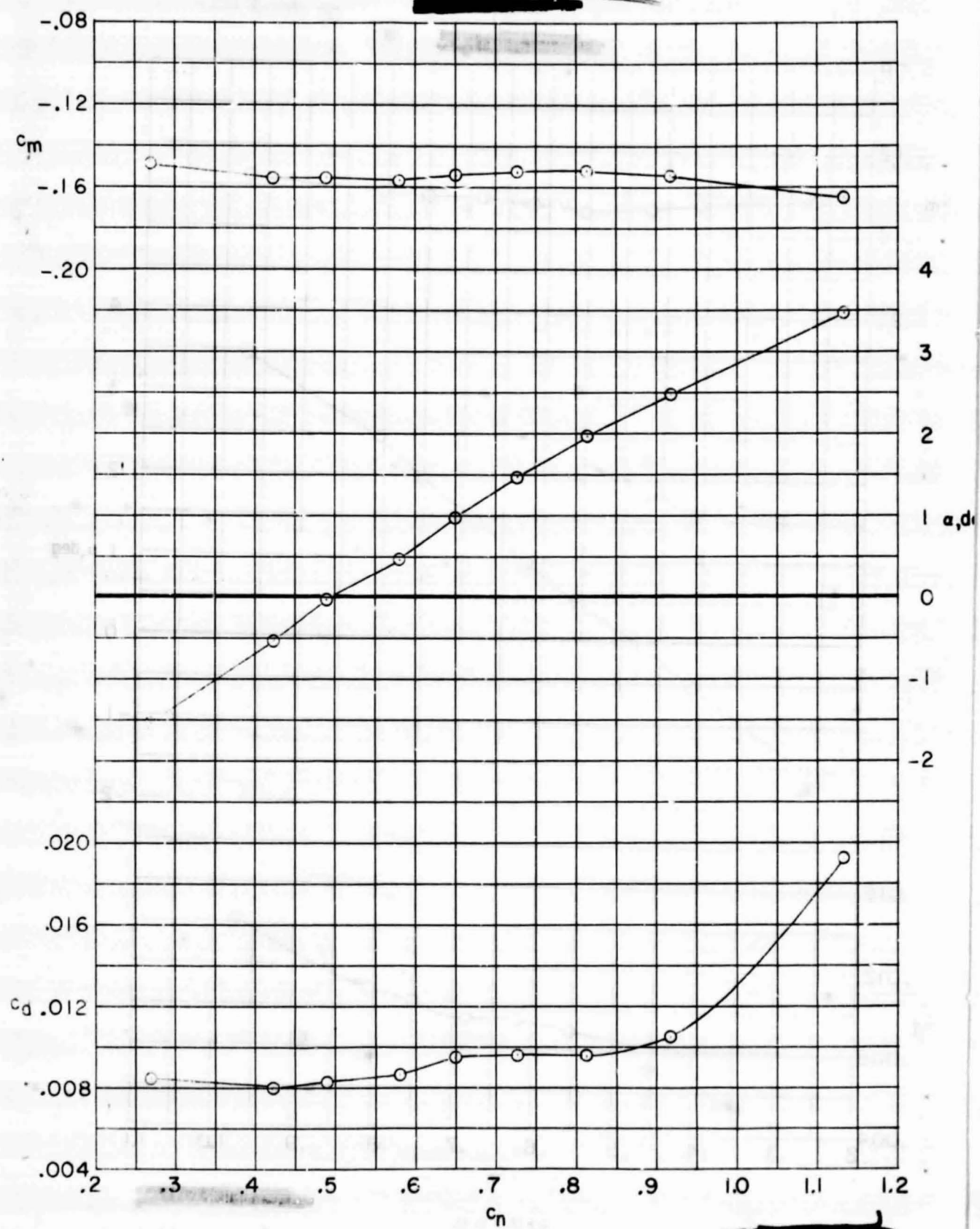
ORIGINAL PAGE IS
OF POOR QUALITY



(b) $M = 0.60$.

Figure 7. - Continued.

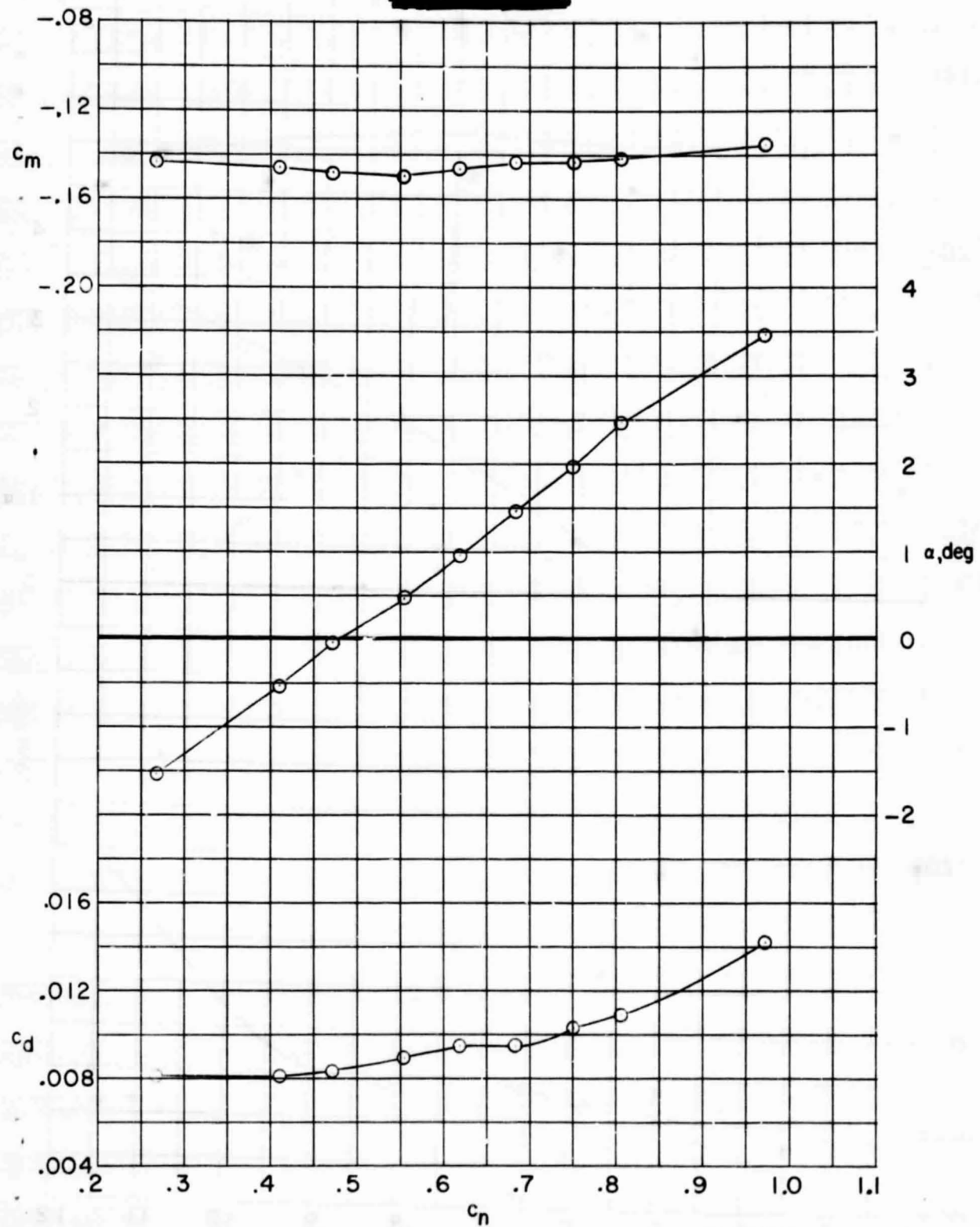
ORIGINAL PAGE IS
OF POOR QUALITY



(d) $M = 0.70$.

Figure 7.- Continued.

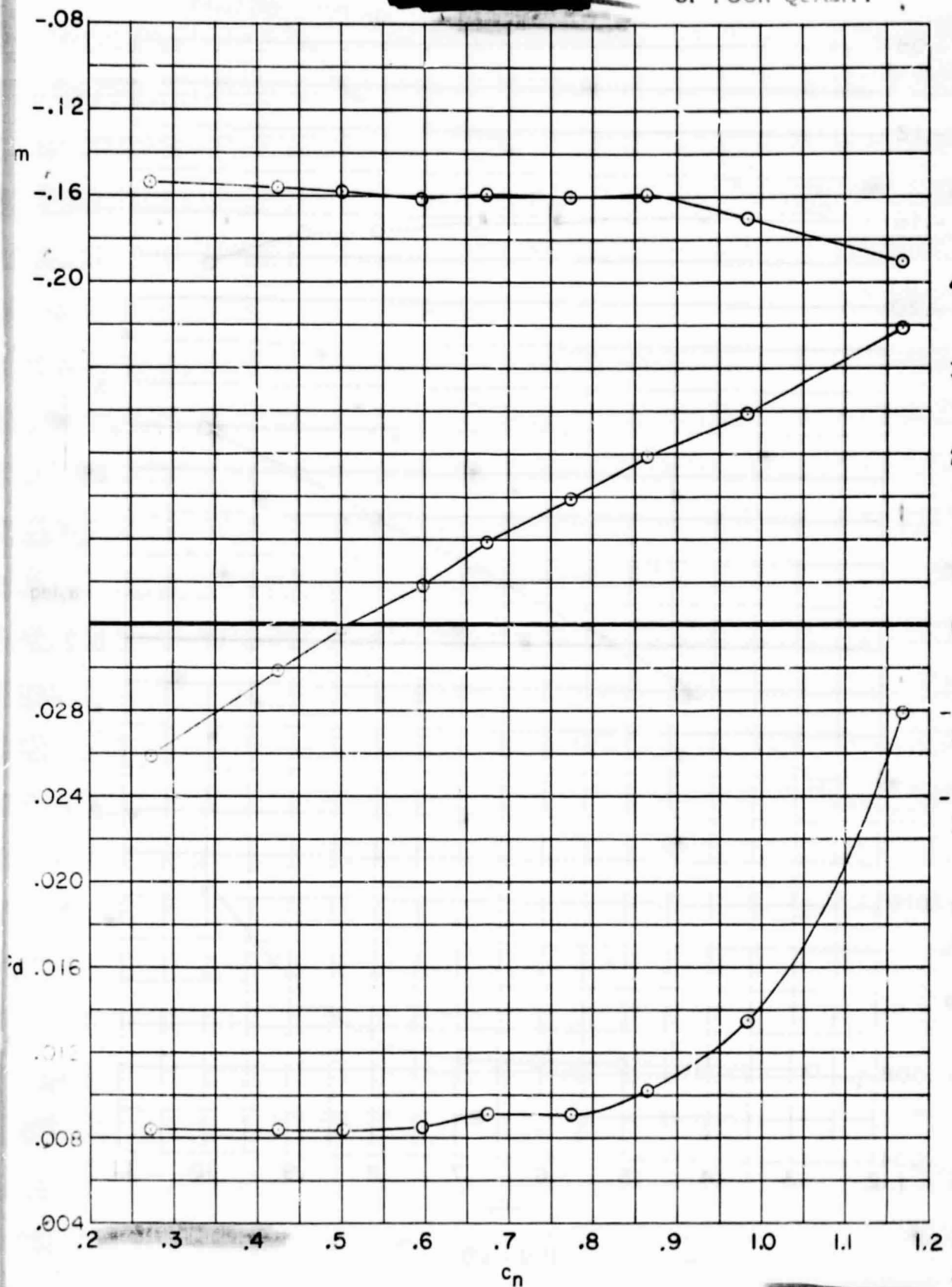
ORIGINAL PAGE IS
OF POOR QUALITY



(c) $M = 0.65.$

Figure 7.- Continued.

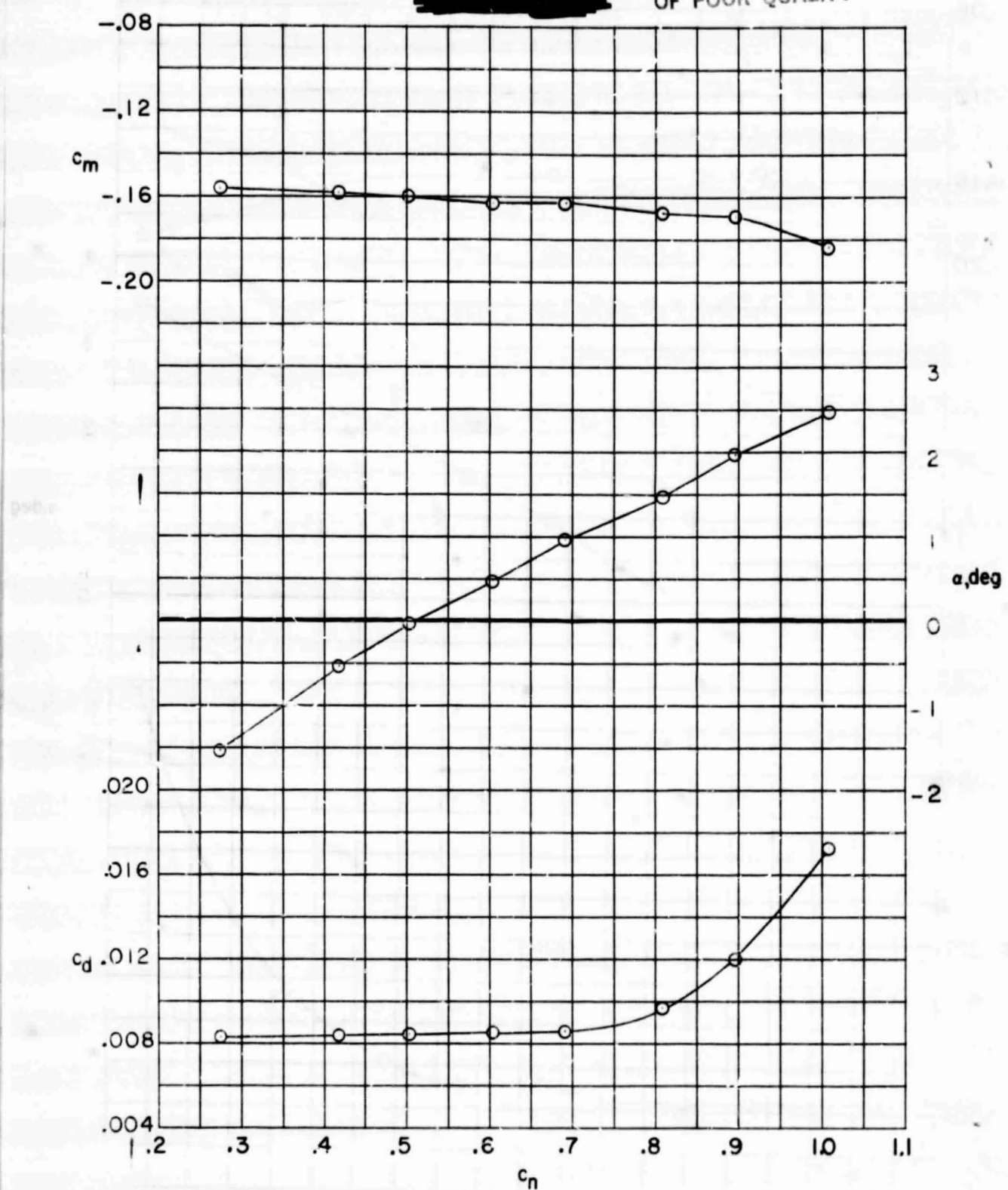
ORIGINAL PAGE IS
OF POOR QUALITY



(e) $M = 0.72$.

Figure 7.- Continued.

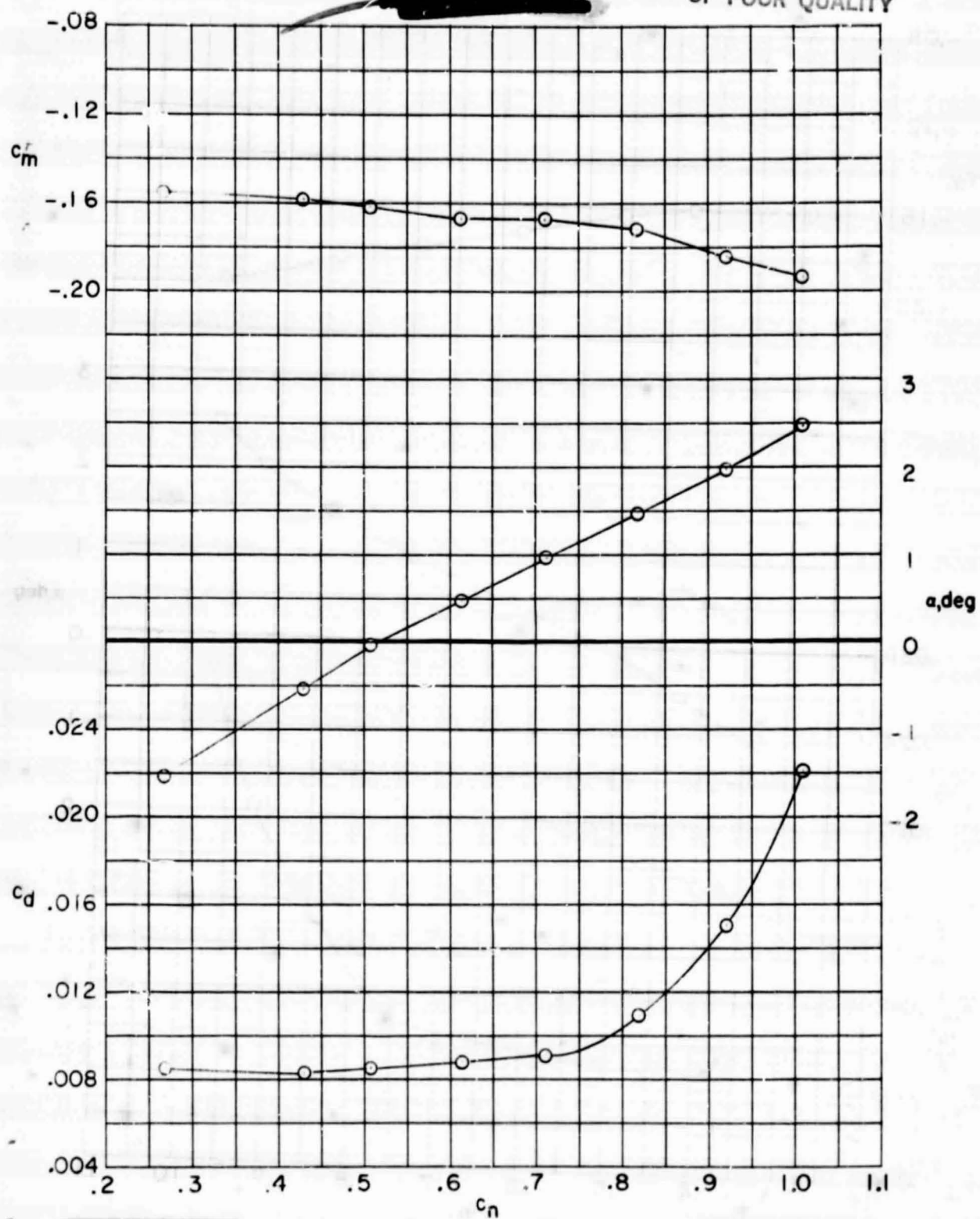
ORIGINAL PAGE IS
OF POOR QUALITY



(f) $M = 0.73$.

Figure 7. - Continued.

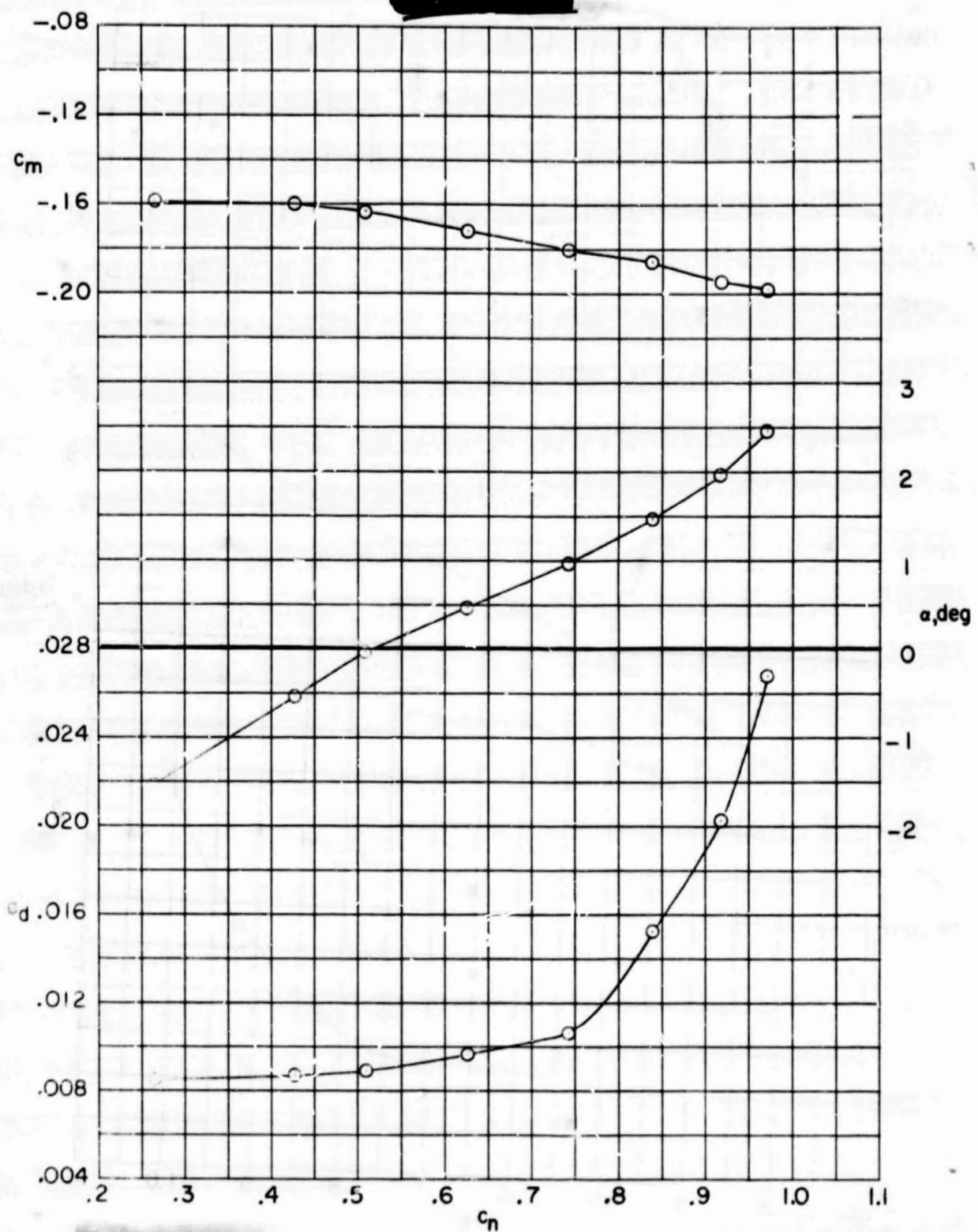
ORIGINAL PAGE IS
OF POOR QUALITY



(g) $M = 0.74$.

Figure 7.- Continued.

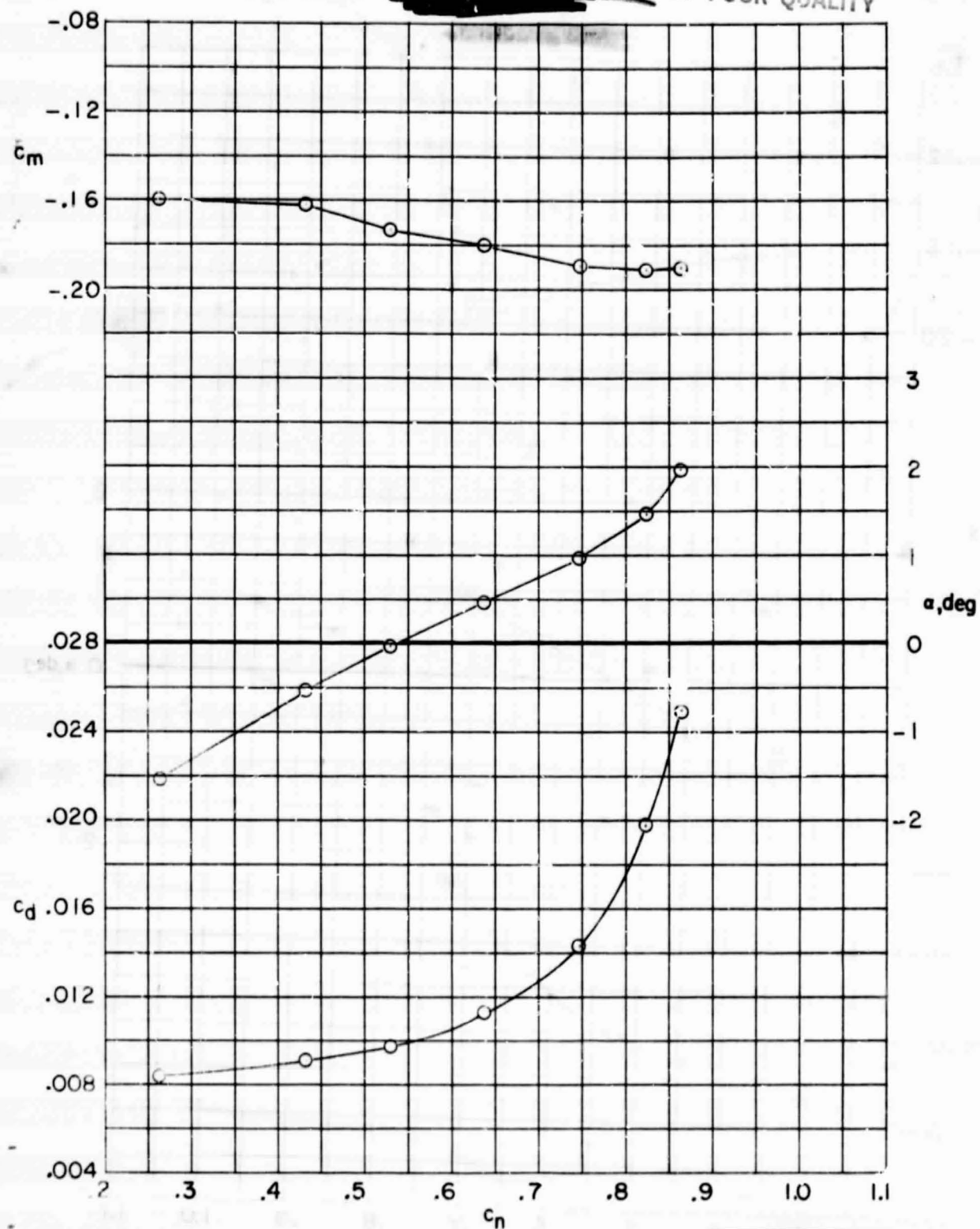
ORIGINAL PAGE IS
OF POOR QUALITY



(h) $M = 0.75$.

Figure 7. - Continued.

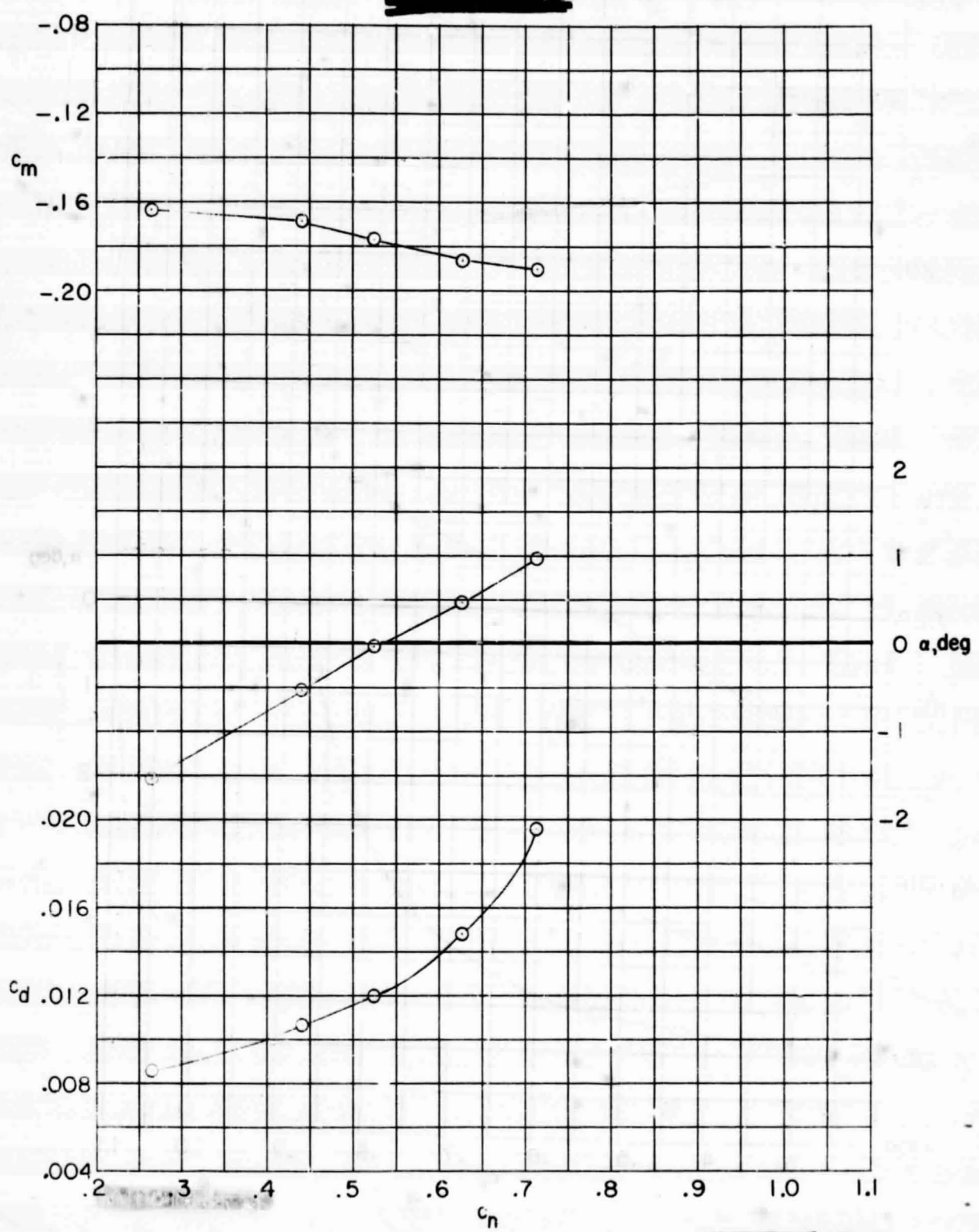
ORIGINAL PAGE IS
OF POOR QUALITY



(i) $M = 0.76$.

Figure 7. - Continued.

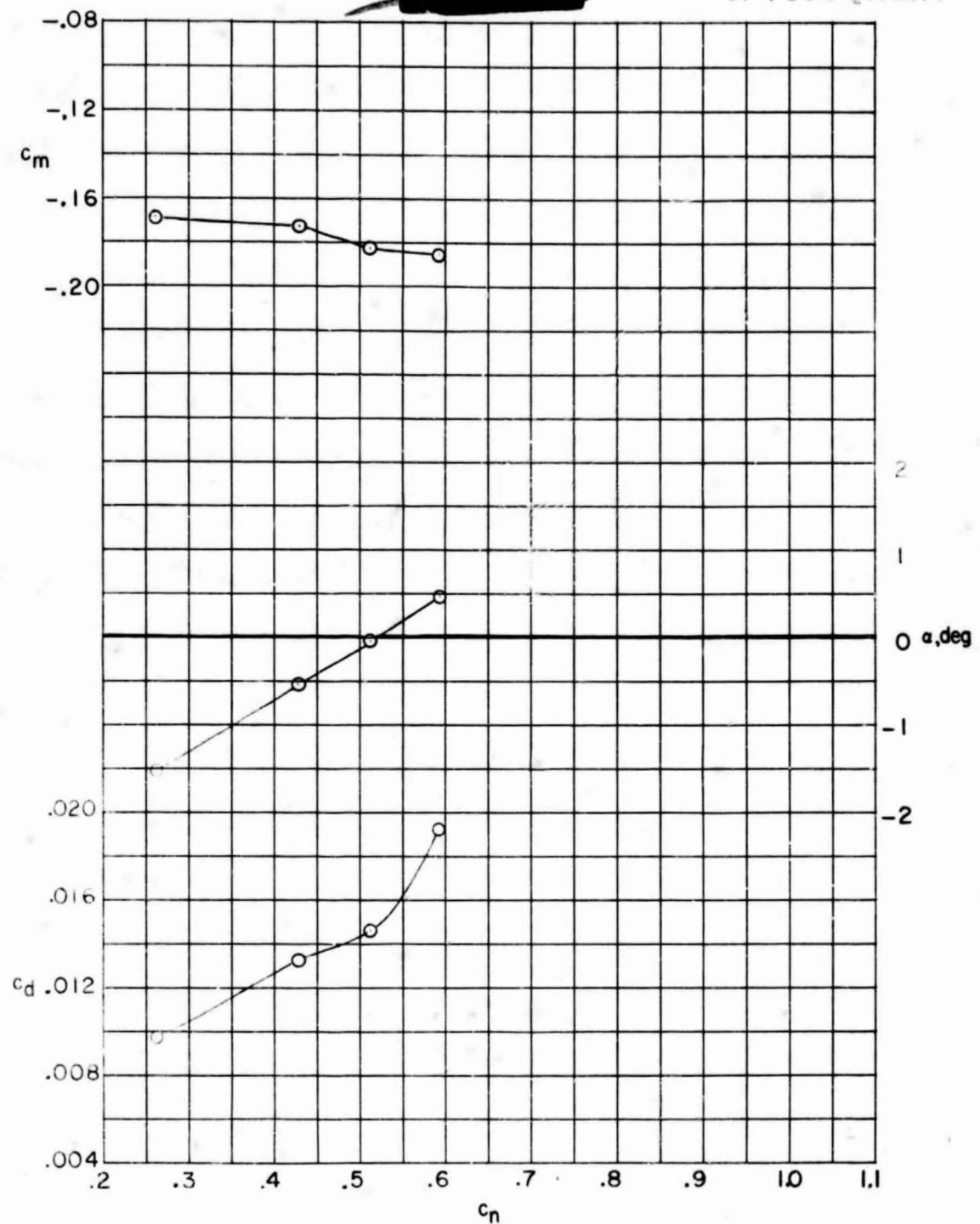
ORIGINAL PAGE IS
OF POOR QUALITY



(j) $M = 0.77$.

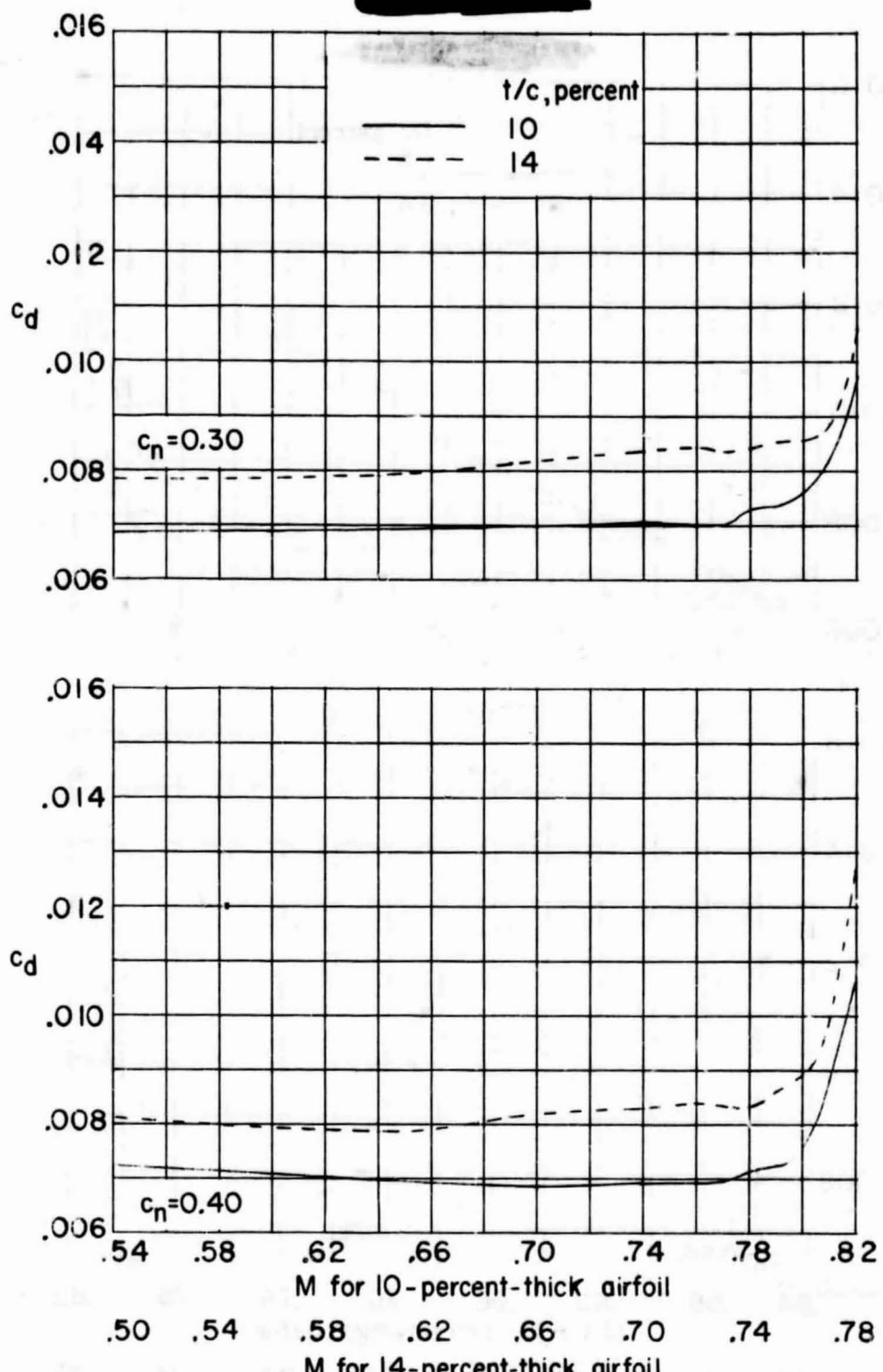
Figure 7. - Continued.

ORIGINAL PAGE IS
OF POOR QUALITY



(k) $M = 0.78$.

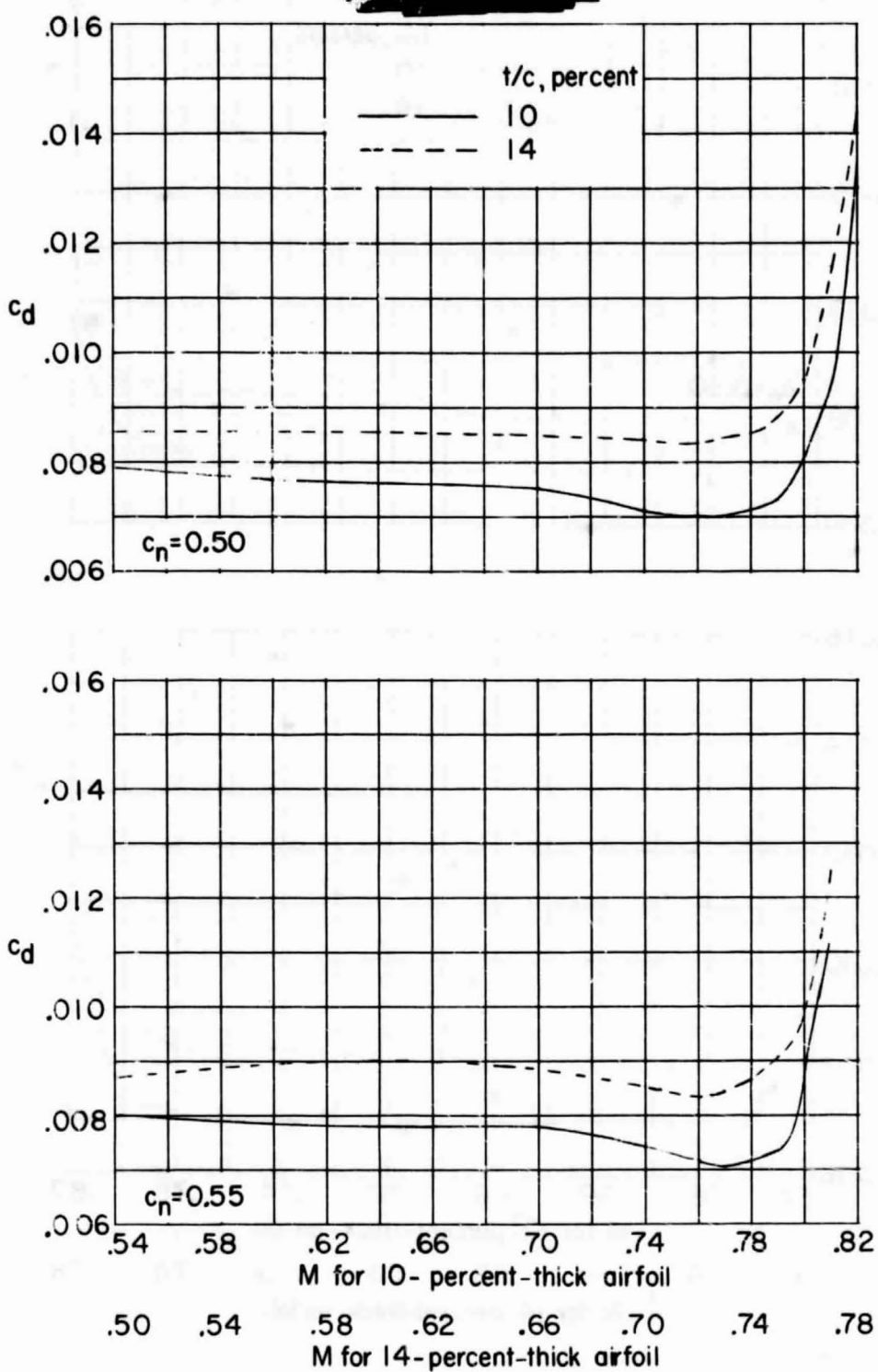
Figure 7.- Concluded.



(a) $c_n = 0.30$ and 0.40 .

Figure 8.- Variation of measured section drag coefficient with Mach number of 14- and 10-percent thick supercritical airfoils.

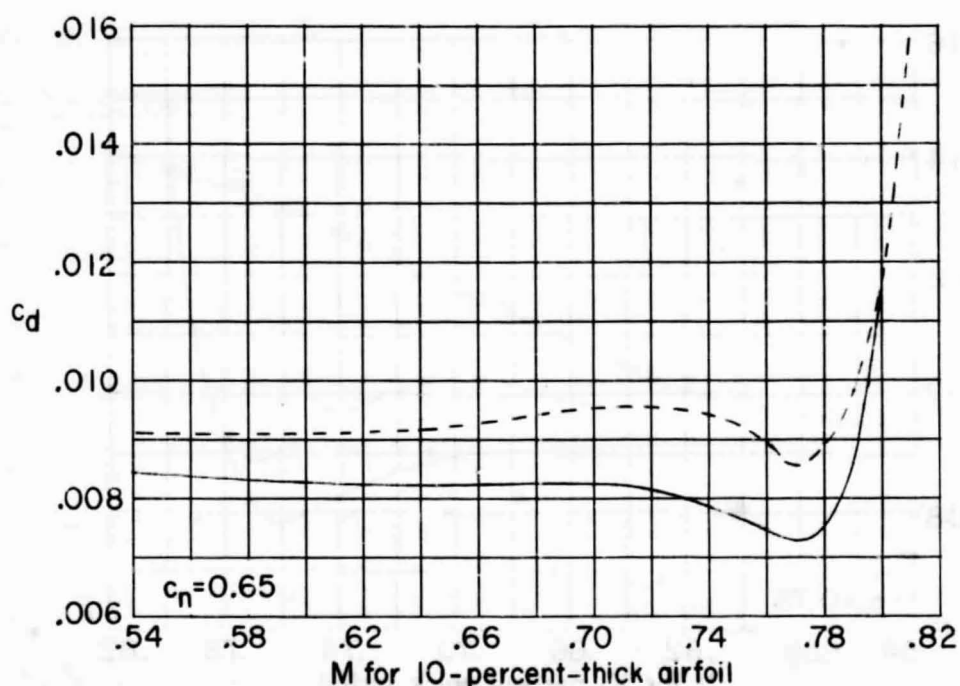
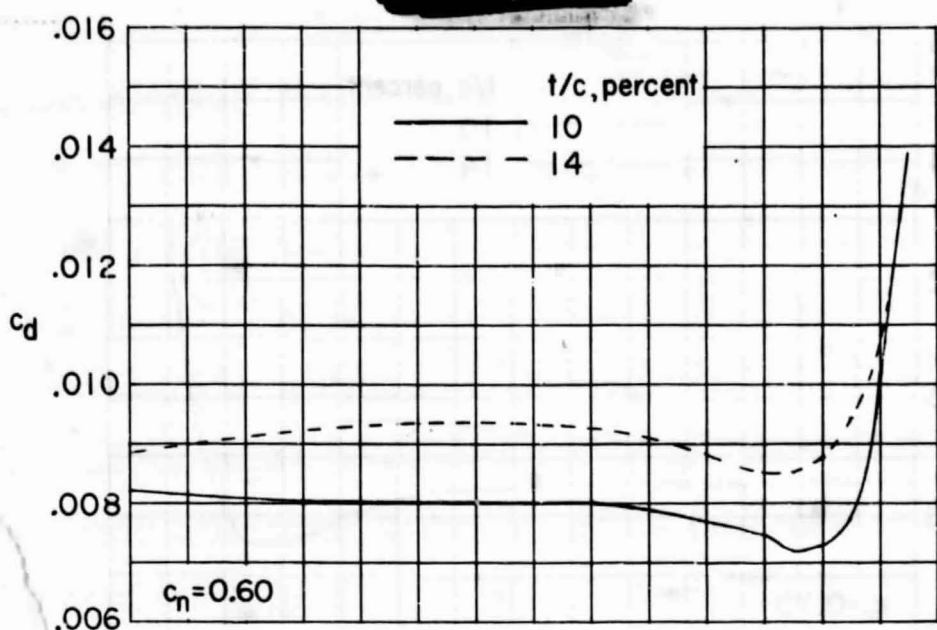
ORIGINAL PAGE IS
OF POOR QUALITY



(b) $c_n = 0.50$ and 0.55.

Figure 8.- Continued.

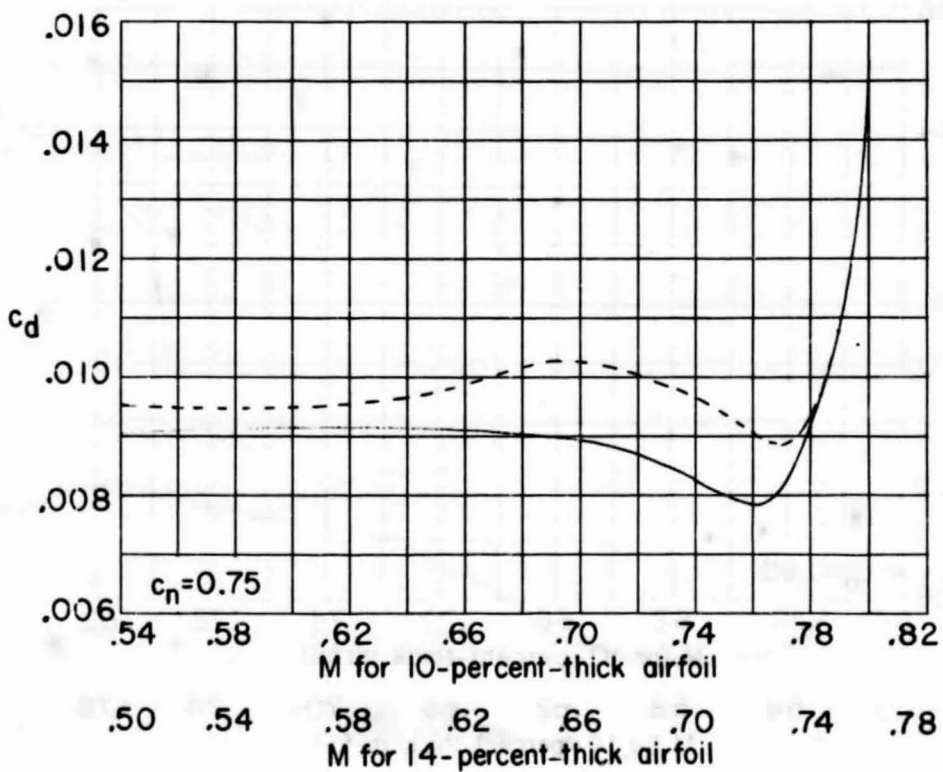
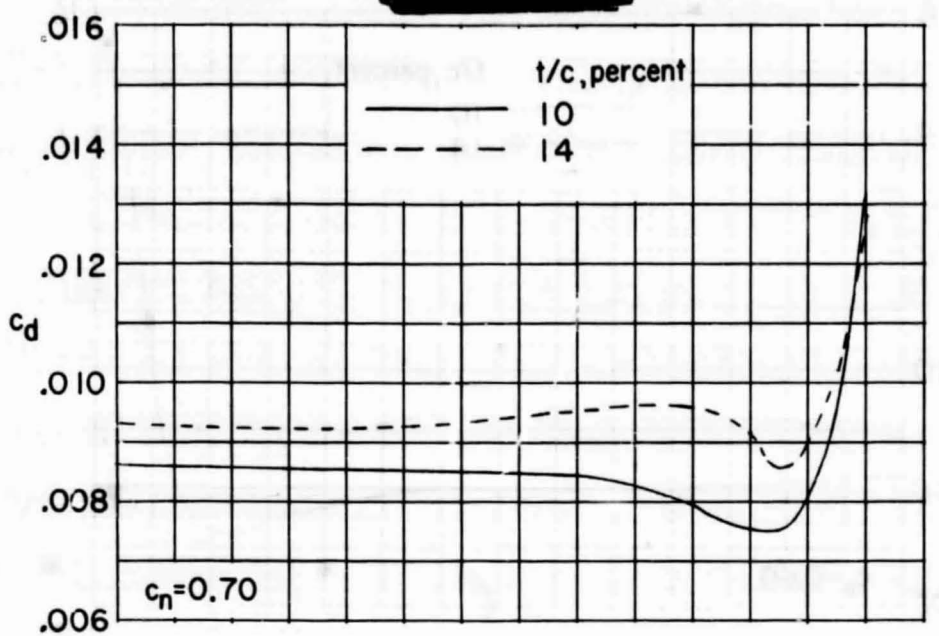
ORIGINAL PAGE IS
OF POOR QUALITY



(c) $c_n = 0.60$ and 0.65 .

Figure 8.- Continued.

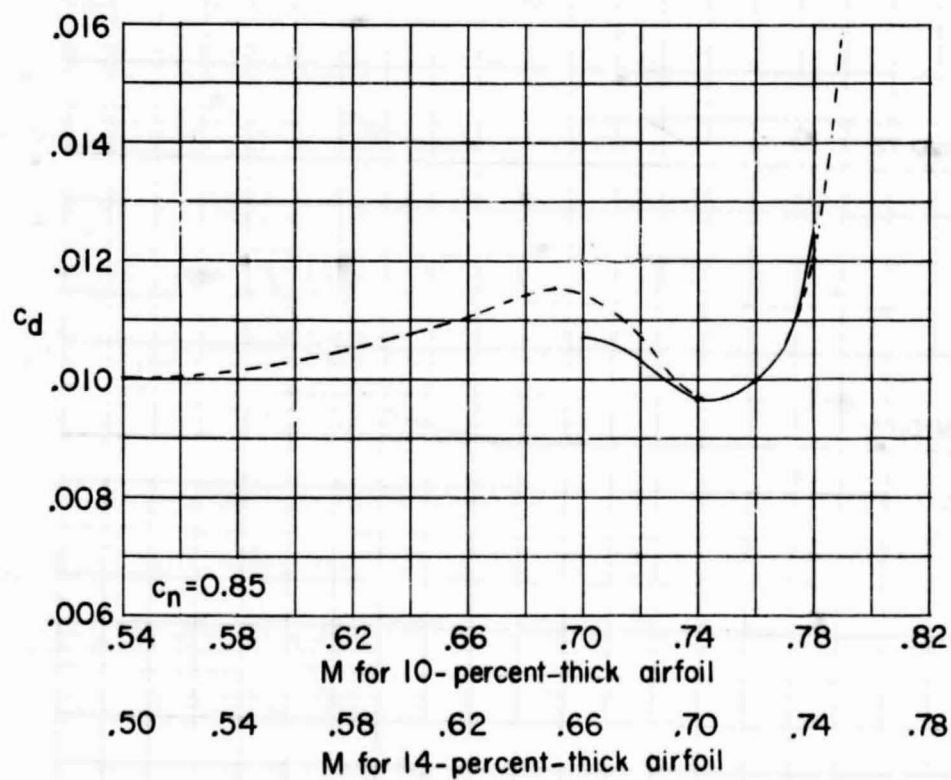
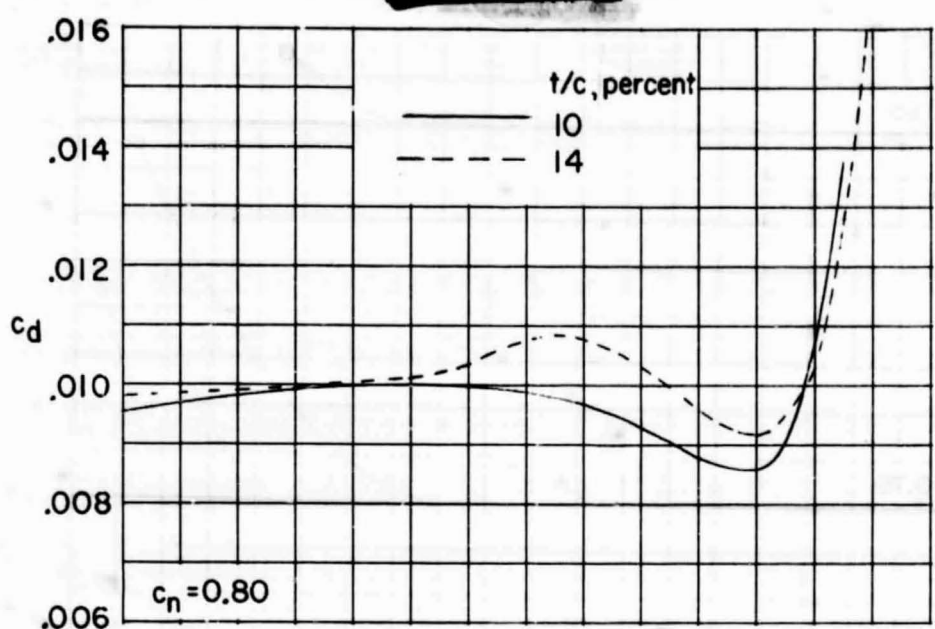
ORIGINAL PAGE IS
OF POOR QUALITY



(d) $c_n = 0.70$ and 0.75 .

Figure 8.- Continued.

ORIGINAL PAGE IS
OF POOR QUALITY



(e) $c_n = 0.80$ and 0.85 .

Figure 8.- Concluded.

ORIGINAL PAGE IS
OF POOR QUALITY

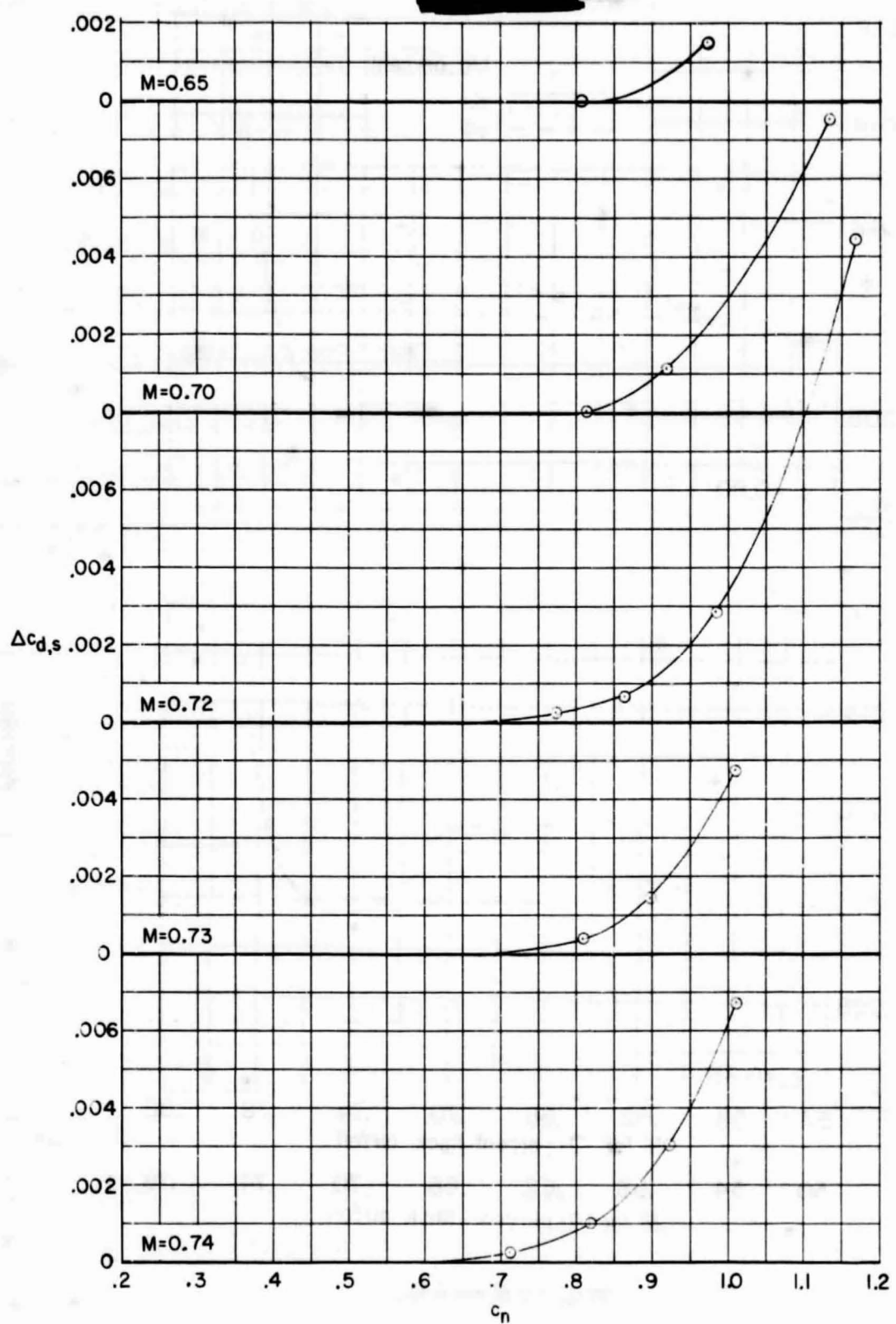


Figure 9. - Drag increment due to shock-wave losses of 14-percent-thick supercritical airfoil.

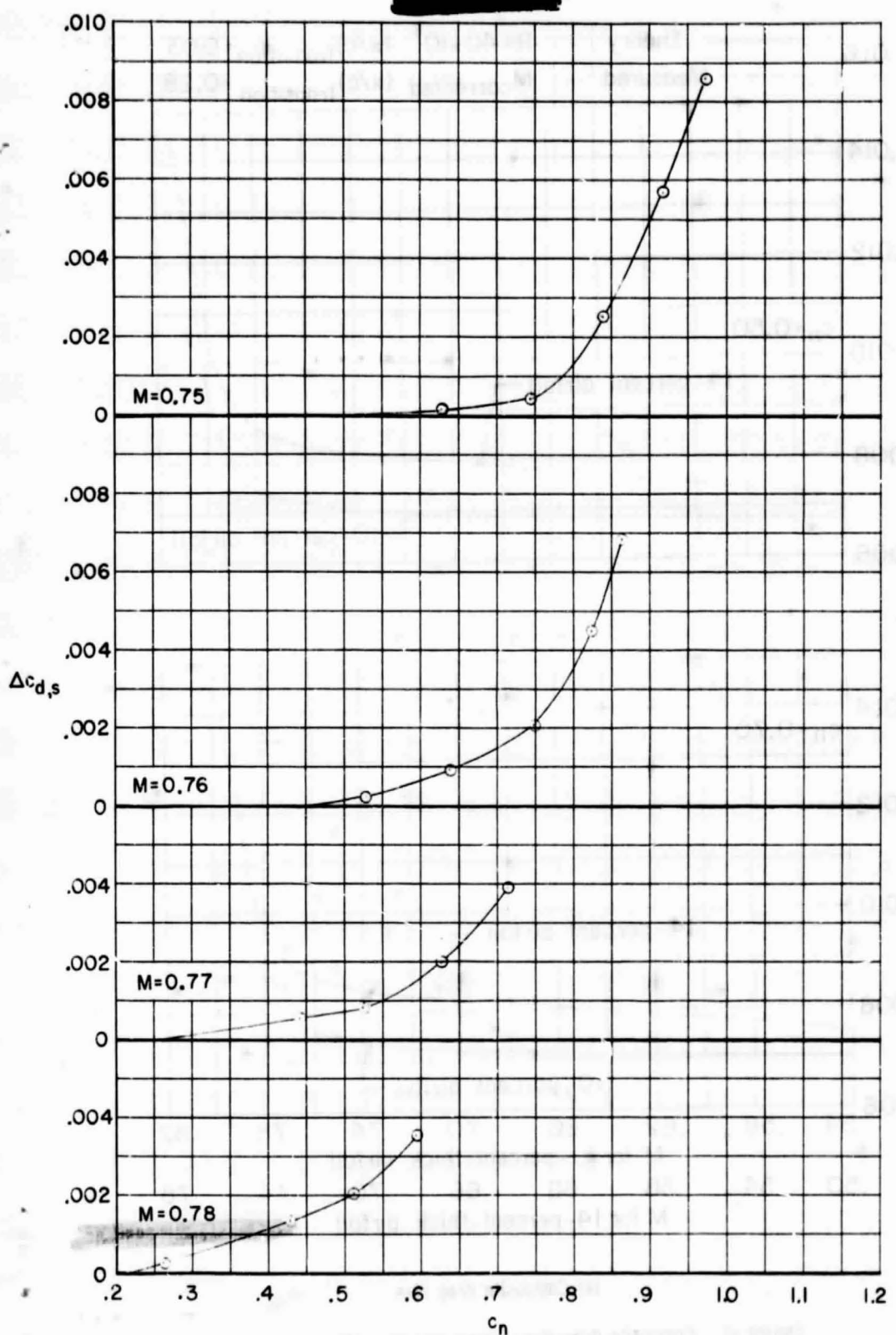
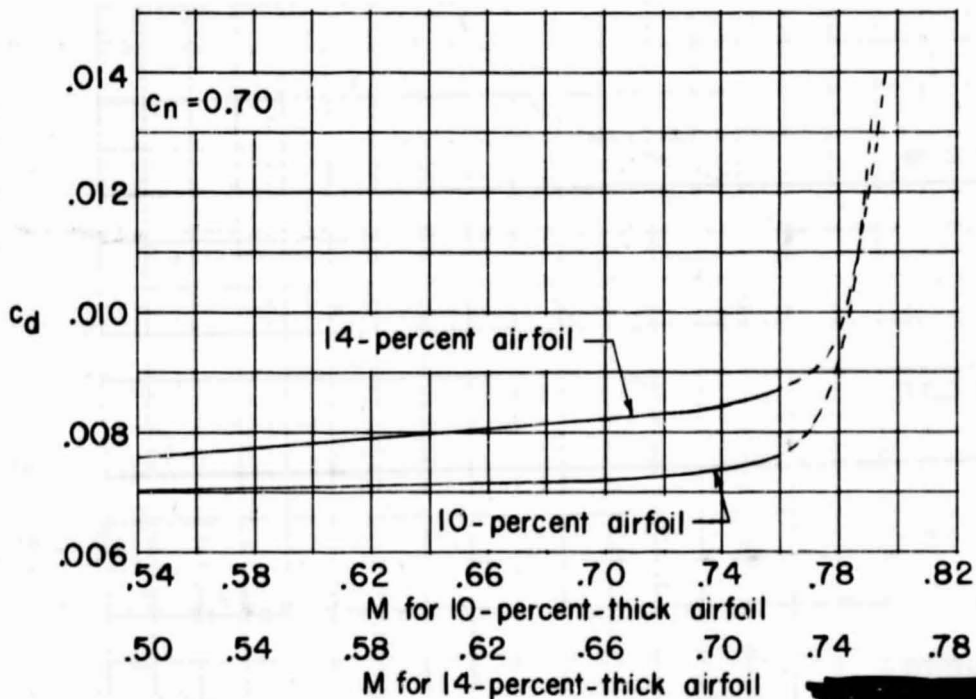
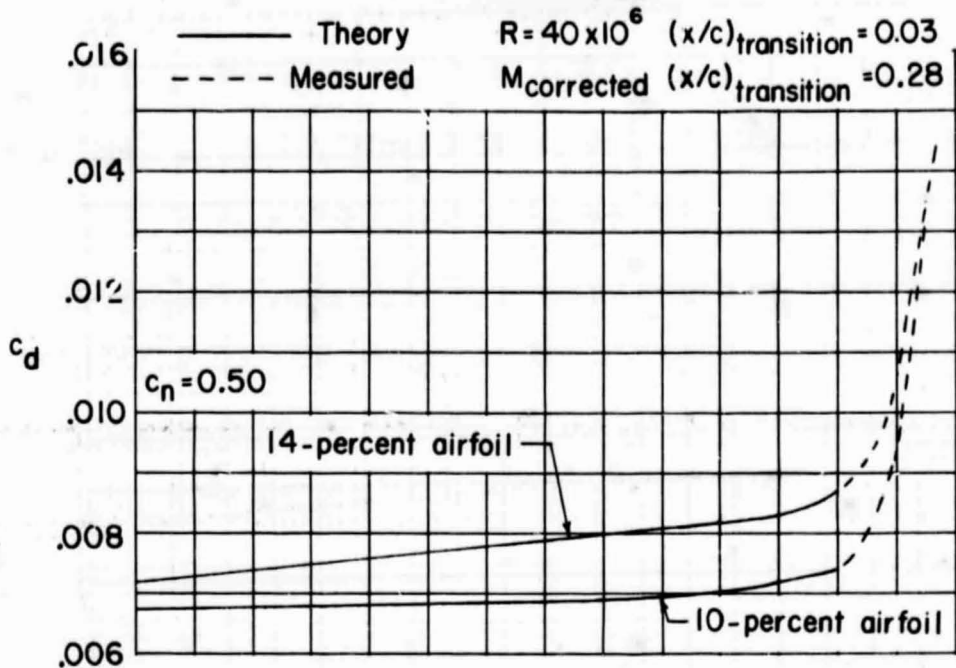


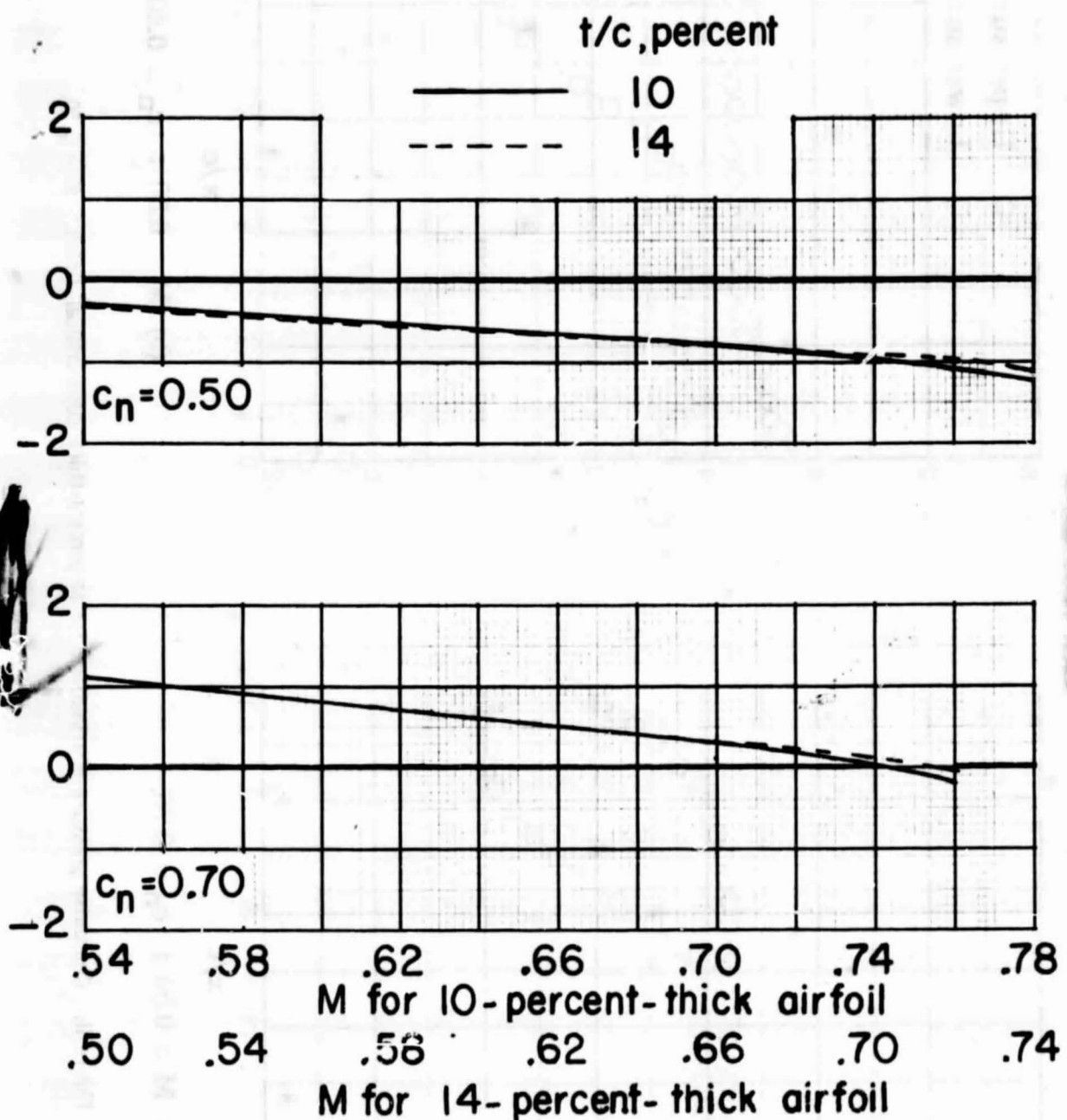
Figure 9. - Concluded.



(a) Composite drag rise.

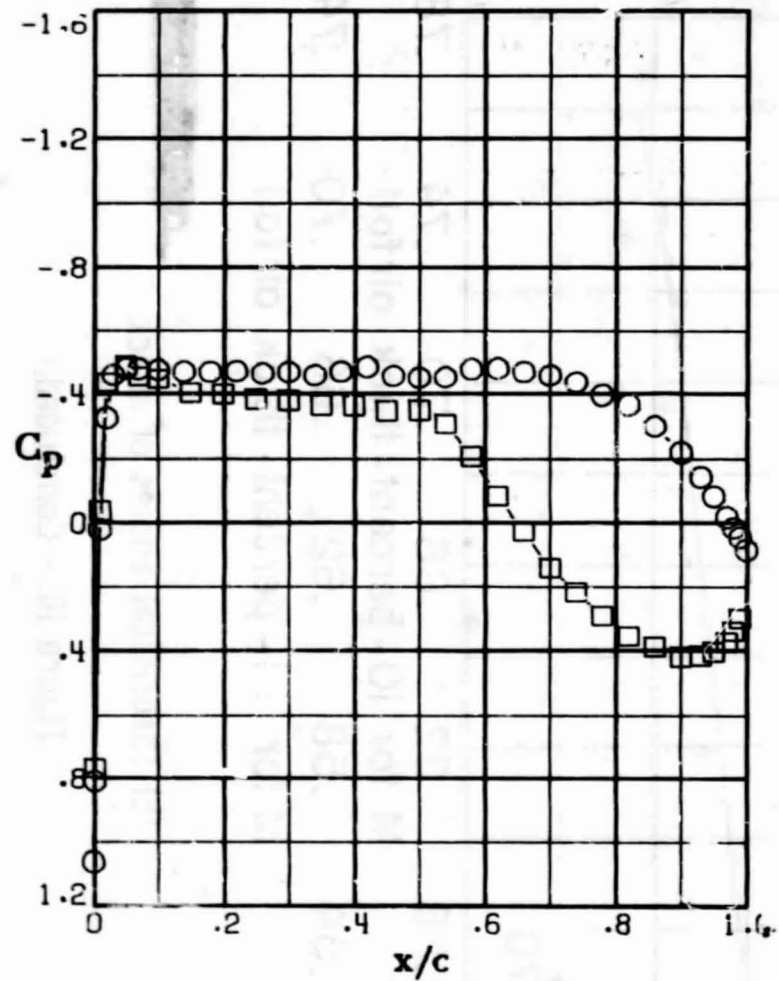
Figure 10.- Composite drag-rise curves and theoretical angles of attack for 14-percent-thick supercritical airfoil and 10-percent-thick supercritical airfoil 33.

ORIGINAL PAGE IS
OF POOR QUALITY

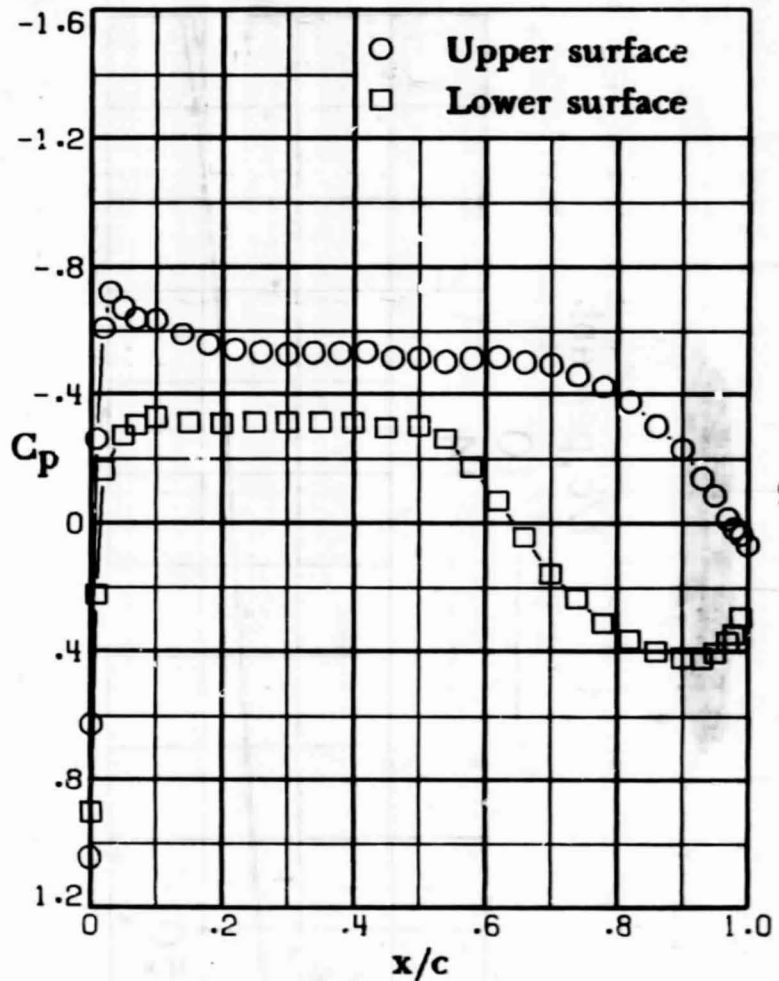


(b) Theoretical angles of attack.

Figure 10.- Concluded.

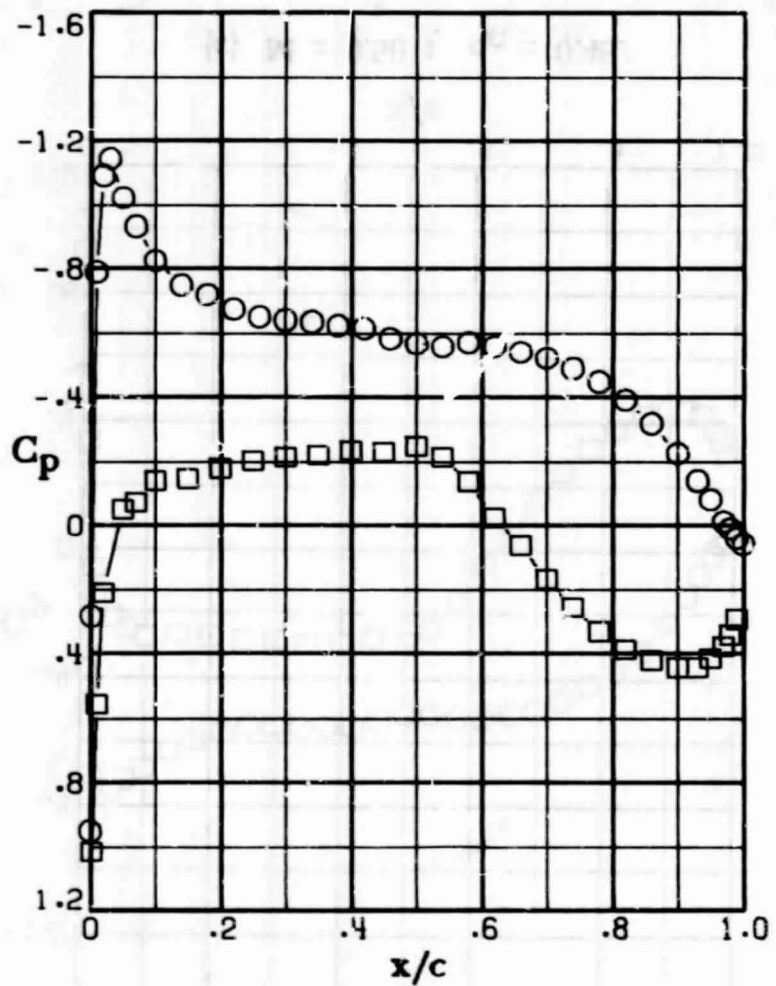


(a) $M = 0.50$; $c_n = 0.28$.

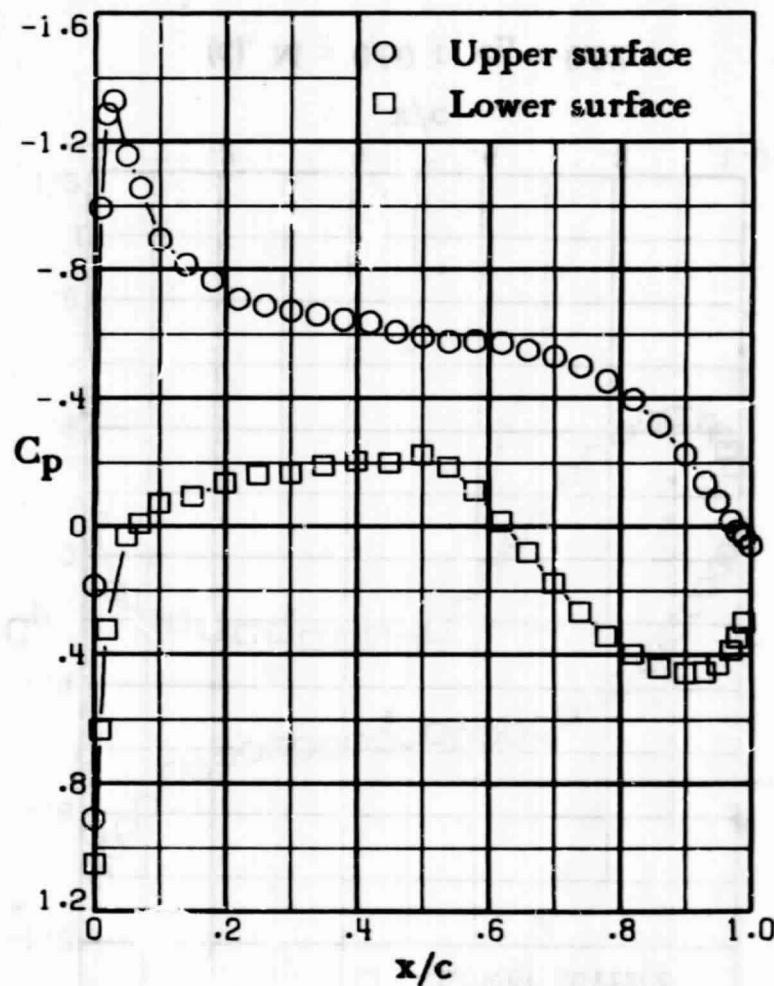


(b) $M = 0.50$; $c_n = 0.40$.

Figure II. - Chordwise pressure distributions for 14-percent-thick supercritical airfoil. $M = 0.50$.



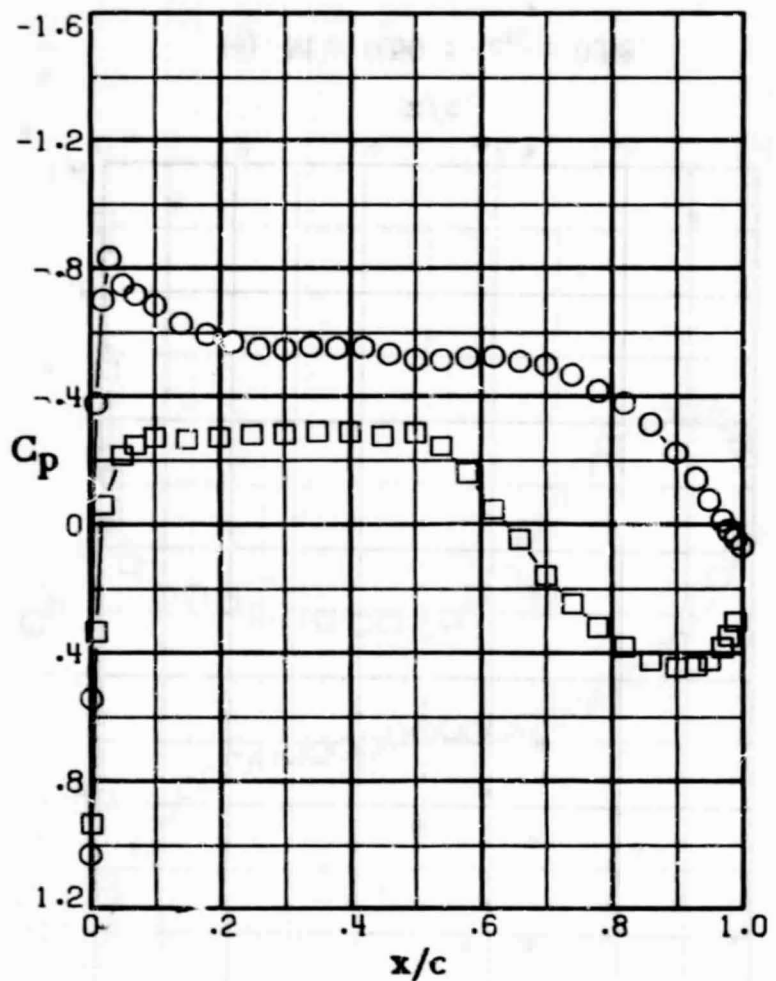
(e) $M = 0.50$; $c_n = 0.58$.



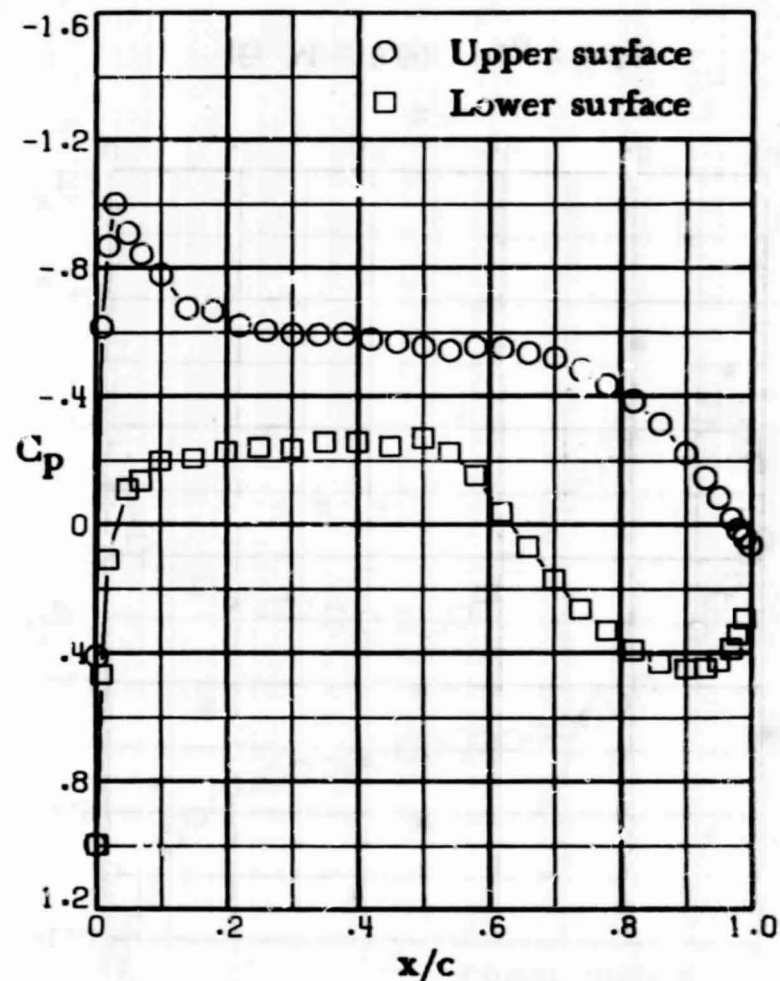
(f) $M = 0.50$; $c_n = 0.64$.

ORIGINAL PAGE IS
OF POOR QUALITY

Figure II. - Continued.



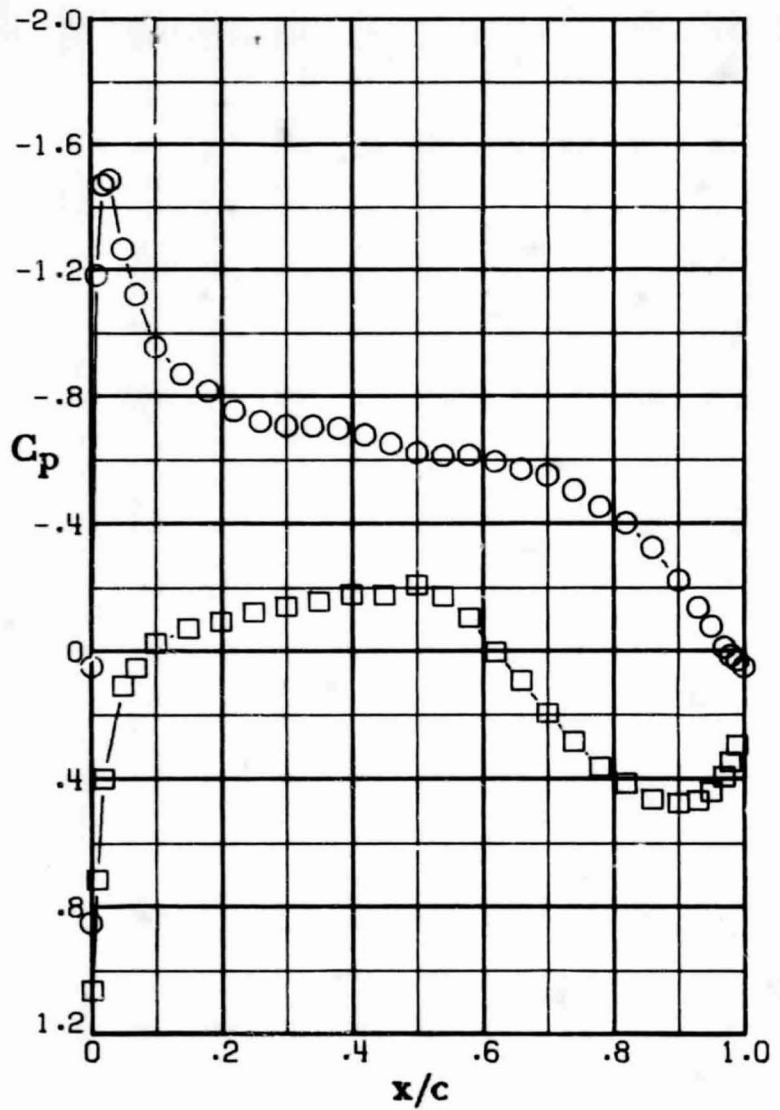
(c) $M = 0.50$; $c_n = 0.45$.



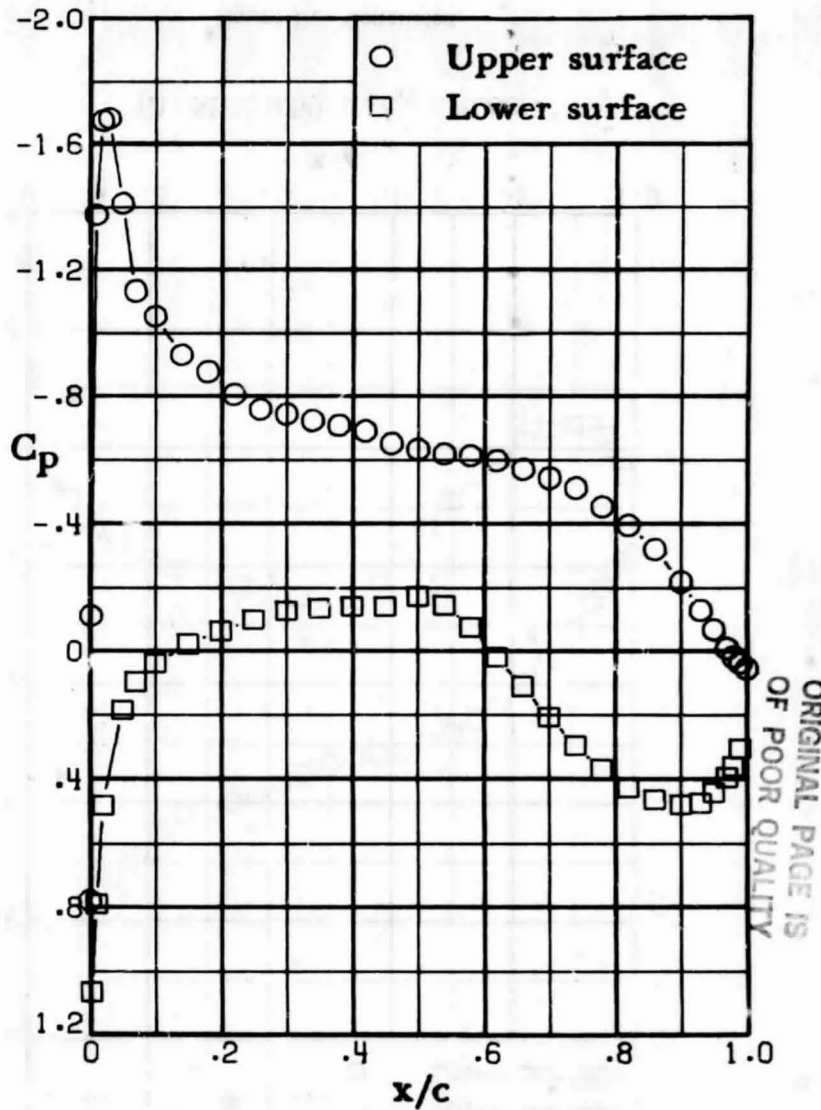
(d) $M = 0.50$; $c_n = 0.52$.

ORIGINAL PAGE IS
OF POOR
QUALITY

Figure II. - Continued.



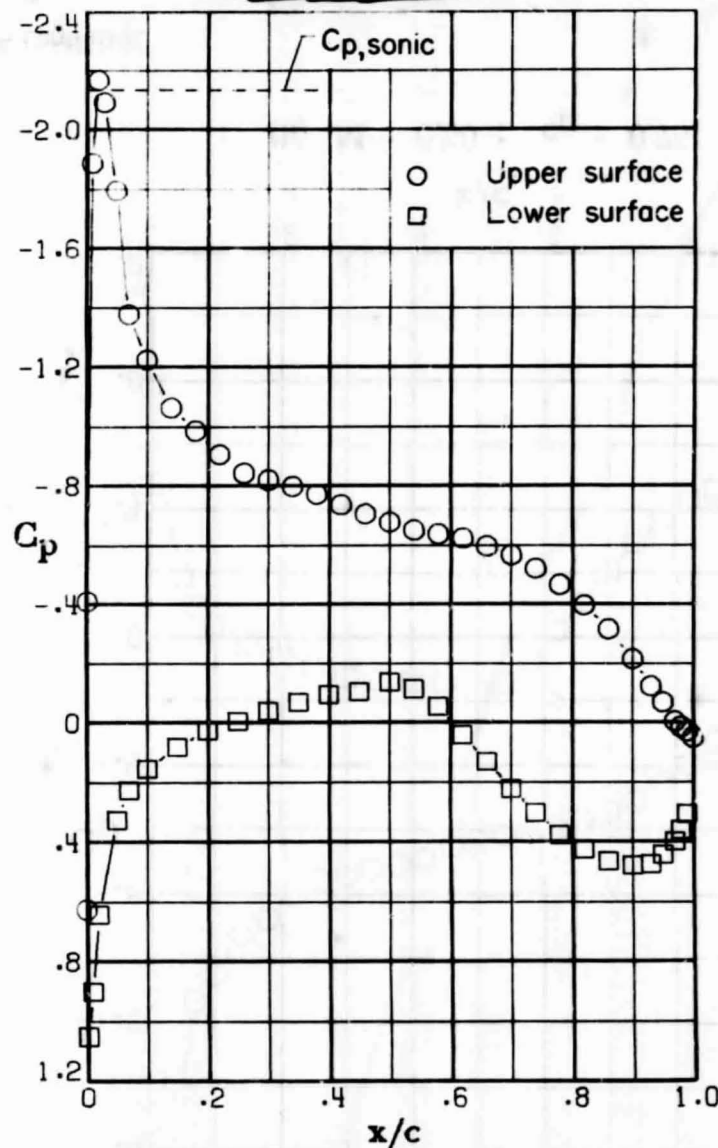
(g) $M = 0.50$; $c_n = 0.70$.



(h) $M = 0.50$; $c_n = 0.75$.

Figure II. - Continued.

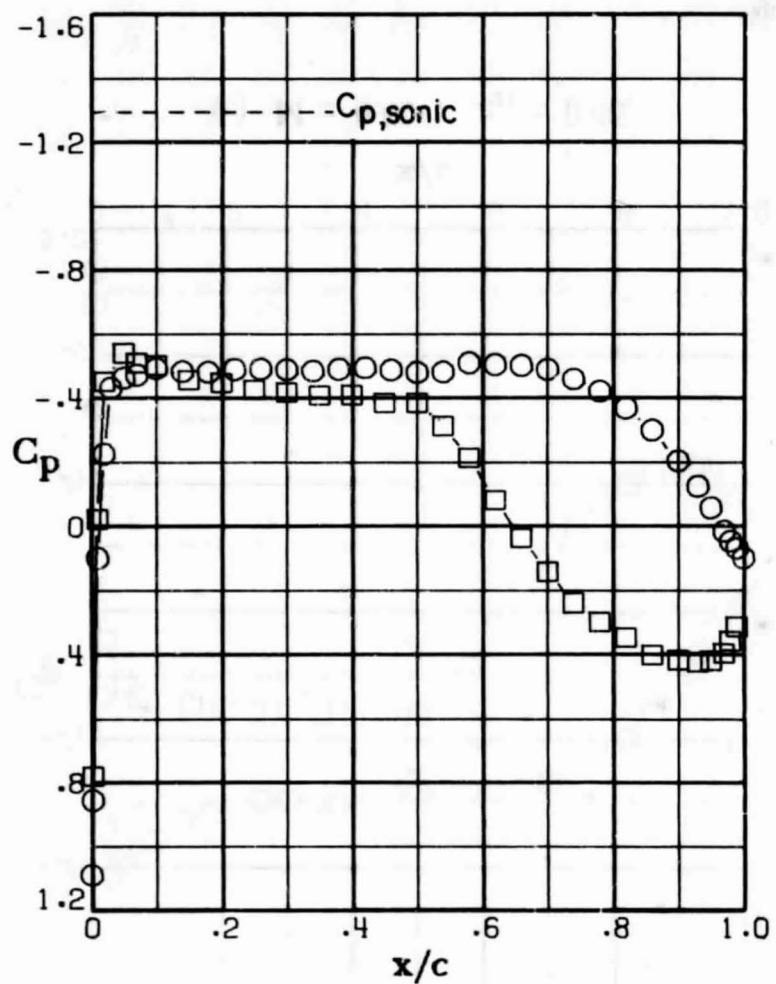
ORIGINAL PAGE IS
OF POOR QUALITY



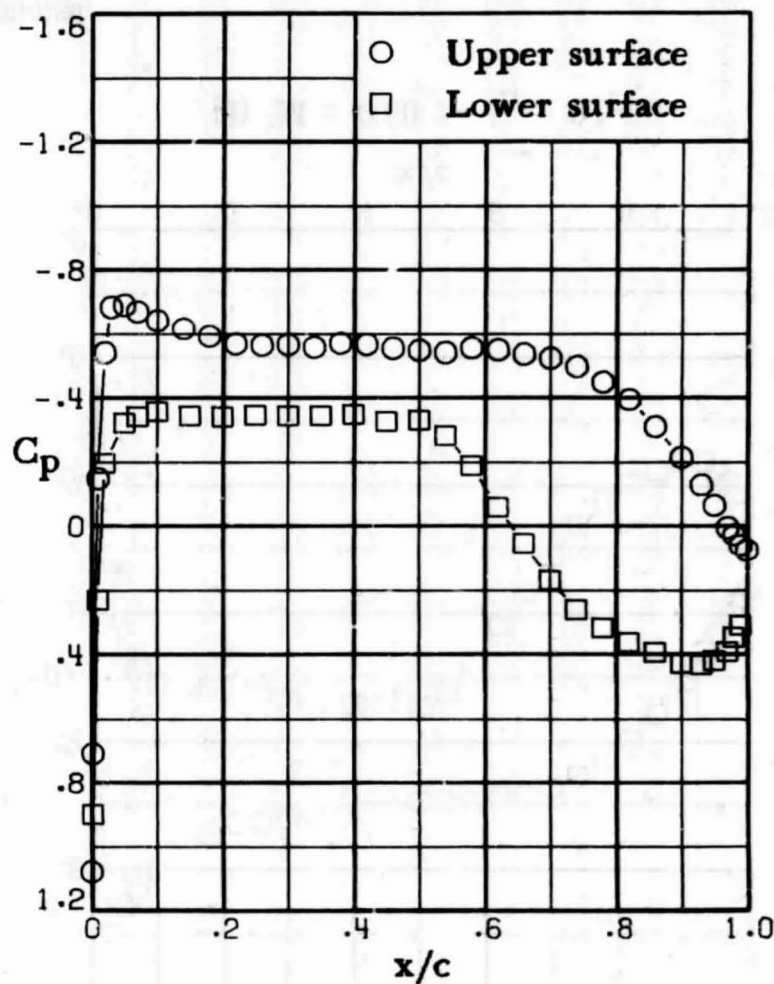
(i) $M = 0.50$: $c_T = 0.88$.

Figure II. - Concluded.

ORIGINAL PAGE IS
OF POOR QUALITY



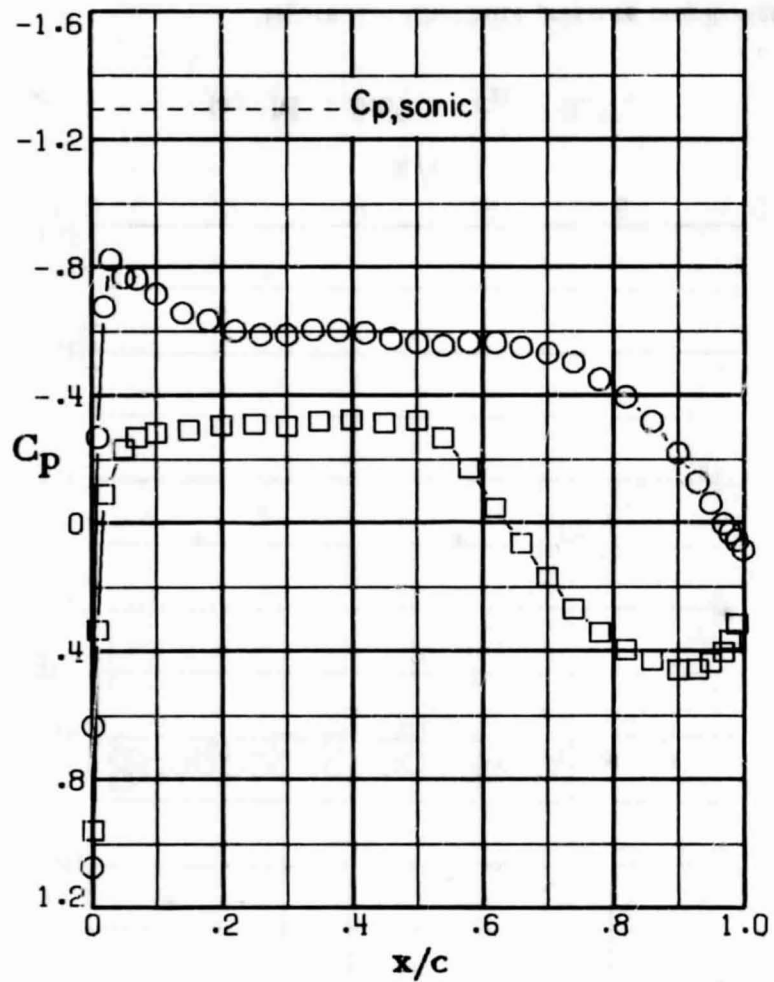
(a) $M = 0.60$; $c_n = 0.27$.



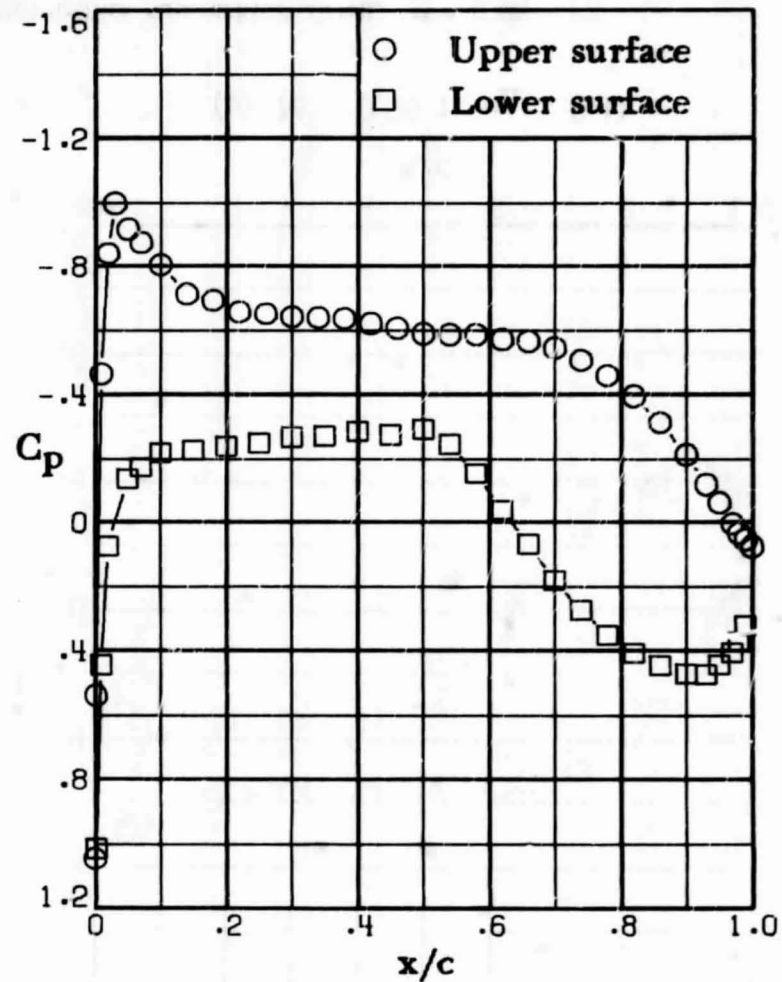
(b) $M = 0.60$; $c_n = 0.41$.

Figure I2. - Chordwise pressure distributions for 14-percent-thick supercritical airfoil. $M = 0.60$.

ORIGINAL PAGE IS
OF POOR QUALITY

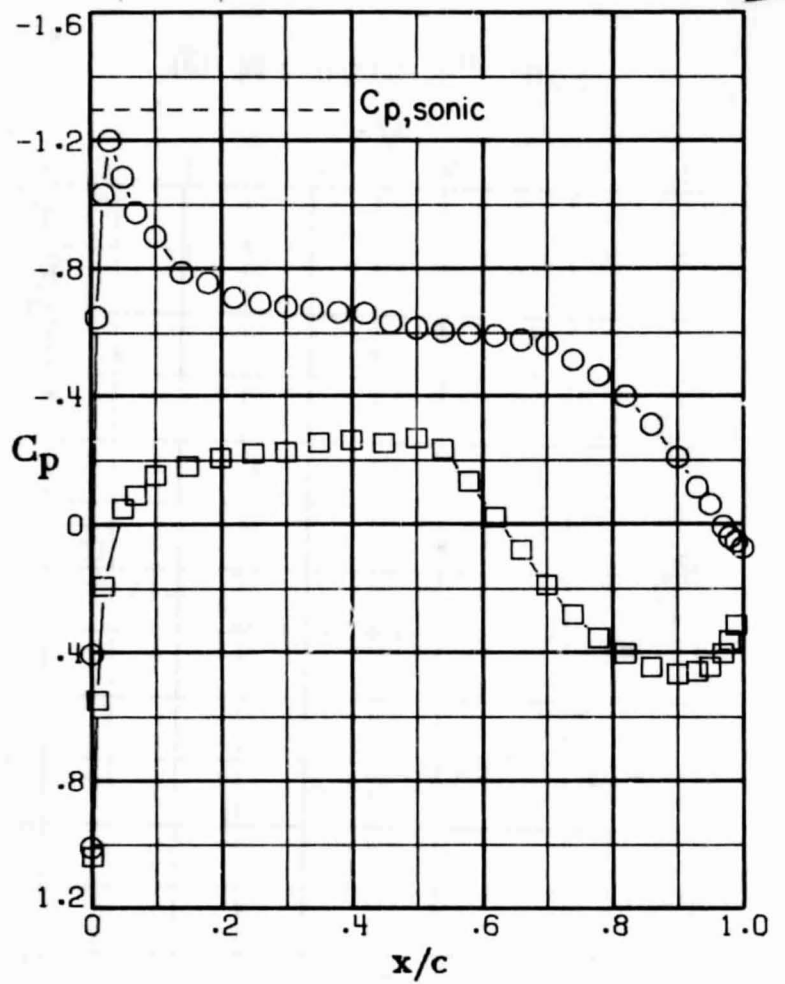


(c) $M = 0.60$: $c_n = 0.46$.

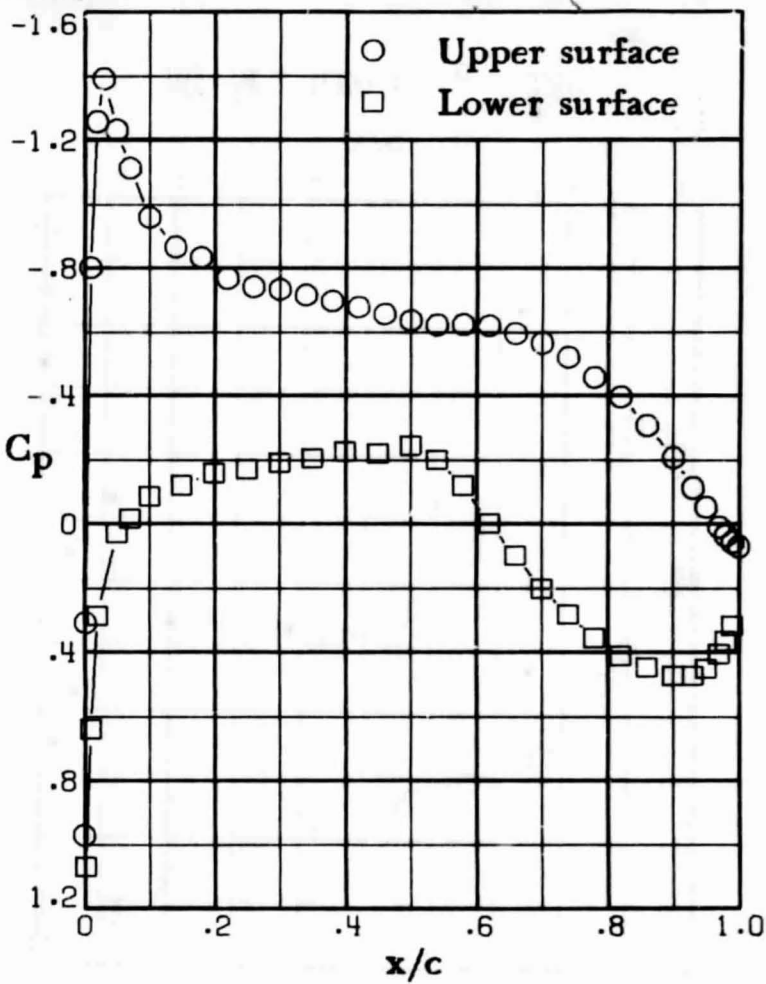


(d) $M = 0.60$: $c_n = 0.54$.

Figure 12.- Continued.



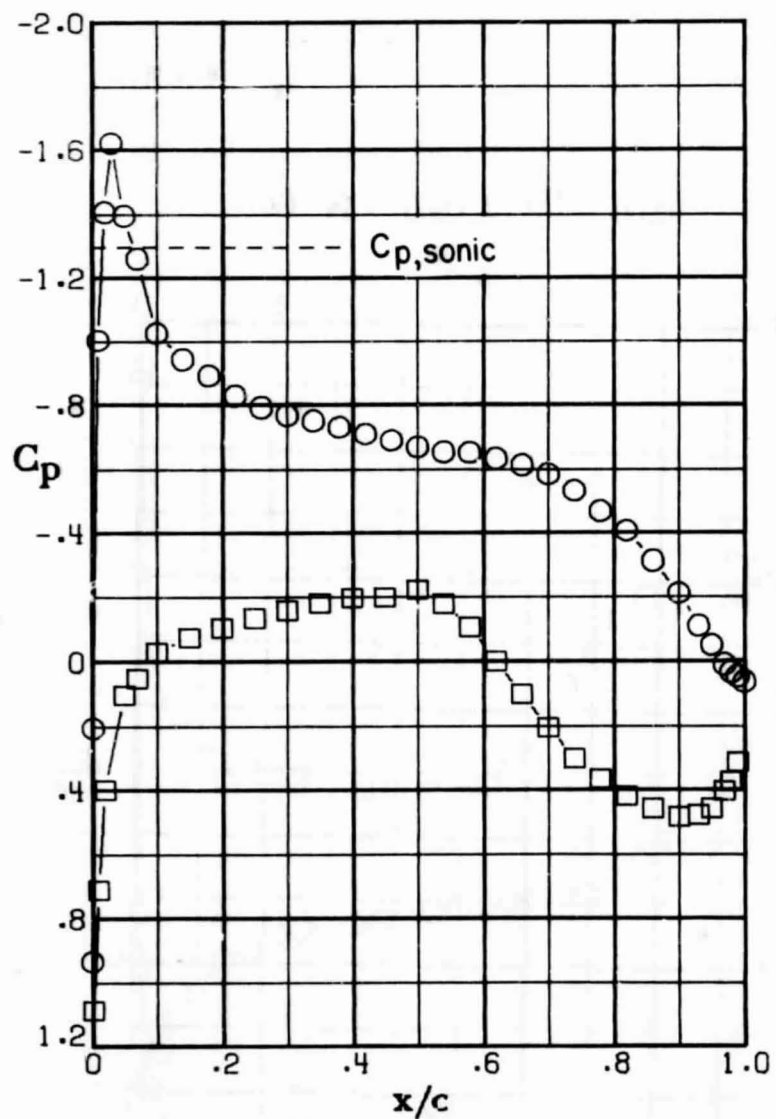
(e) $M = 0.60$; $c_n = 0.60$.



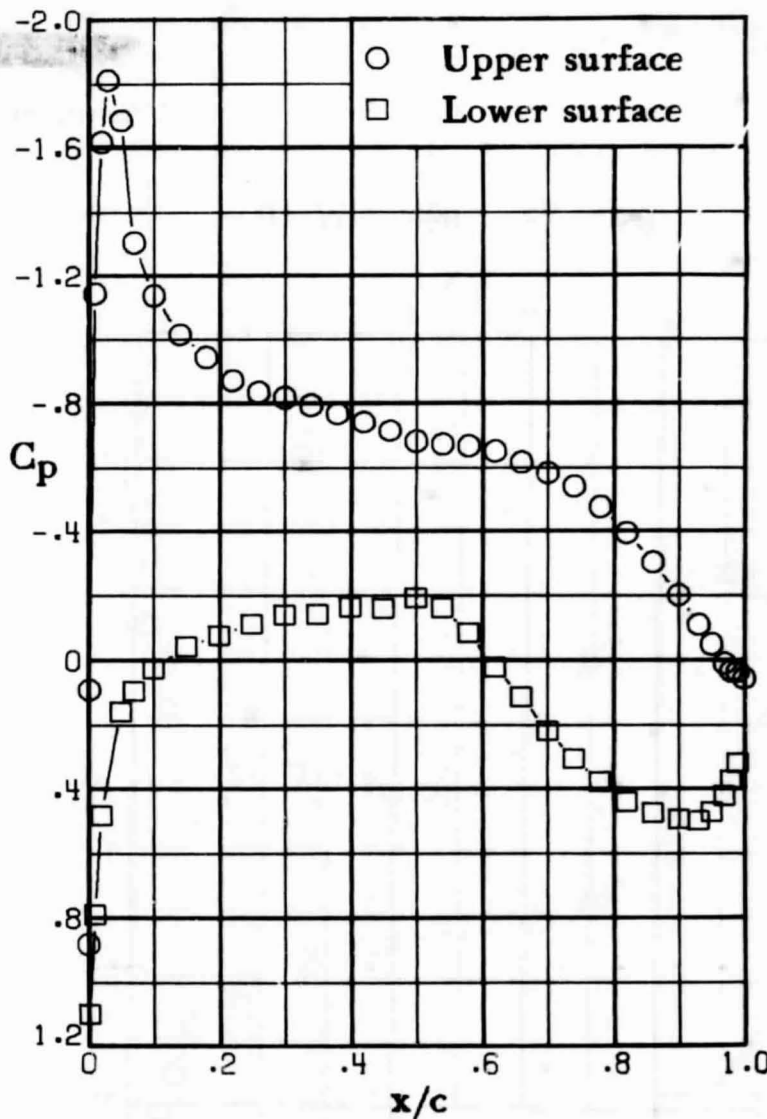
(f) $M = 0.60$; $c_n = 0.67$.

Figure I2.- Continued.

SHEET 8



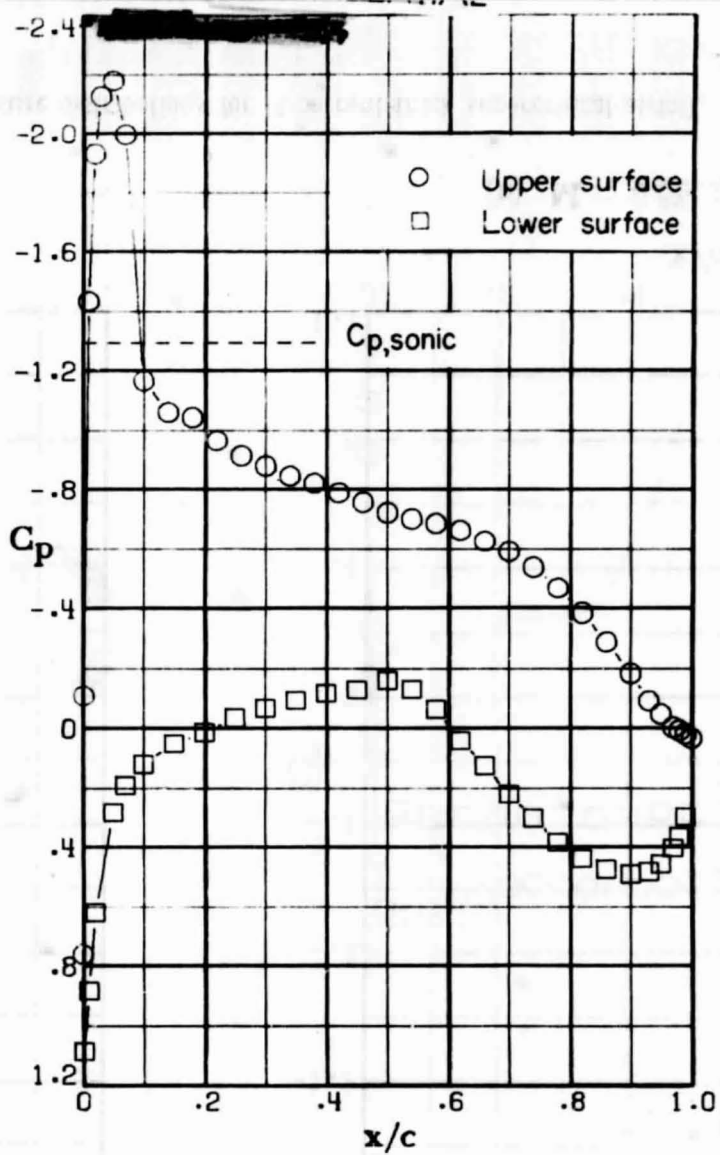
(g) $M = 0.60$; $c_n = 0.73$.



(h) $M = 0.60$; $c_n = 0.80$.

ORIGINAL PAGE IS
OF POOR
QUALITY

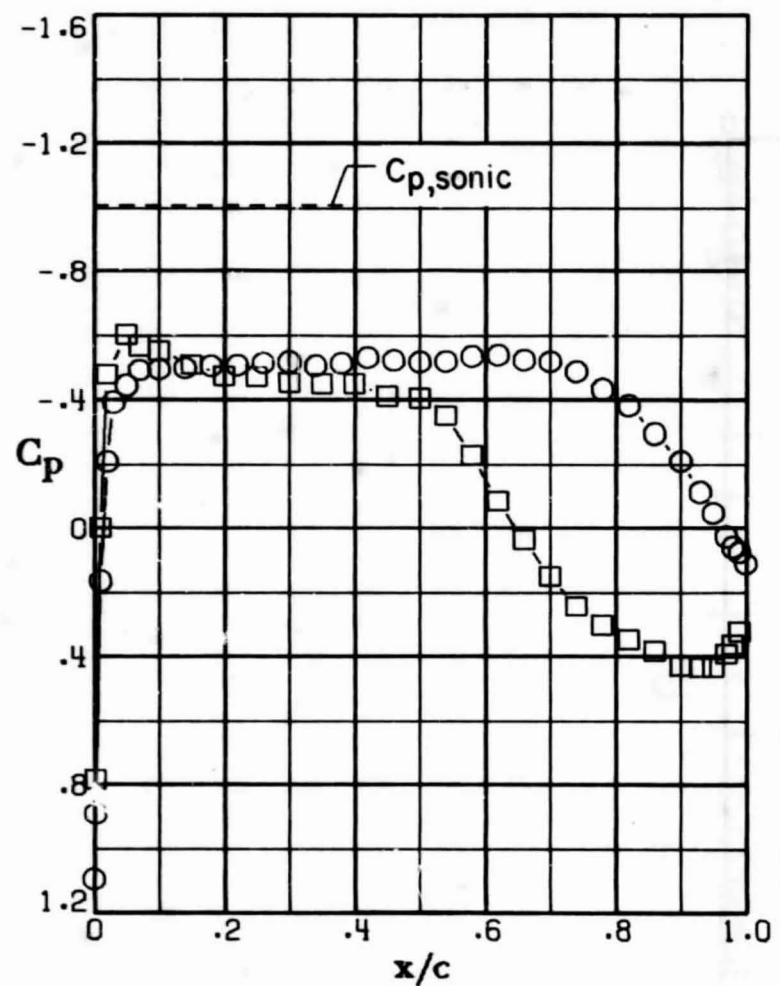
ORIGINAL PAGE IS
OF POOR QUALITY



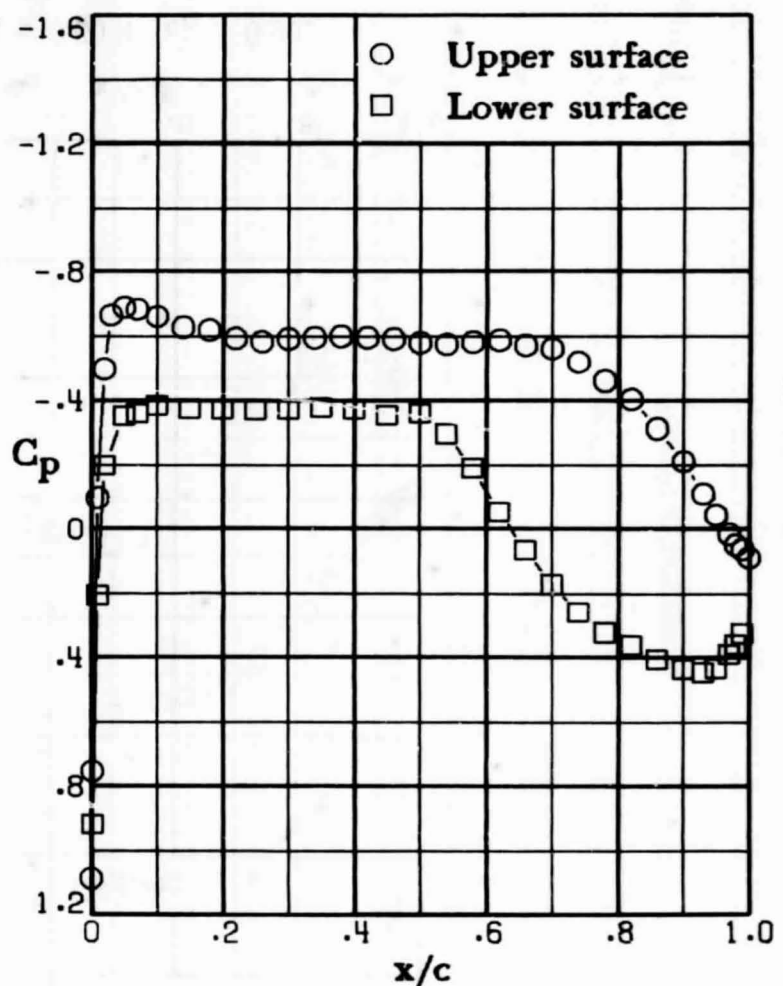
(i) $M = 0.60$; $c_n = 0.90$.

Figure 12.- Concluded.

ORIGINAL PAGE IS
OF POOR QUALITY

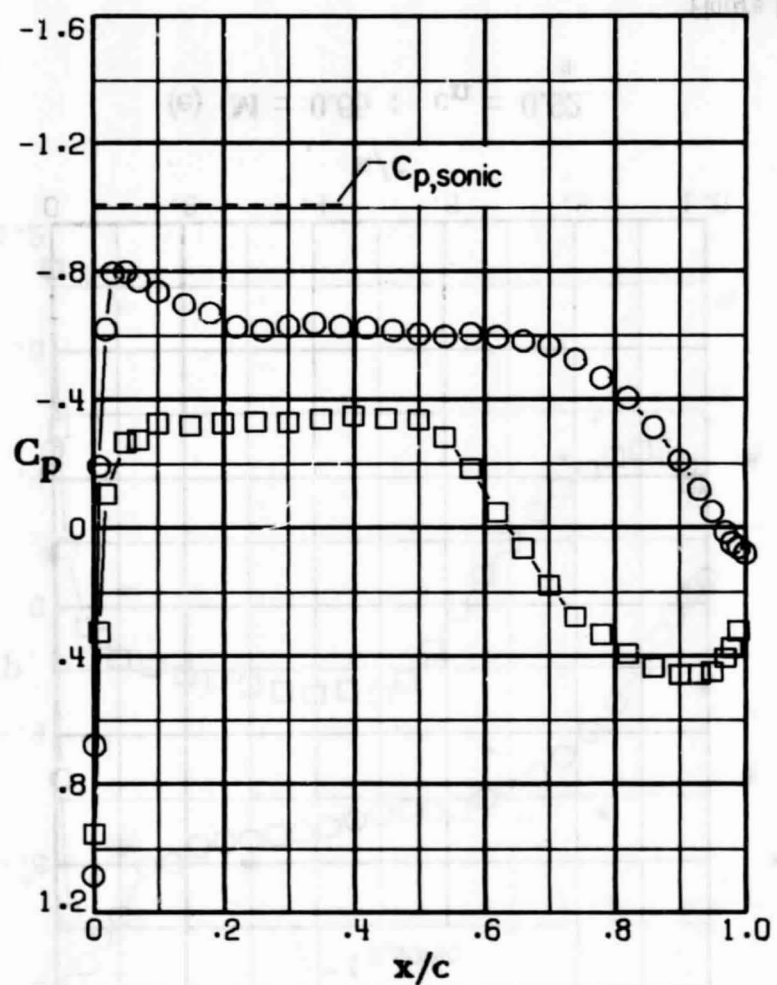


(a) $M = 0.65$; $c_n = 0.27$.

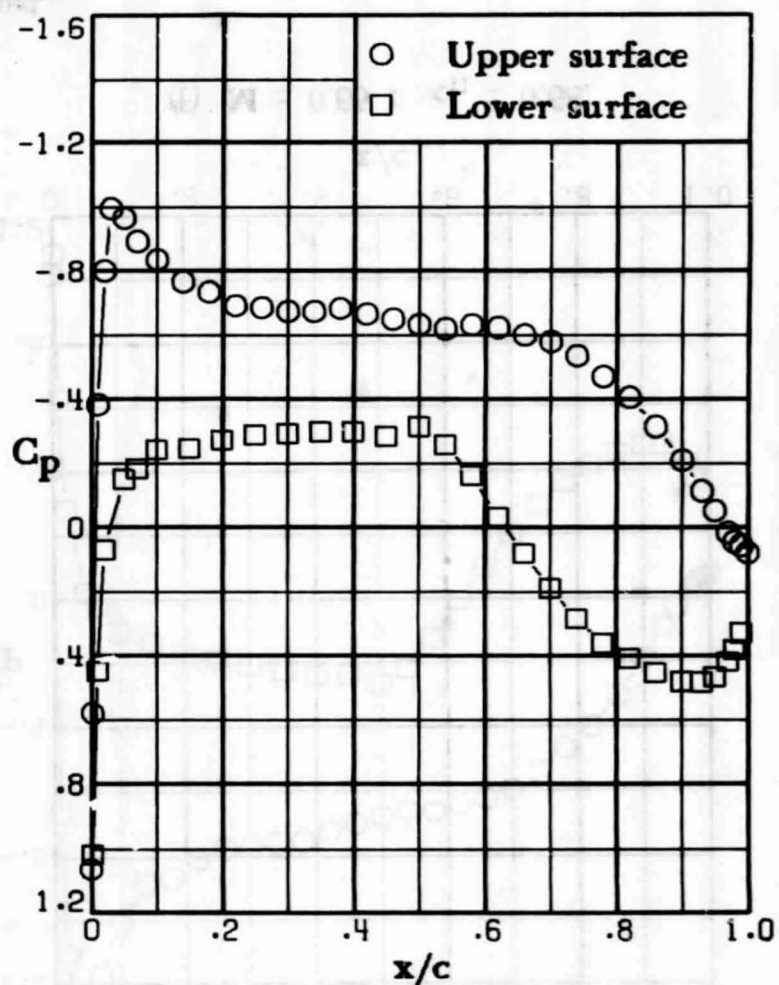


(b) $M = 0.65$; $c_n = 0.41$.

Figure I3.- Chordwise pressure distributions for 14-percent-thick supercritical airfoil. $M = 0.65$.



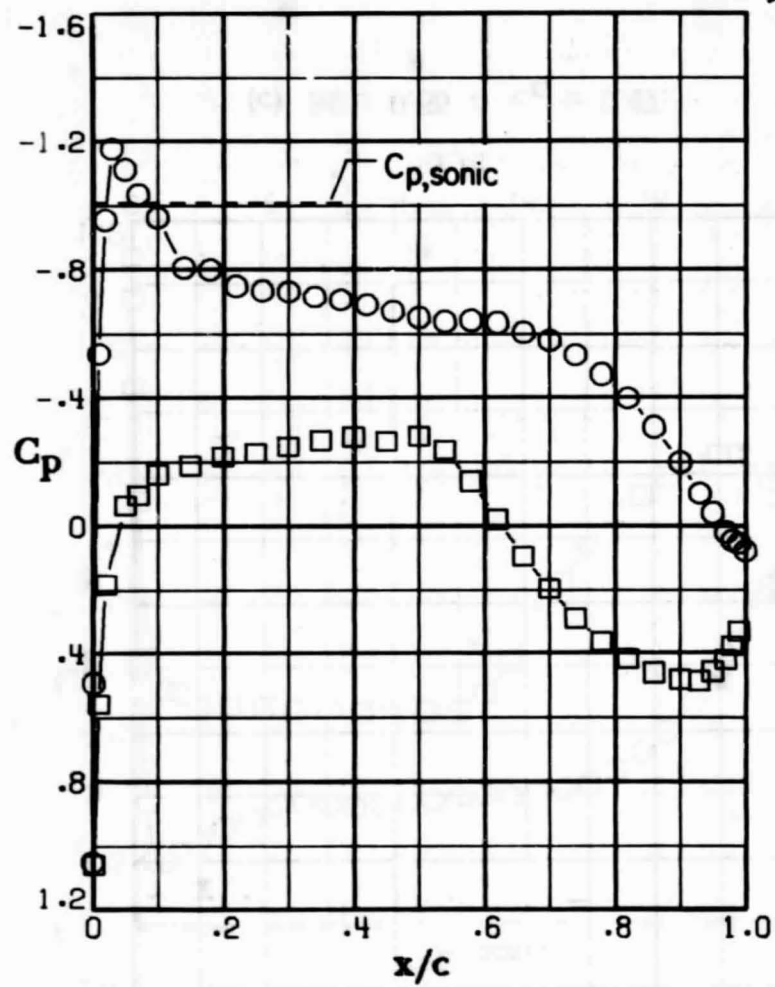
$$(c) M = 0.65 ; c_n = 0.47.$$



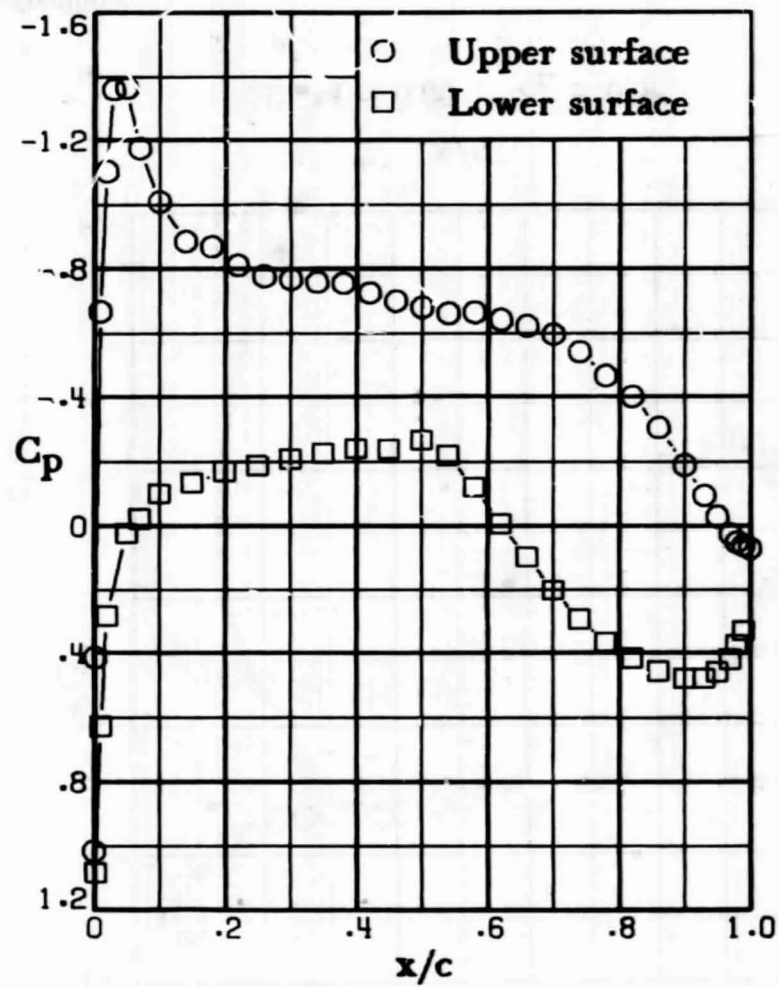
$$(d) M = 0.65 ; c_n = 0.56.$$

Figure 13. - Continued.

ORIGINAL PAGE IS
OF POOR QUALITY

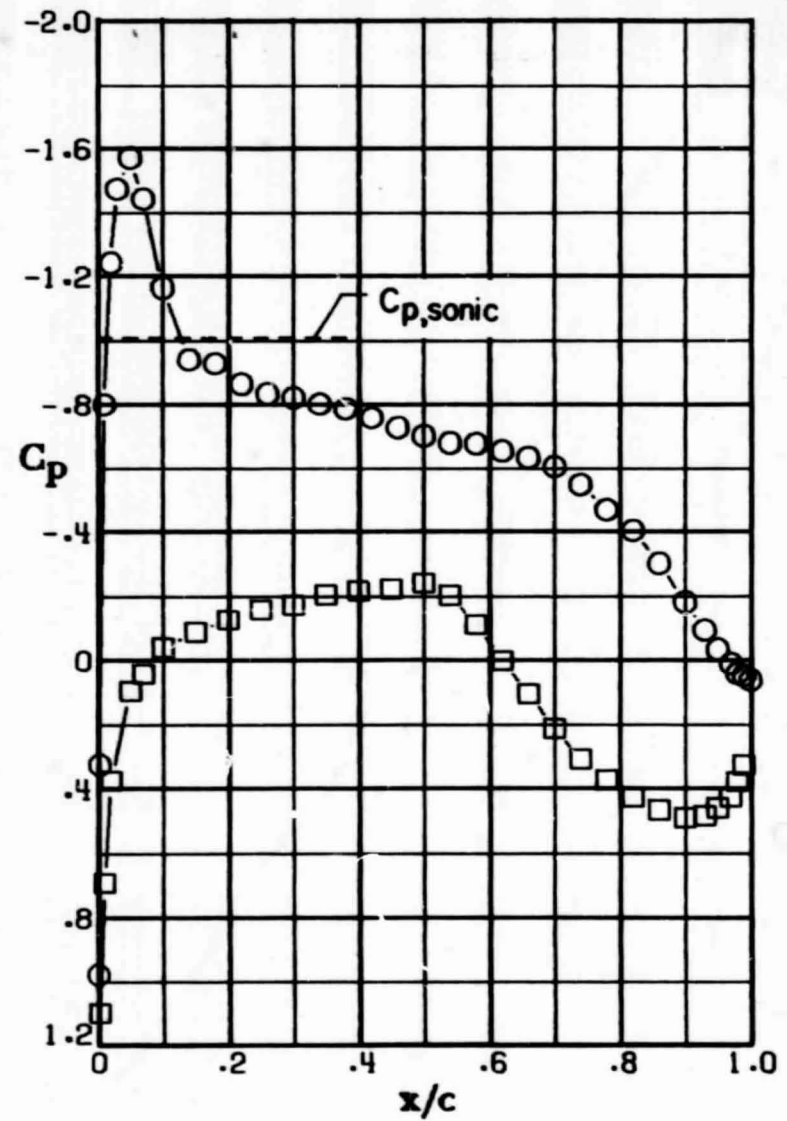


(e) $M = 0.65$; $c_n = 0.62$.

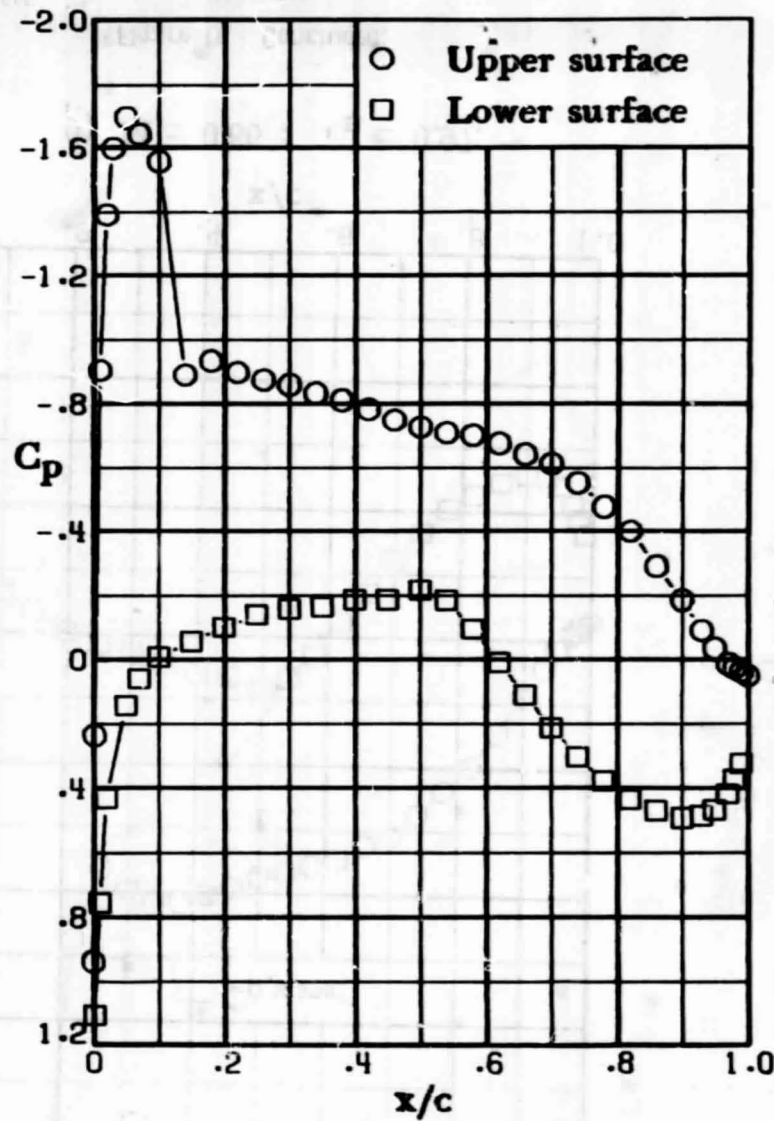


(f) $M = 0.65$; $c_n = 0.68$.

Figure 13. - Continued.



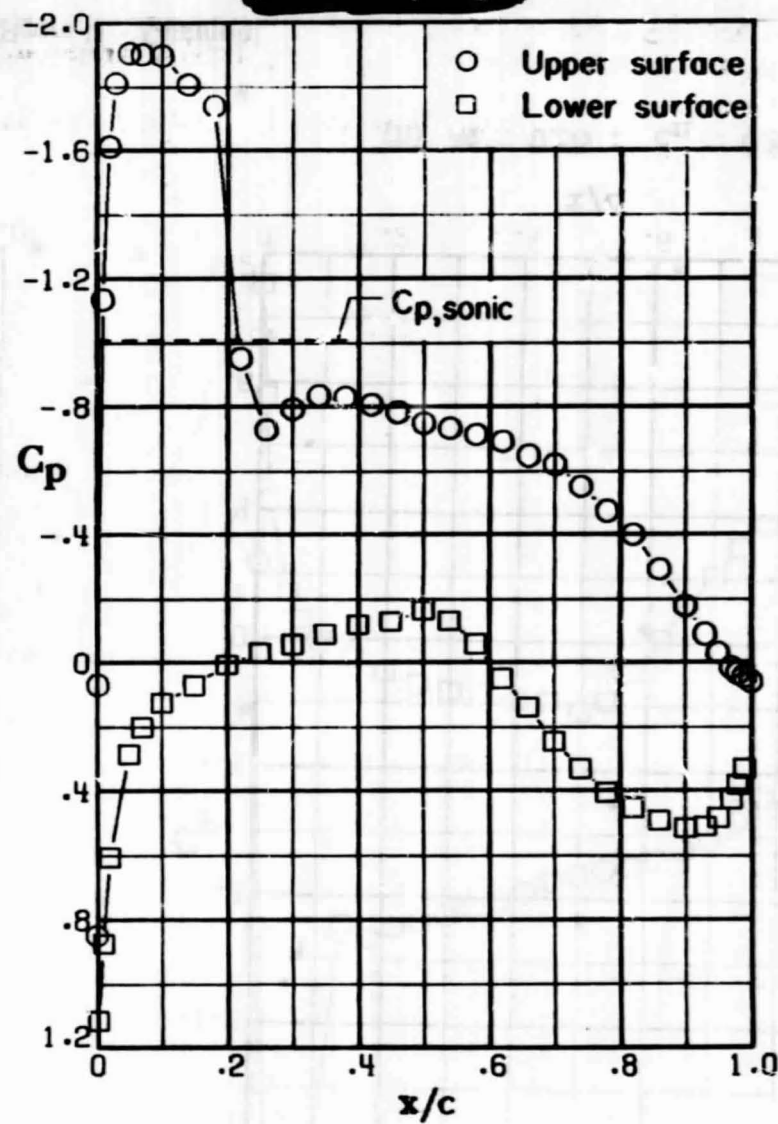
(g) $M = 0.65 : c_n = 0.75.$



(h) $M = 0.65 : c_n = 0.81.$

Figure I3. - Continued.

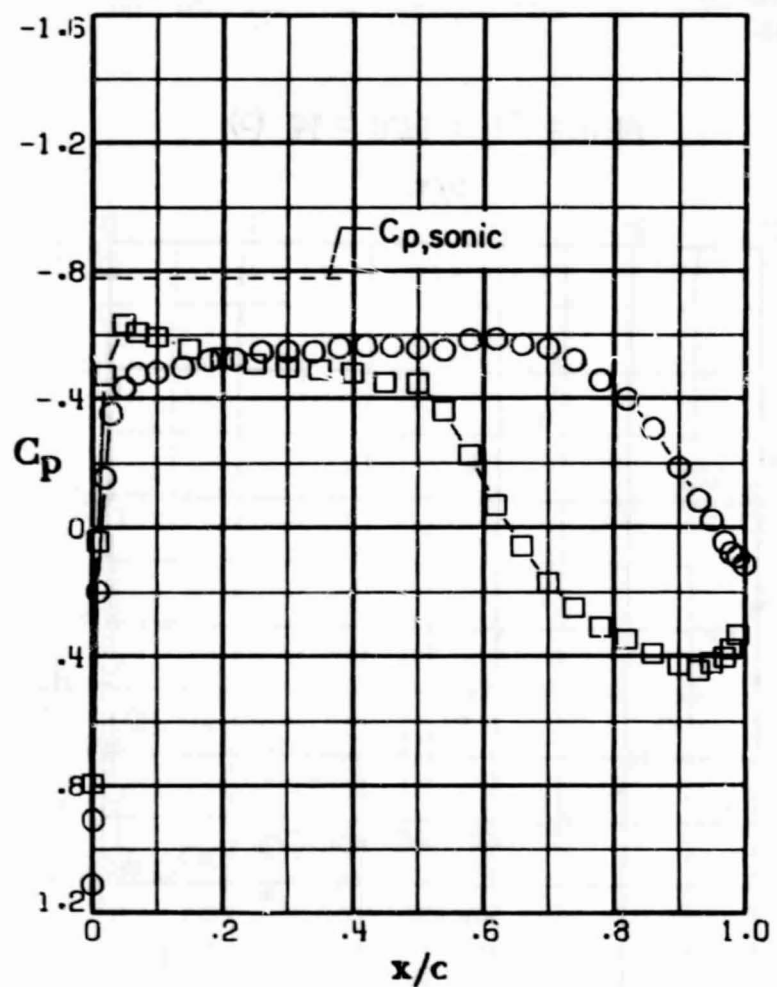
ORIGINAL PAGE IS
OF POOR QUALITY



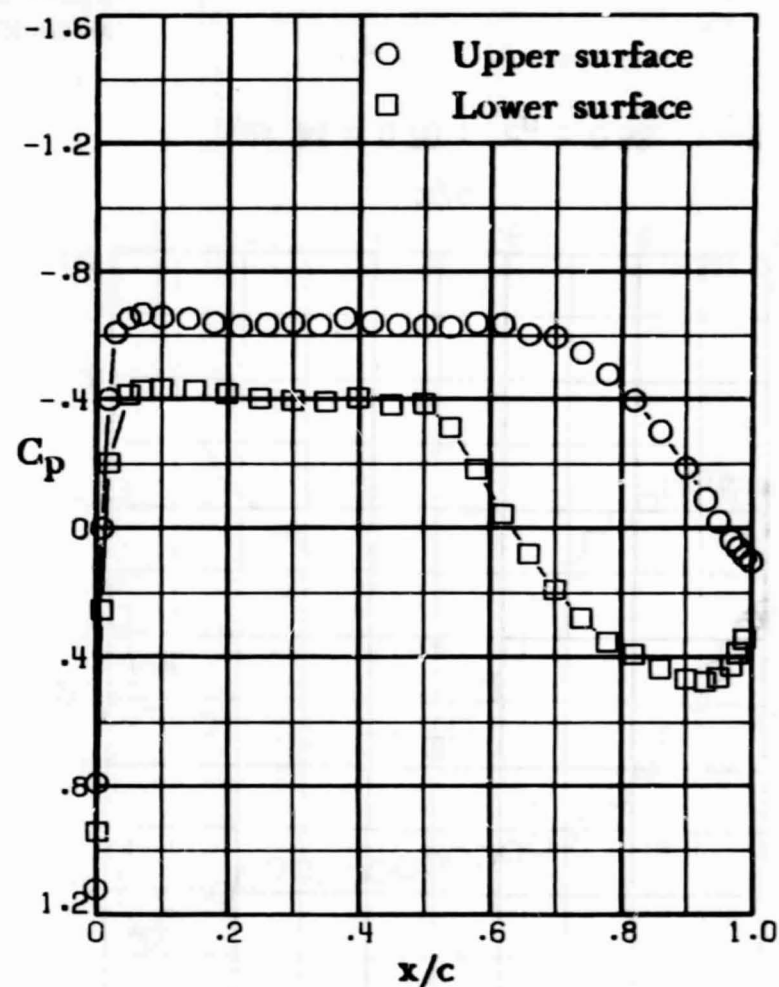
(i) $M = 0.65$: $c_n = 0.97$.

Figure I3. - Concluded.

ORIGINAL PAGE IS
OF POOR QUALITY

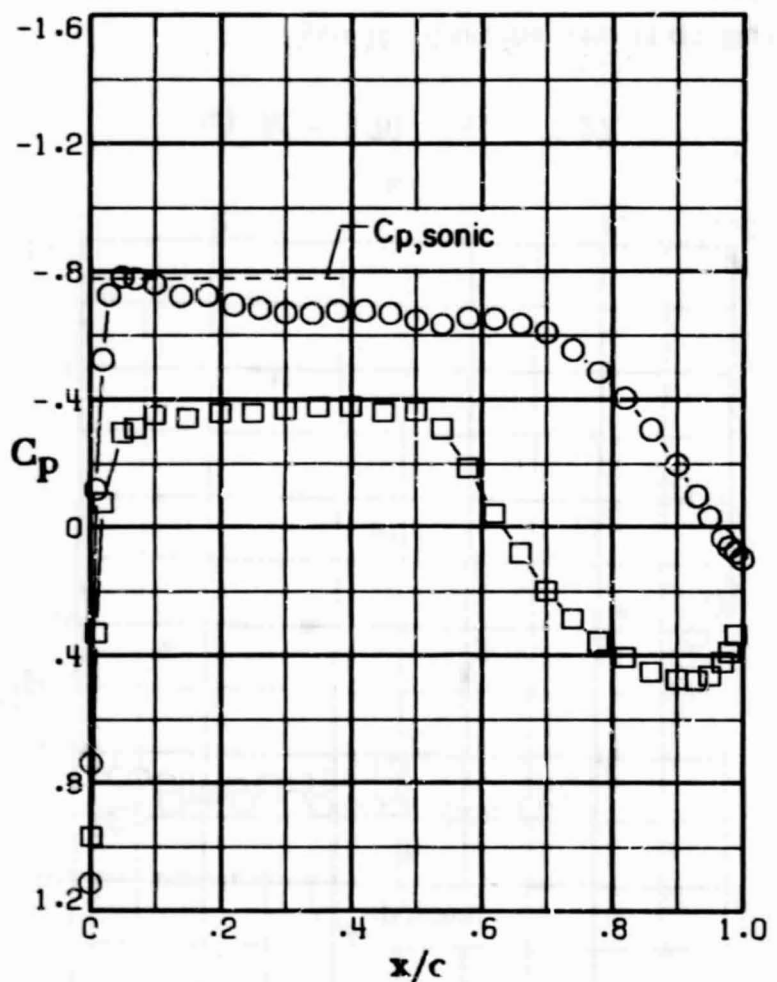


(a) $M = 0.70$; $c_n = 0.27$.

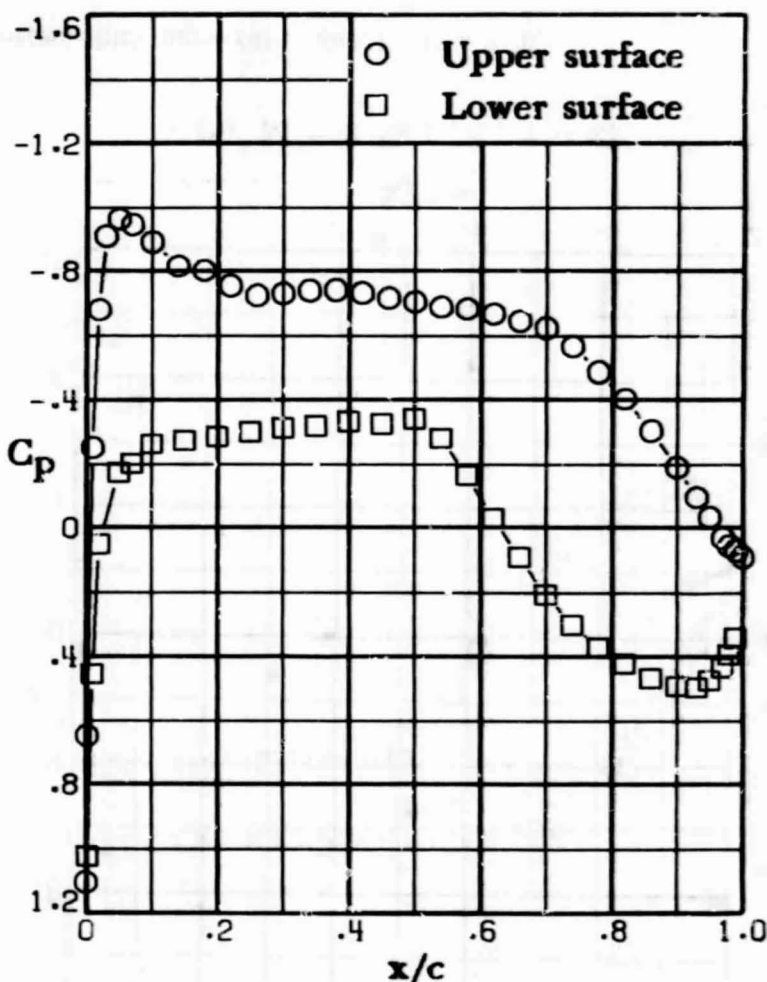


(b) $M = 0.70$; $c_n = 0.42$.

Figure 14. - Chordwise pressure distributions for 14-percent-thick supercritical airfoil. $M = 0.70$.



(c) $M = 0.70$; $c_n = 0.49$.



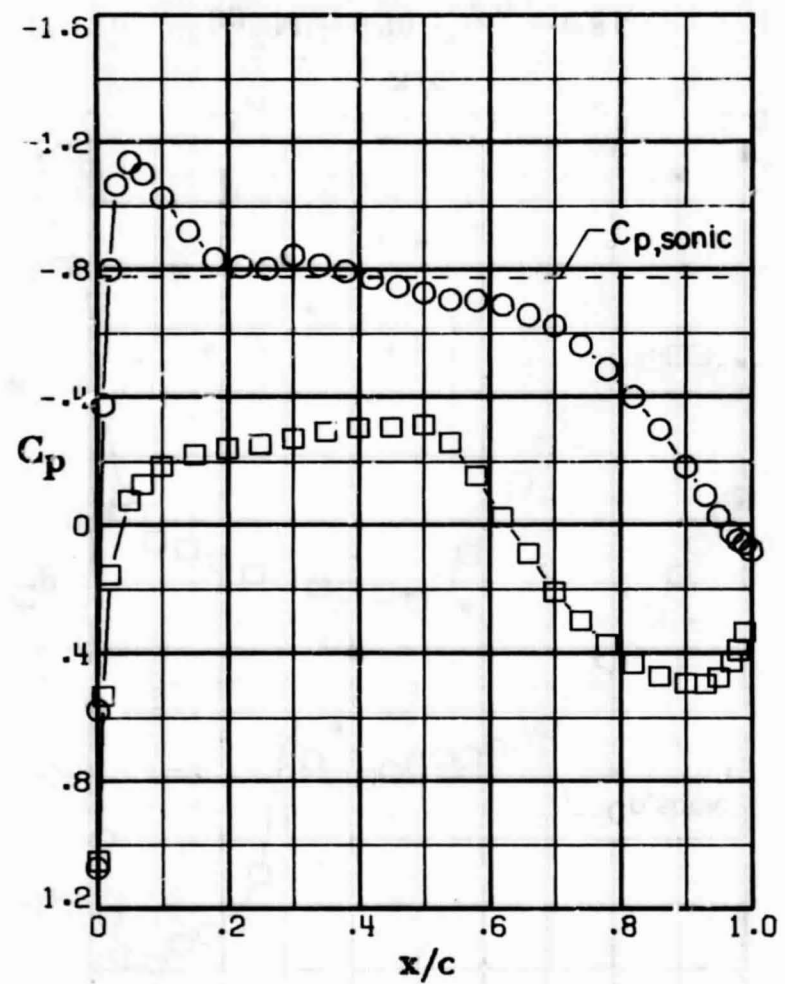
(d) $M = 0.70$; $c_n = 0.58$.

Figure 14. - Continued.

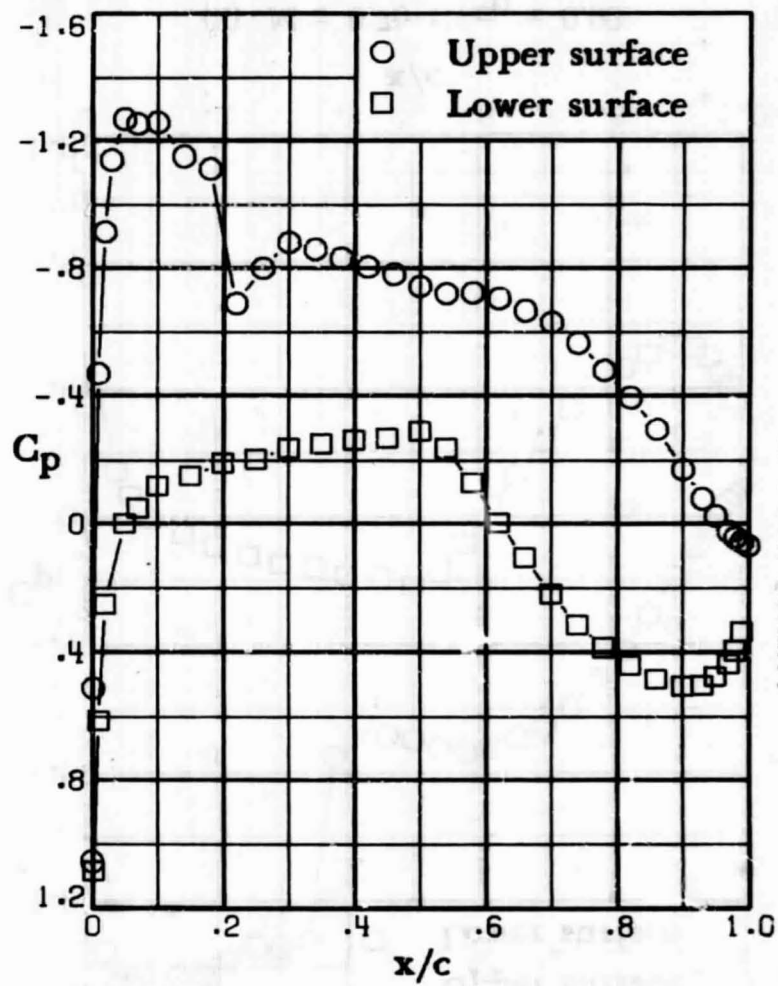
SHEET17

ORIGINAL PAGE IS
OF POOR QUALITY

ORIGINAL PAGE IS
OF POOR QUALITY



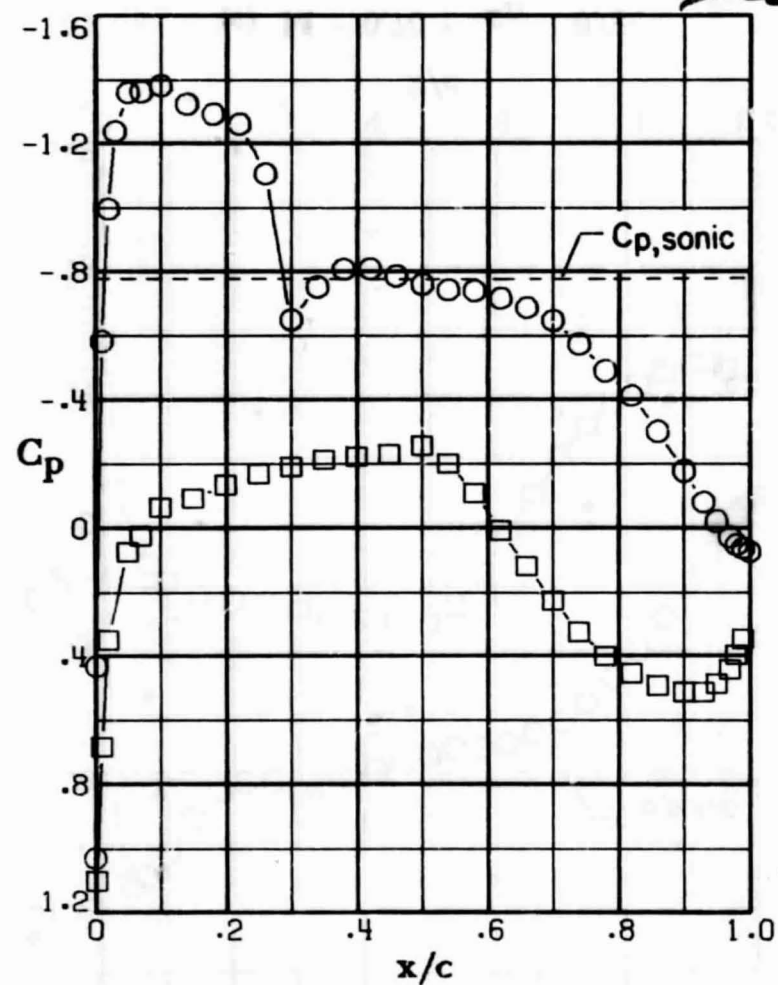
(e) $M = 0.70$; $c_n = 0.65$.



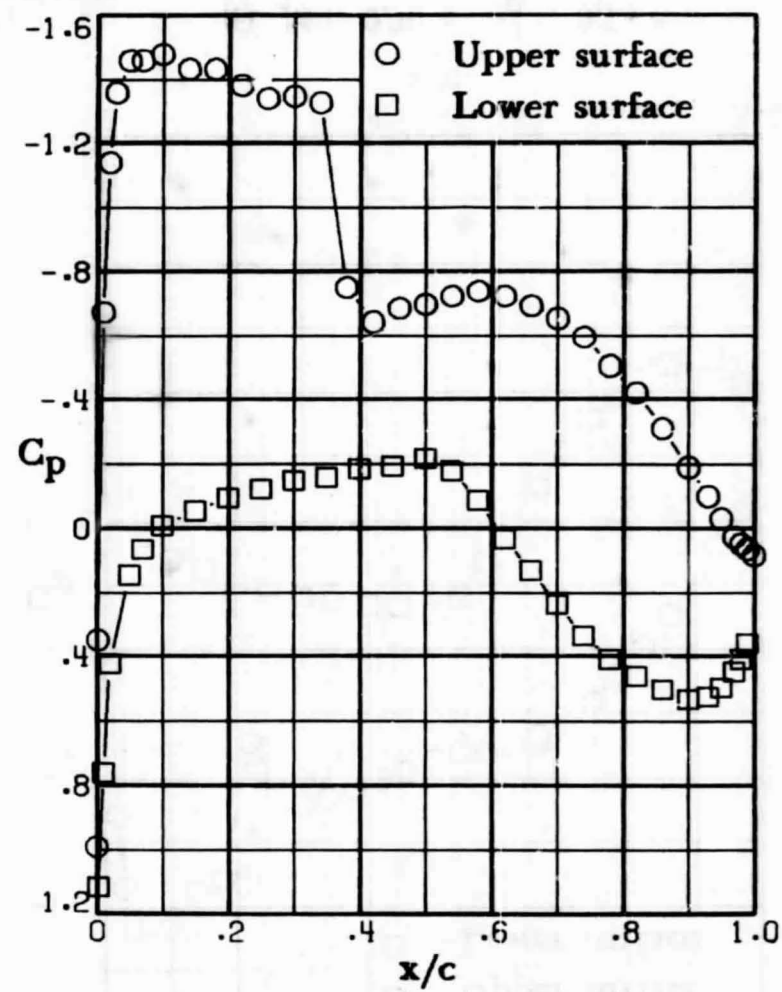
(f) $M = 0.70$; $c_n = 0.73$.

Figure 14. - Continued.

ORIGINAL PAGE IS
OF POOR QUALITY



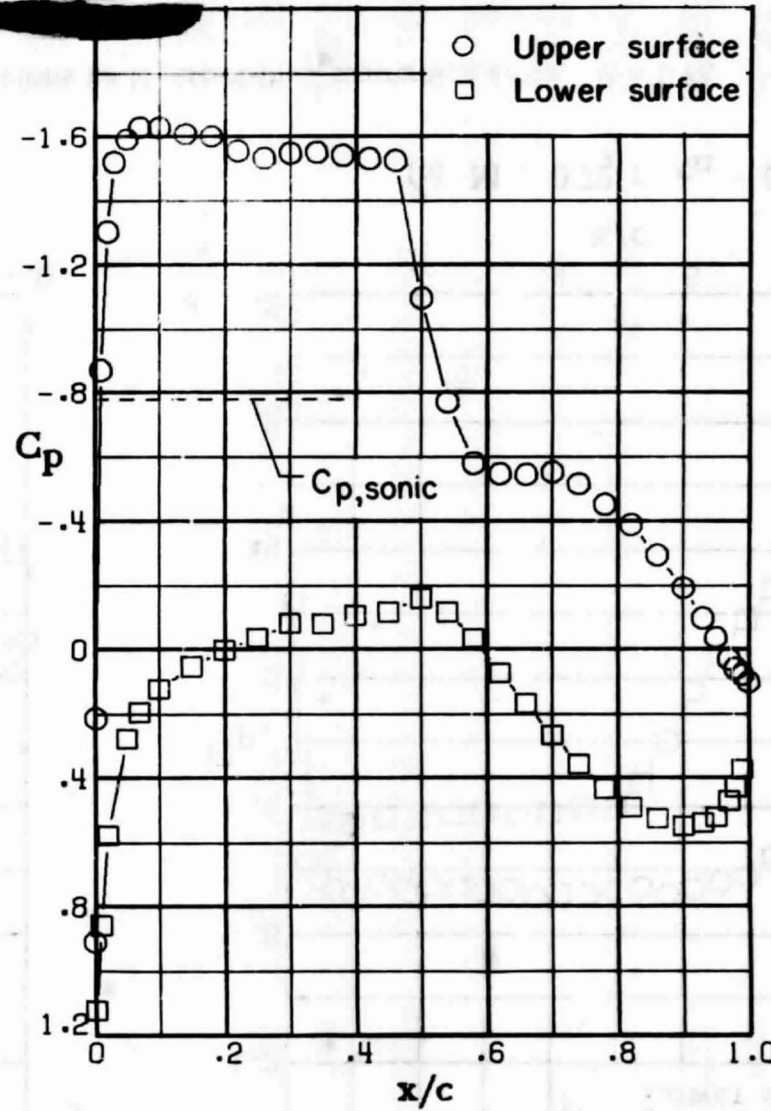
(g) $M = 0.70$: $c_n = 0.81$.



(h) $M = 0.70$: $c_n = 0.92$.

Figure 14.- Continued.

אַתָּה תִּשְׁמַע אֱלֹהִים

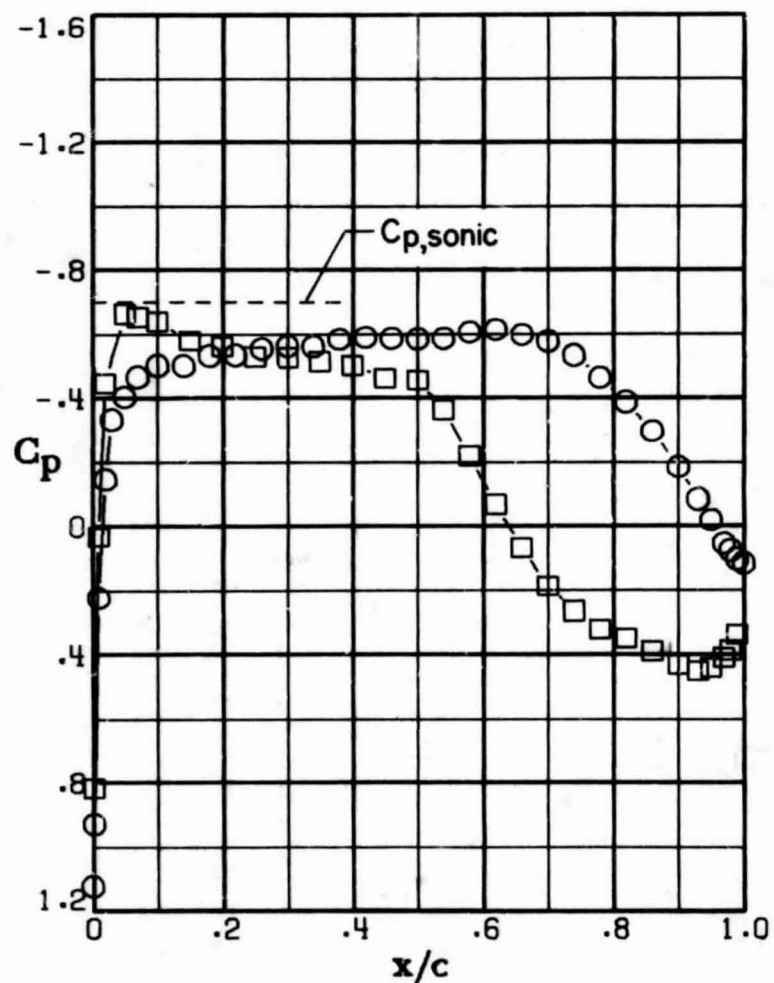


$$(i) \quad M = 0.70 ; \quad c_n = 1.13.$$

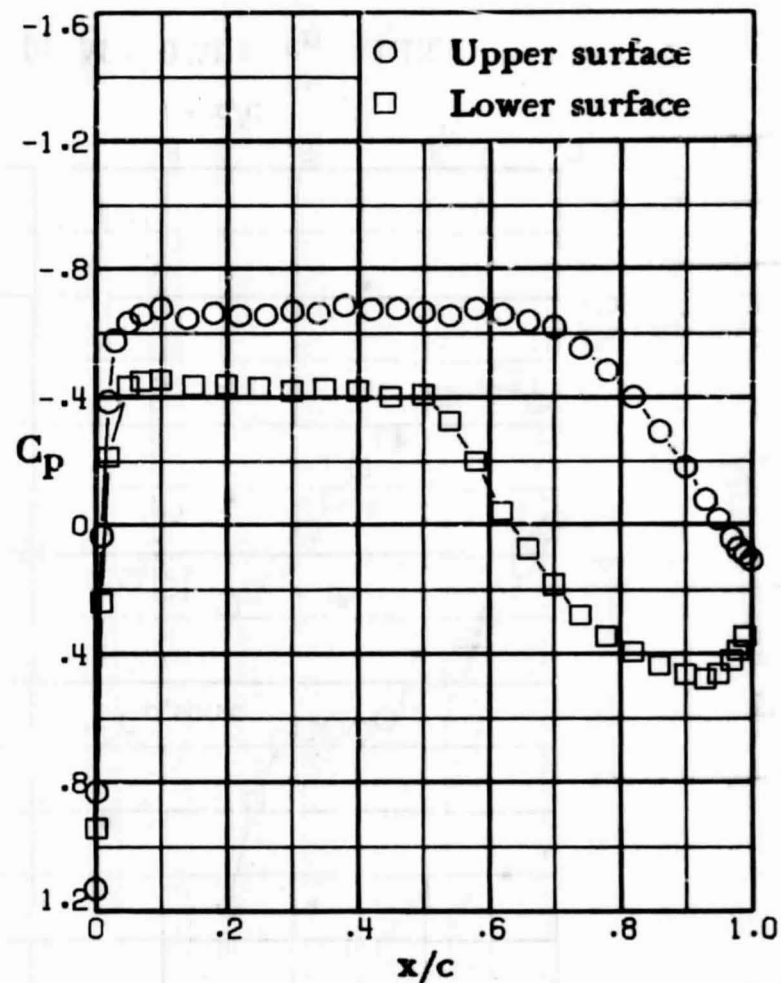
ORIGINAL PAGE IS
OF POOR QUALITY

Figure 14. - Concluded

ORIGINAL PAGE IS
OF POOR QUALITY

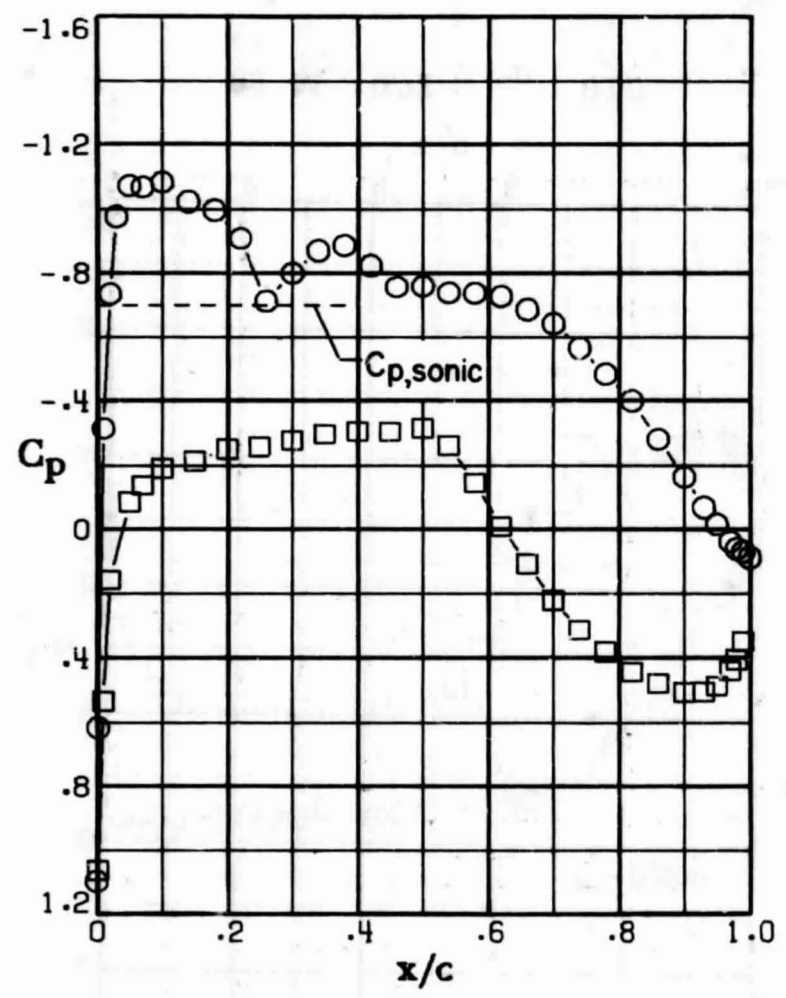


(a) $M = 0.72$; $c_n = 0.27$.

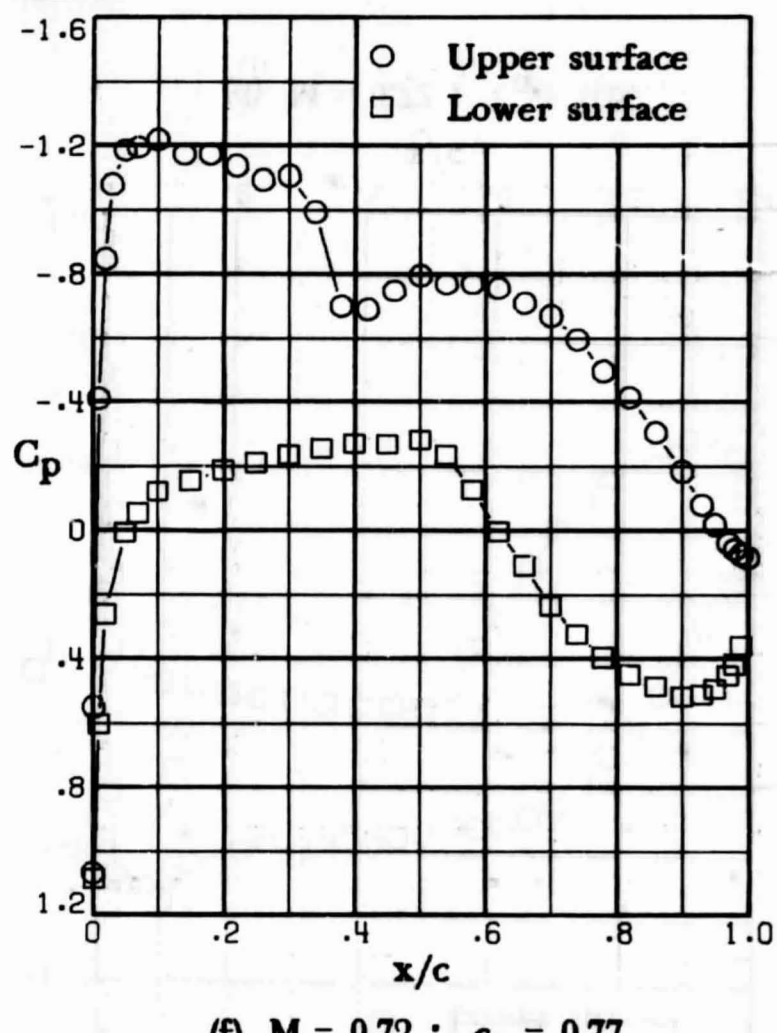


(b) $M = 0.72$; $c_n = 0.43$.

Figure 15. - Chordwise pressure distributions for 4-percent-thick supercritical airfoil. $M = 0.72$.

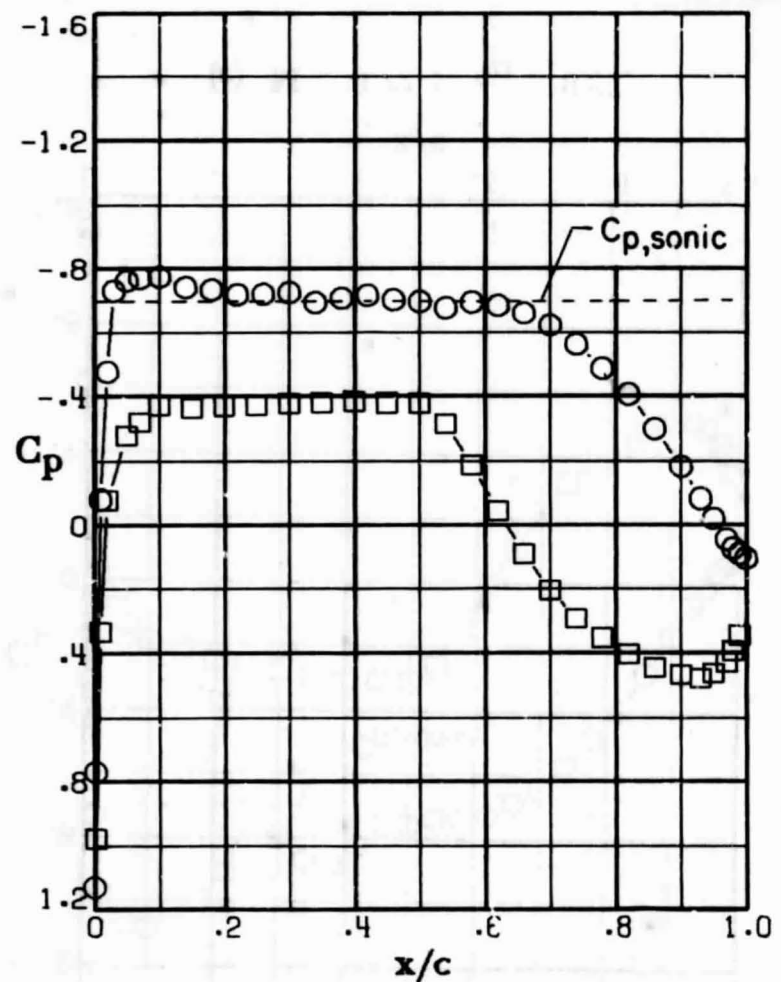


(e) $M = 0.72$; $c_n = 0.67$.

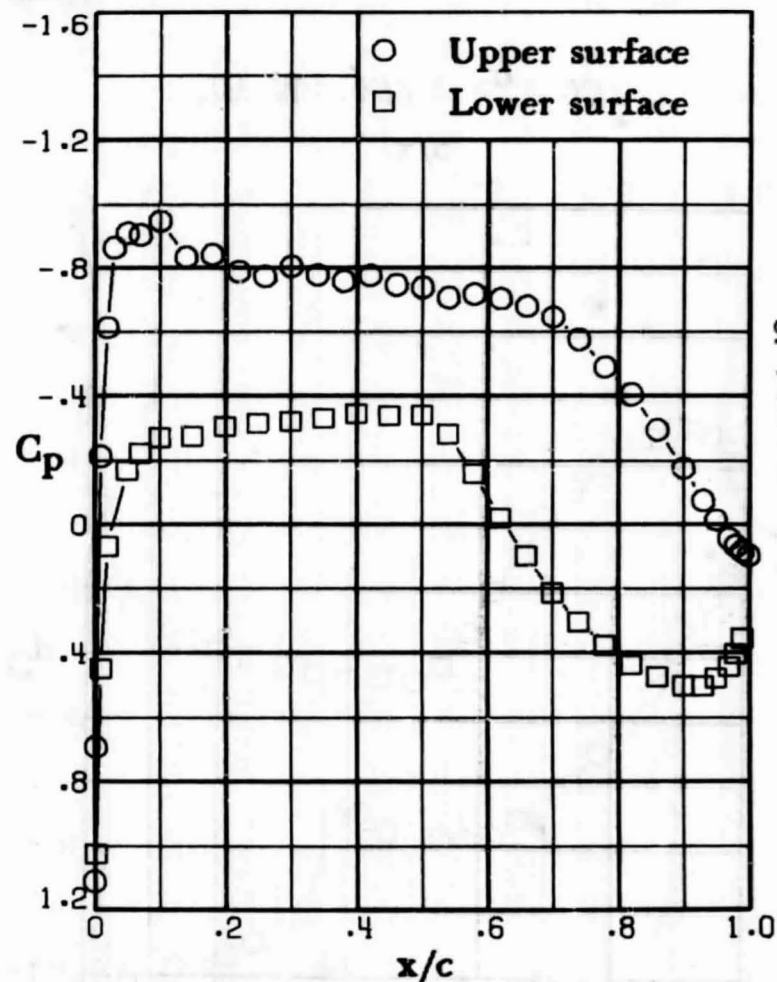


(f) $M = 0.72$; $c_n = 0.77$.

Figure 15.- Continued.

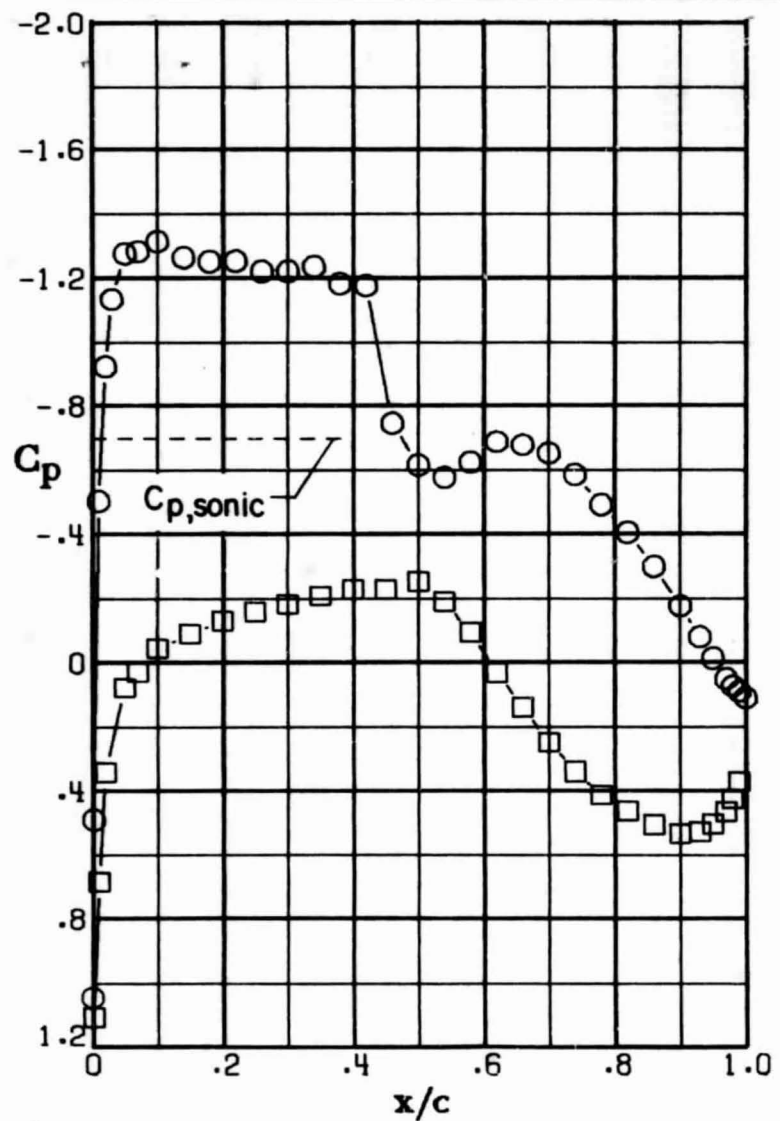


(c) $M = 0.72$; $c_n = 0.50$.

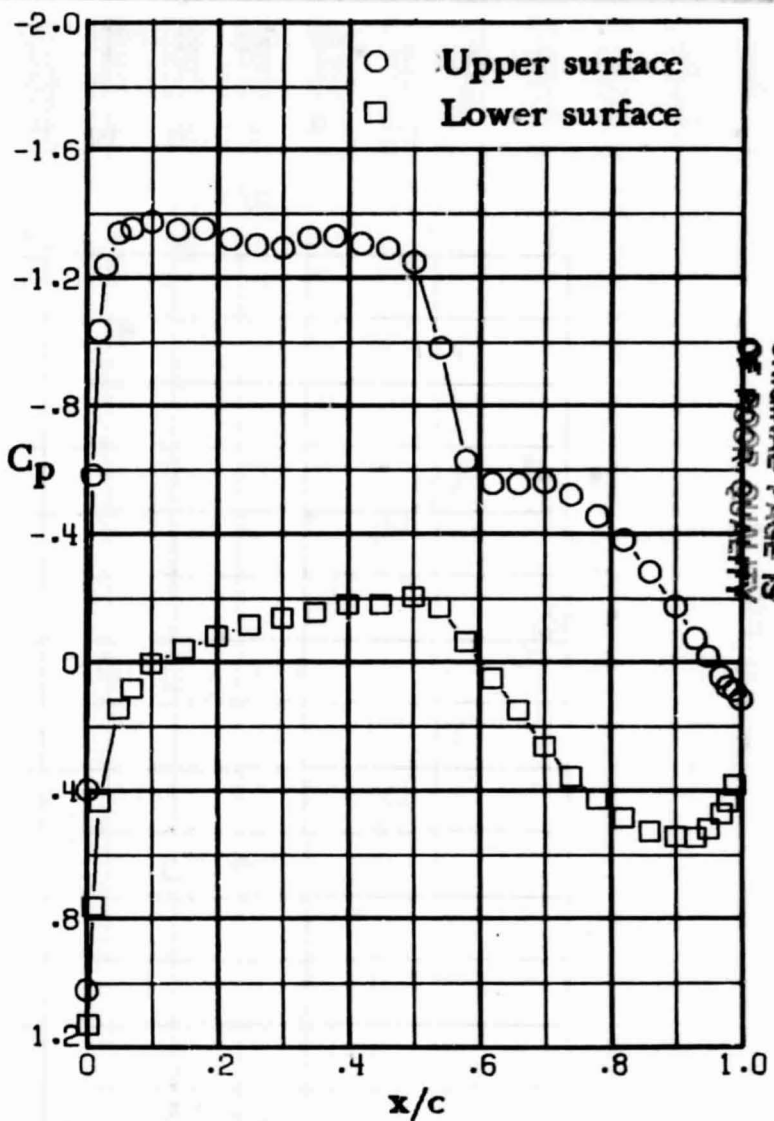


(d) $M = 0.72$; $c_n = 0.60$.

Figure 15.- Continued.



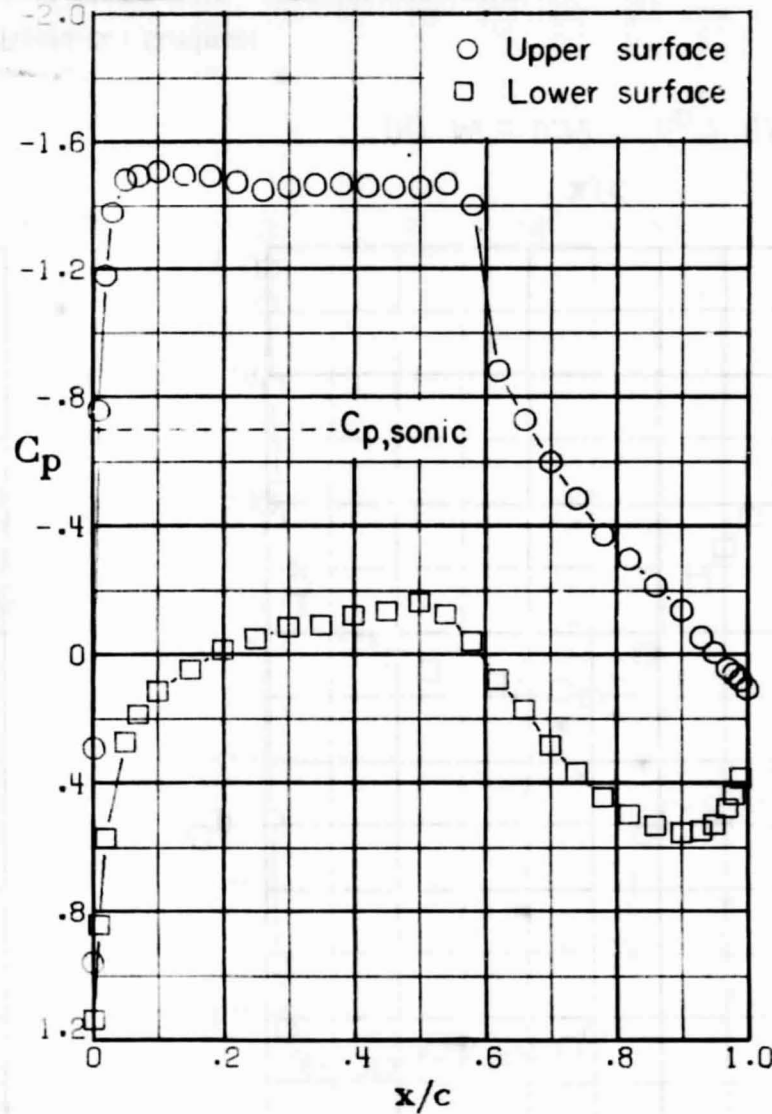
(g) $M = 0.72$; $c_n = 0.86$.



(h) $M = 0.72$; $c_n = 0.98$.

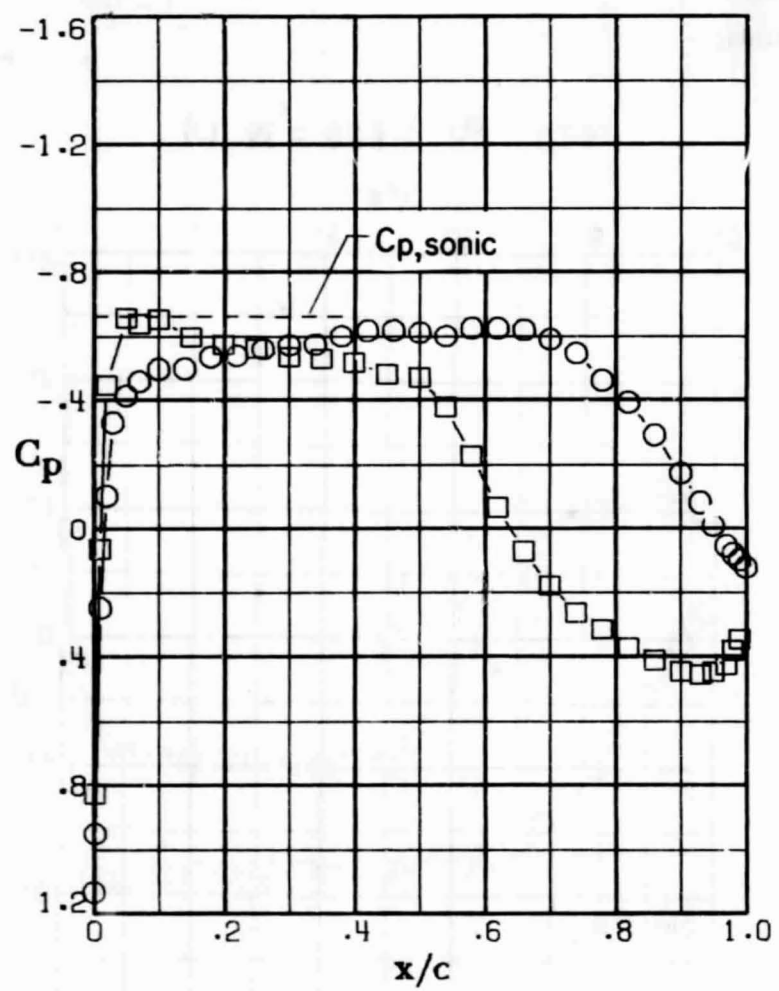
Figure 15. - Continued.

ORIGINAL PAGE IS
OF POOR
QUALITY

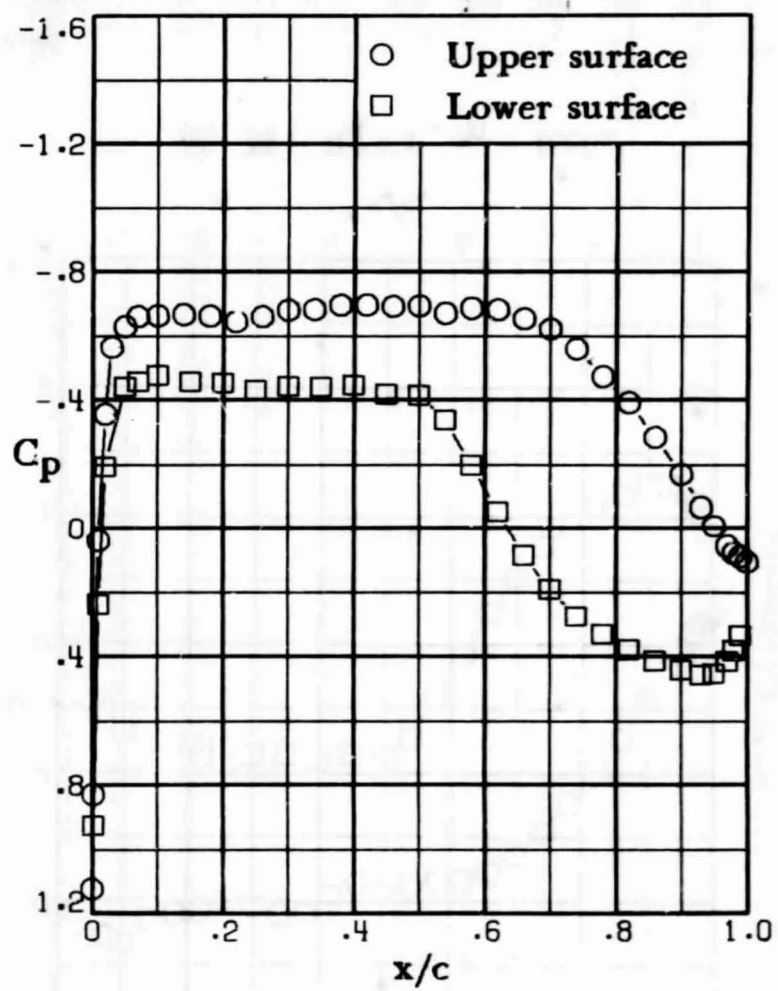


(i) $M = 0.72$; $c_n = 1.17$.

Figure 15.- Concluded.

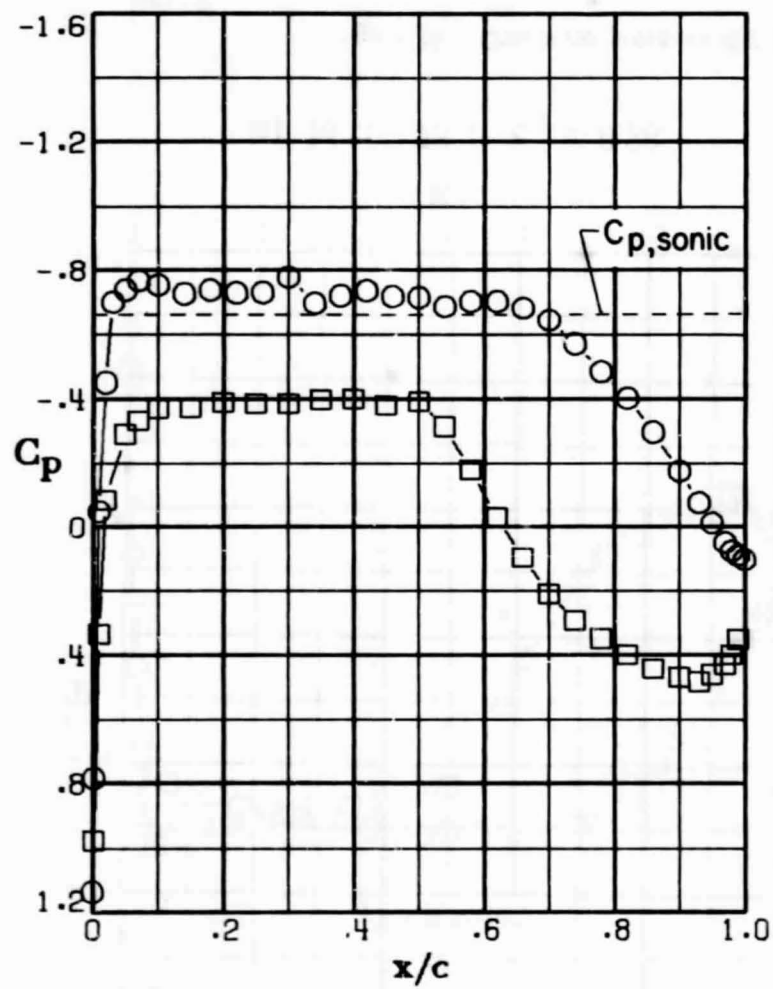


(a) $M = 0.73$: $c_n = 0.28$.

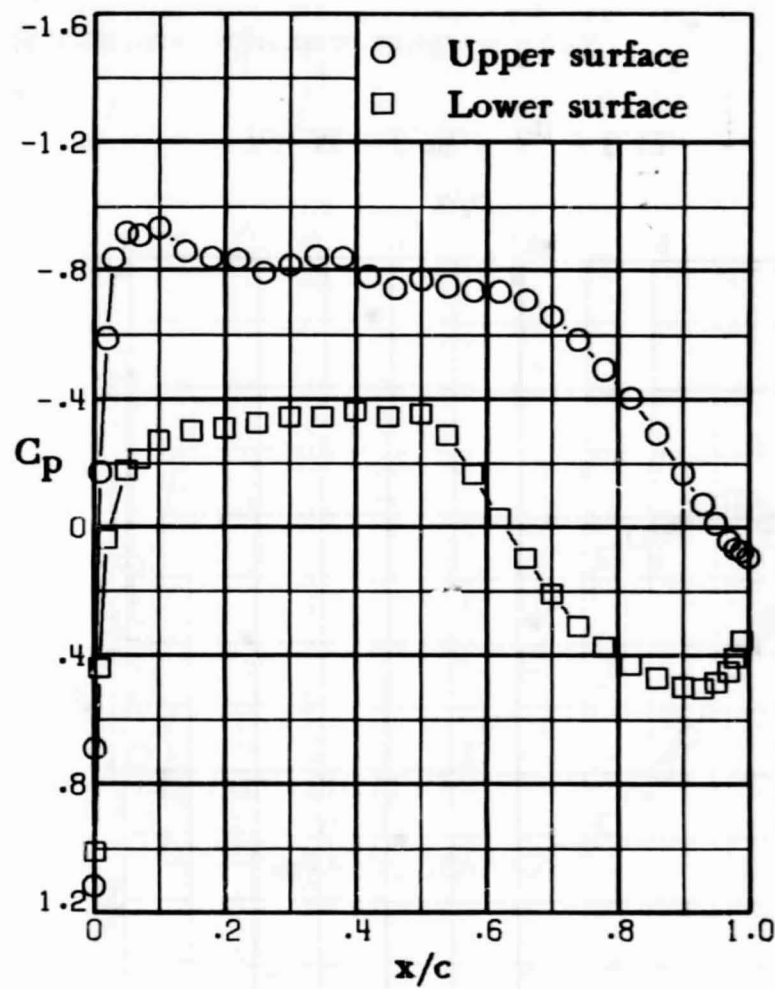


(b) $M = 0.73$: $c_n = 0.42$.

Figure 16. - Chordwise pressure distributions for 14-percent-thick supercritical airfoil. $M = 0.73$.

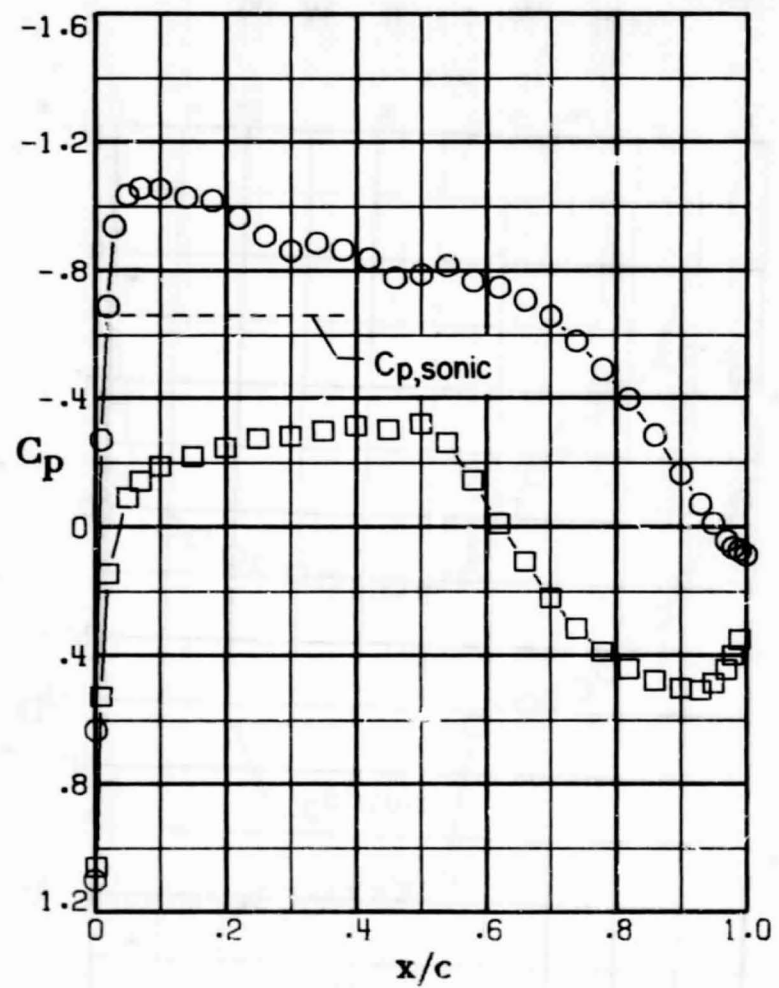


(c) $M = 0.73$; $c_n = 0.50$.

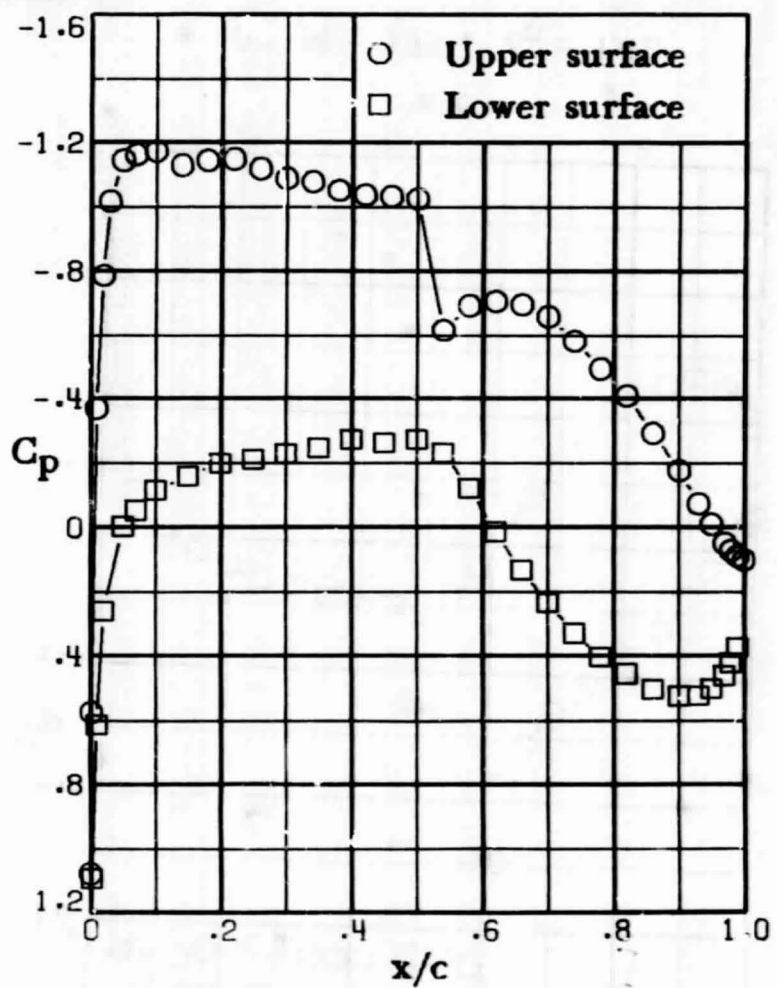


(d) $M = 0.73$; $c_n = 0.60$.

ORIGINAL PAGE IS
OF POOR QUALITY

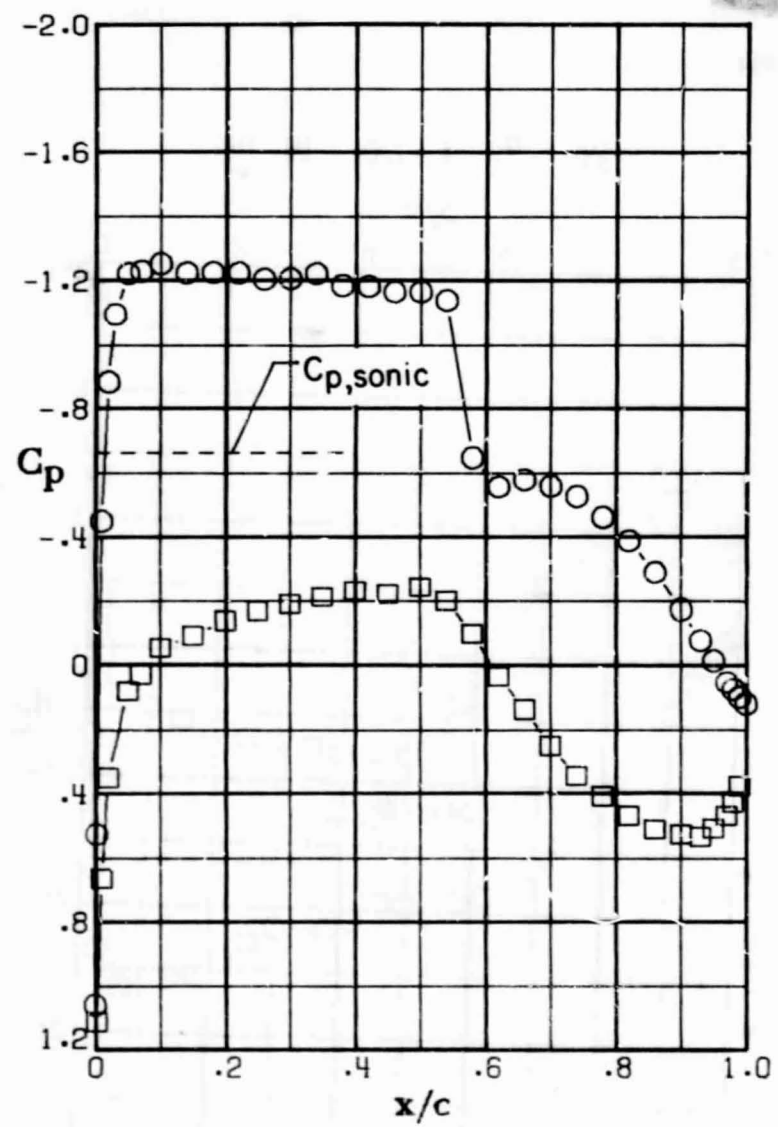


(e) $M = 0.73 ; c_n = 0.69.$

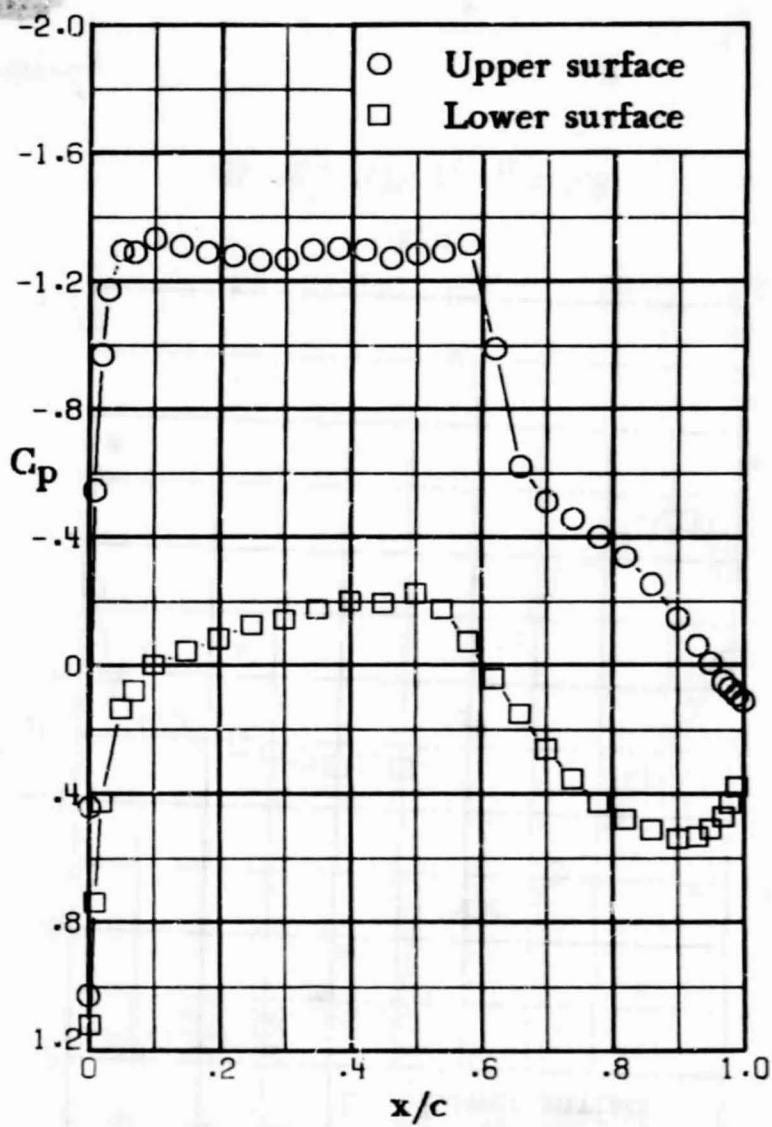


(f) $M = 0.73 ; c_n = 0.81.$

Figure I6.- Continued.

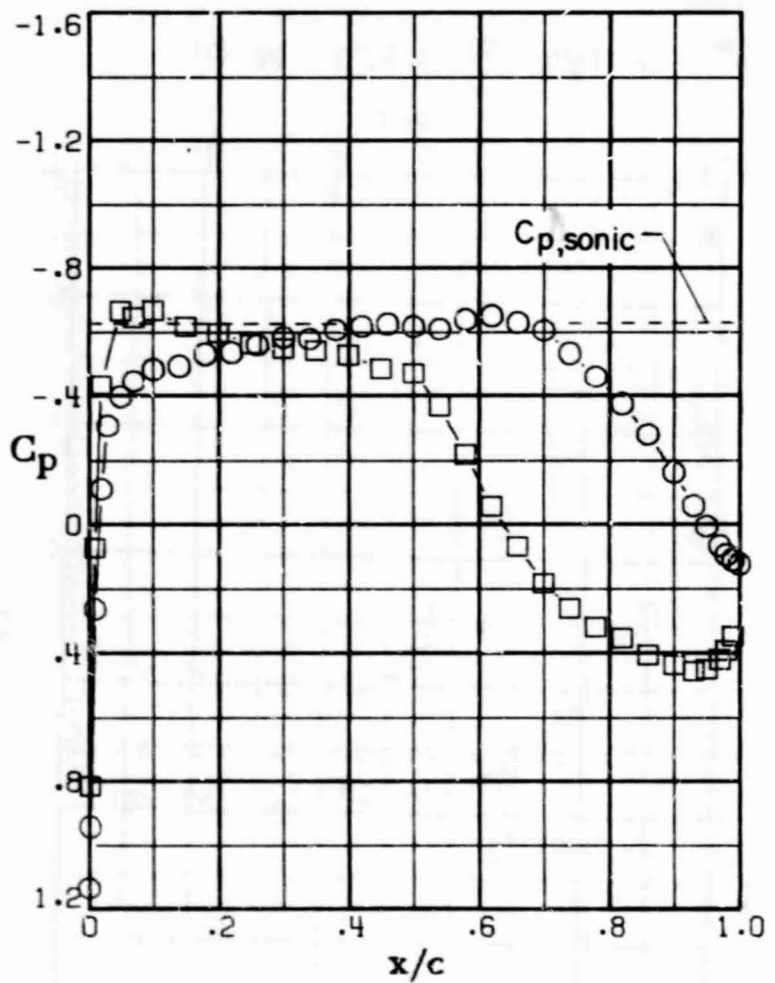


(g) $M = 0.73 ; c_n = 0.90.$

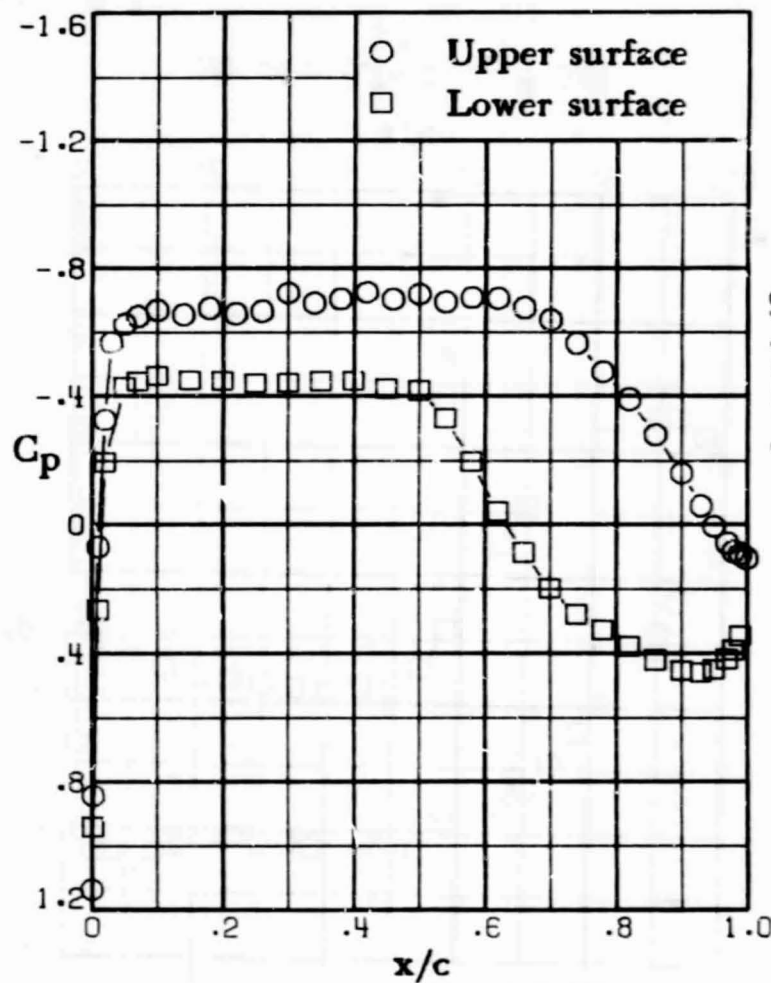


(h) $M = 0.73 ; c_n = 1.01.$

ORIGINAL PAGE IS
OF POOR QUALITY



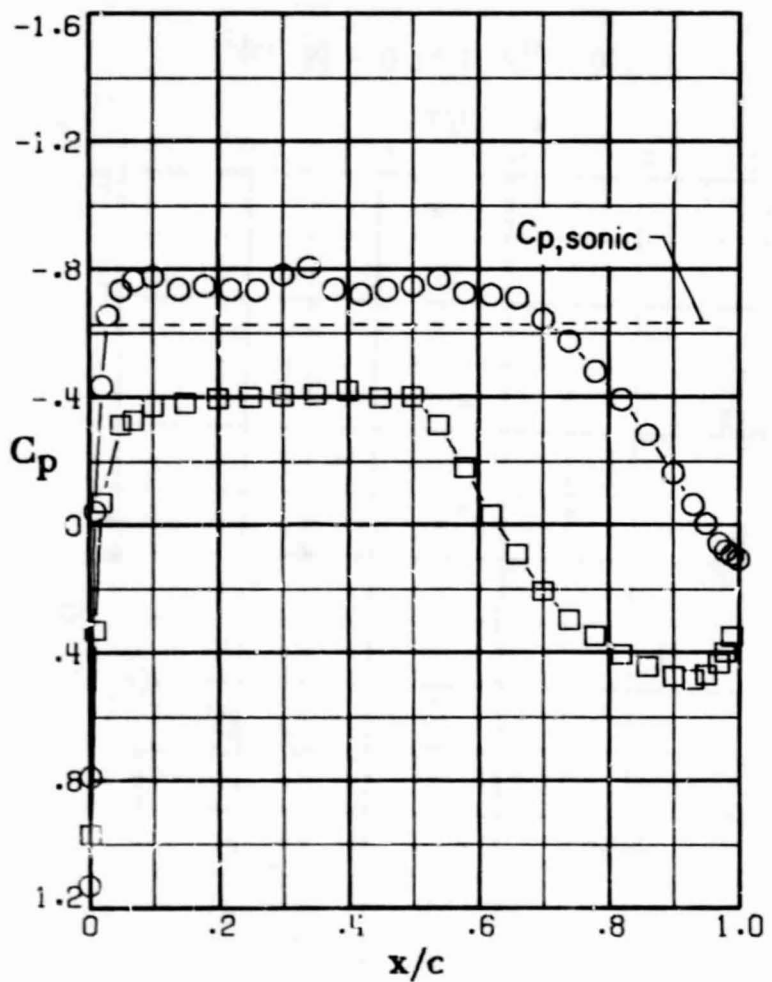
(a) $M = 0.74$; $c_n = 0.27$.



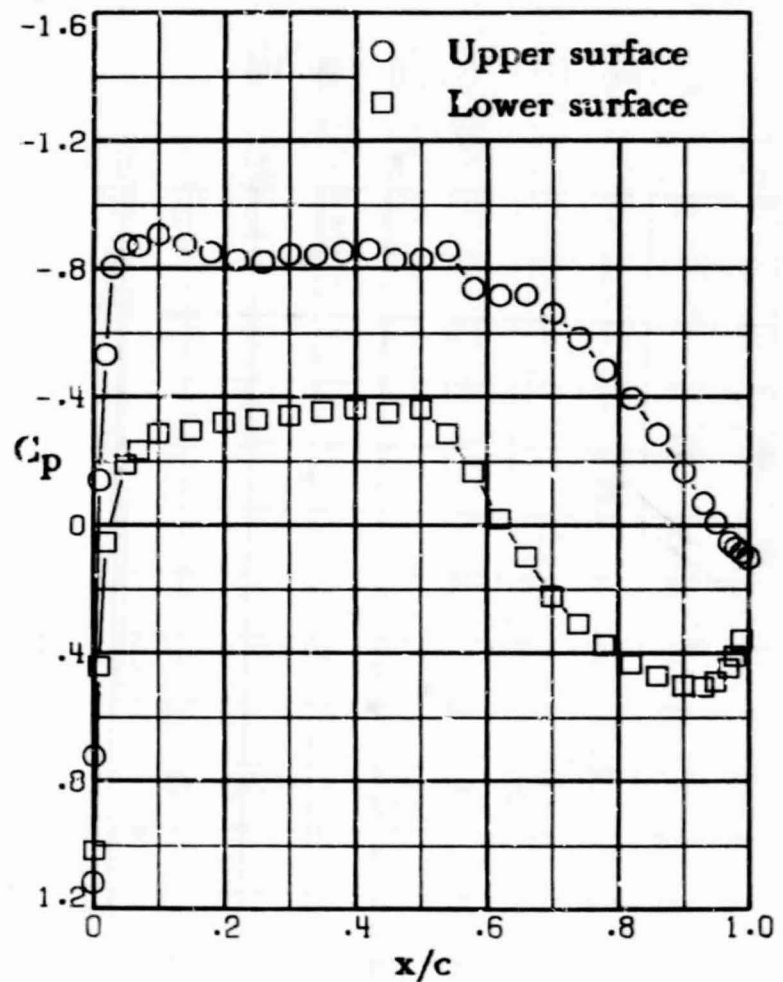
(b) $M = 0.74$; $c_n = 0.43$.

Figure 17. - Chordwise pressure distributions for 14-percent-thick supercritical airfoil. $M = 0.74$.

ORIGINAL PAGE IS
OF POOR QUALITY

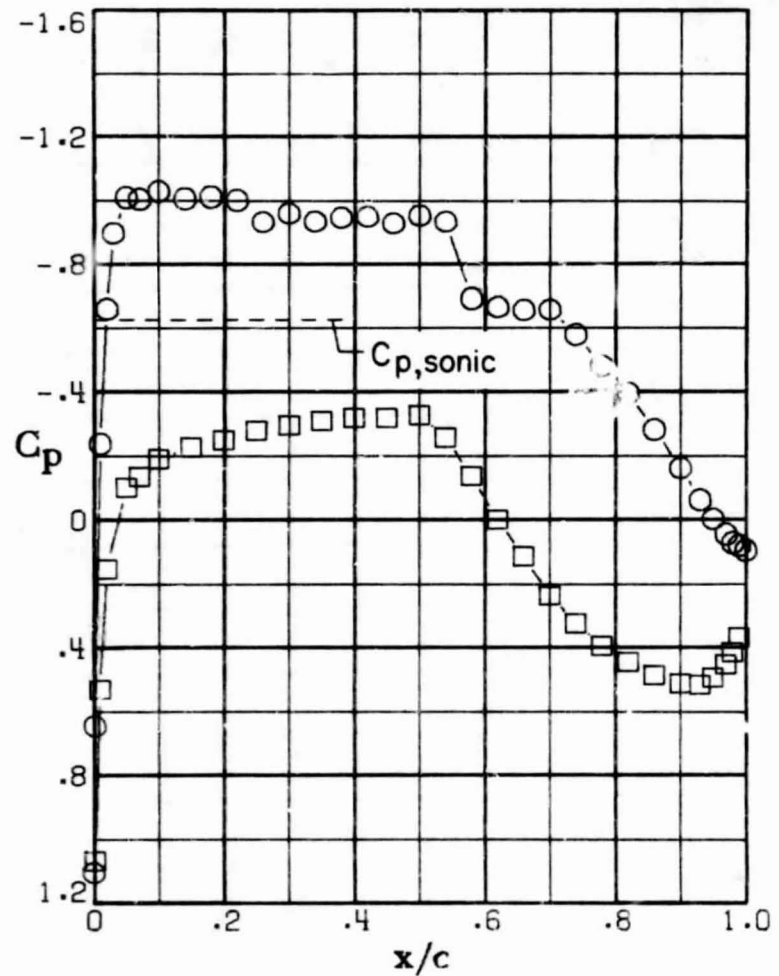


(c) $M = 0.74$; $c_n = 0.51$.

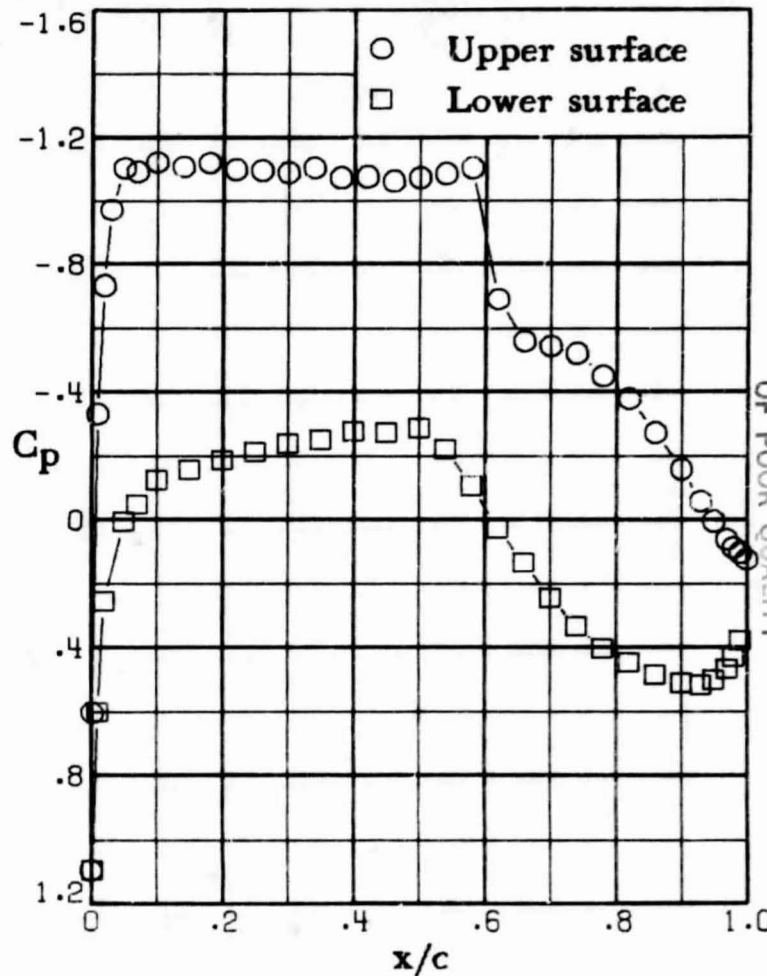


(d) $M = 0.74$; $c_n = 0.61$.

Figure 17.- Continued.

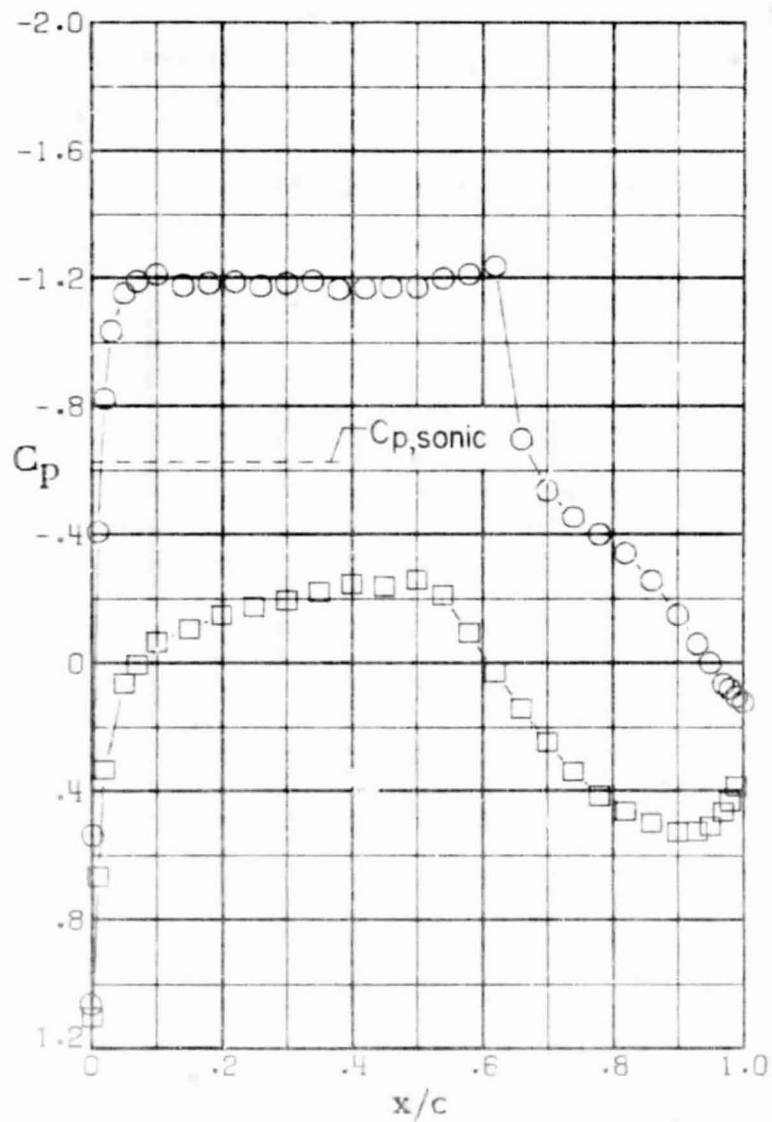


(e) $M = 0.74 ; c_n = 0.71.$

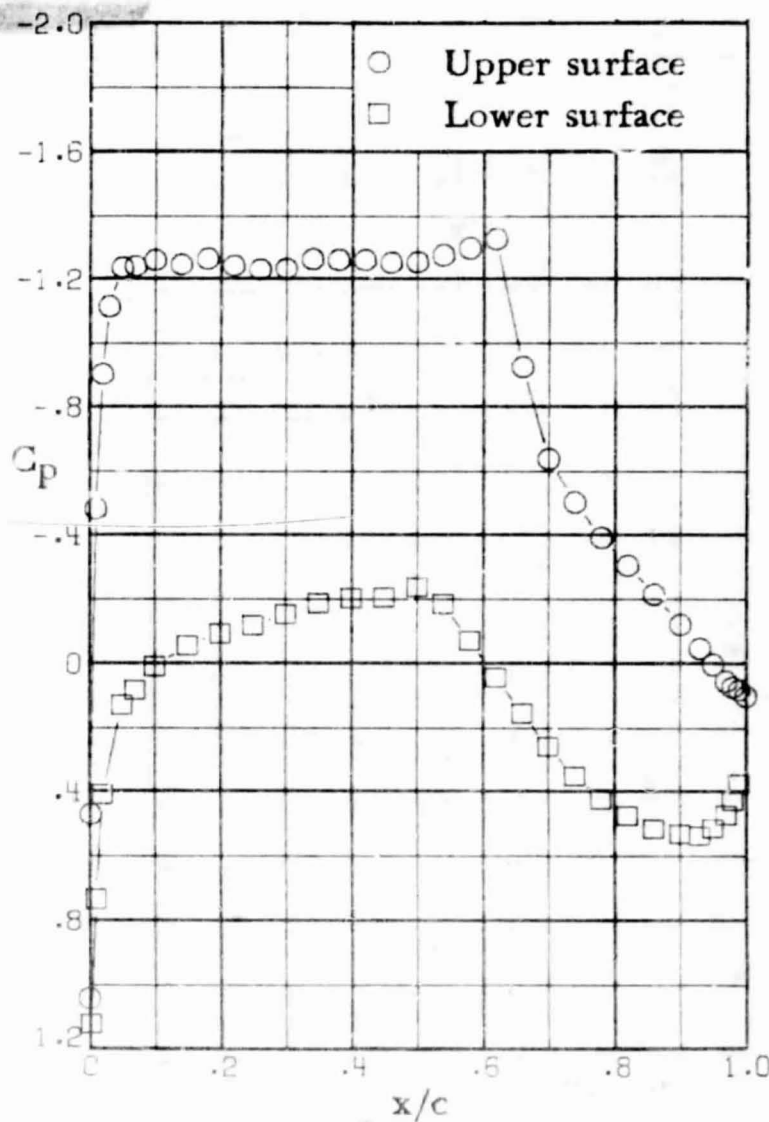


(f) $M = 0.74 ; c_n = 0.82.$

Figure 17. - Continued.



(g) $M = 0.74$: $c_n = 0.92$.

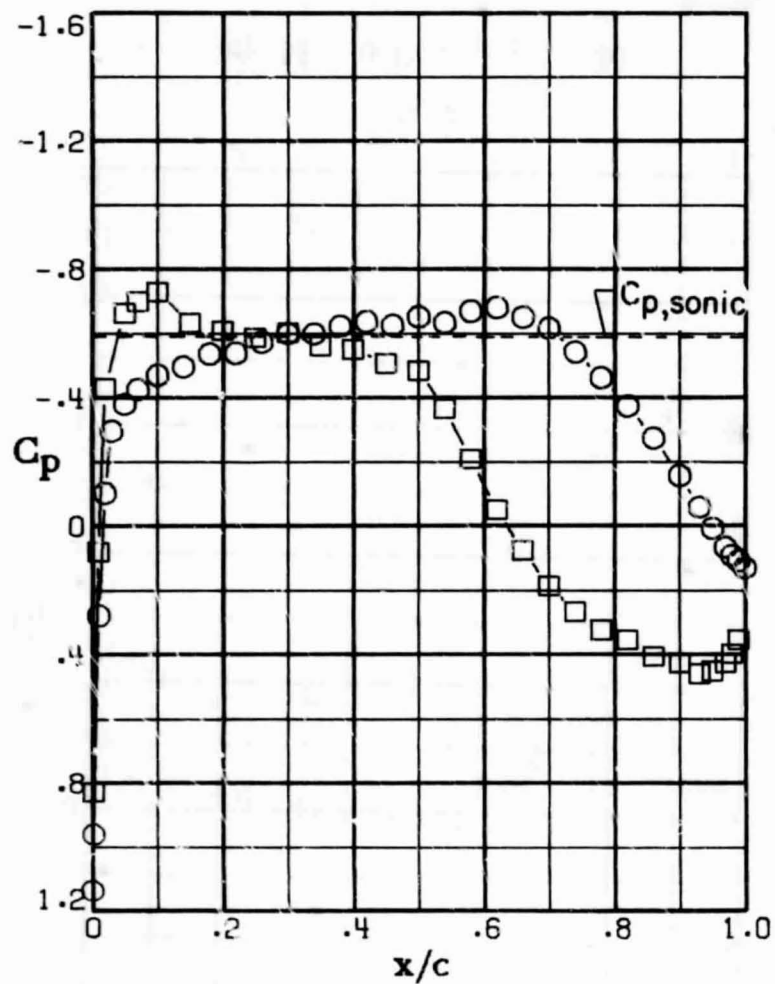


(h) $M = 0.74$: $c_n = 1.01$.

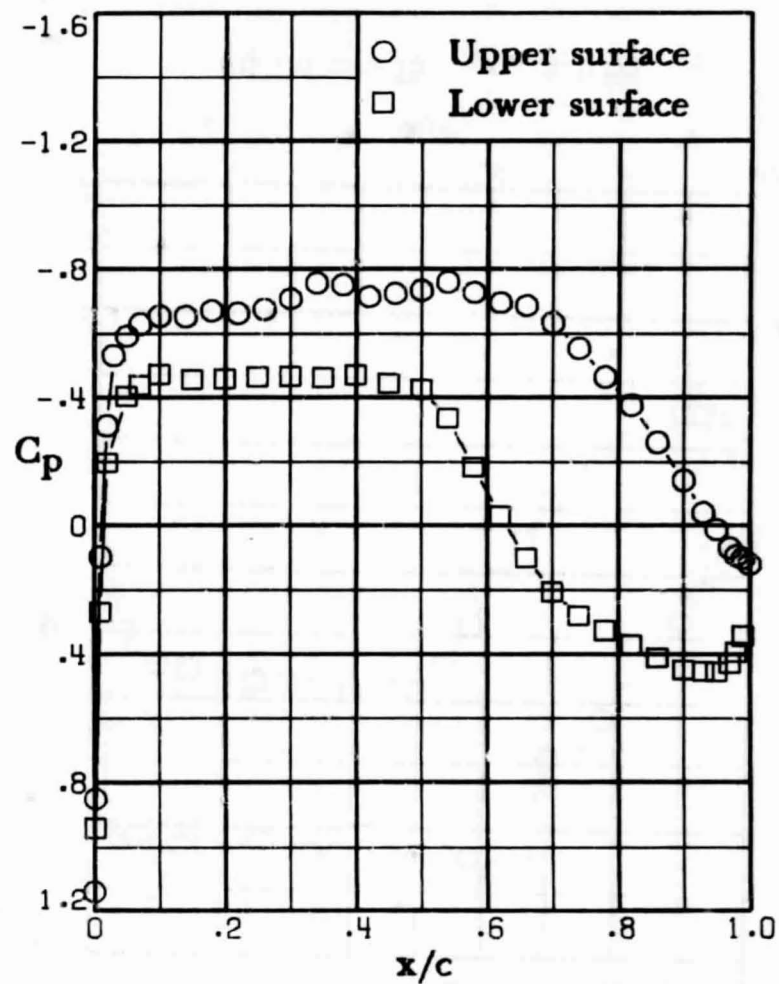
ORIGINAL PAGE IS
OF POOR
QUALITY

Figure 17. - Concluded.

ORIGINAL PAGE IS
OF POOR QUALITY

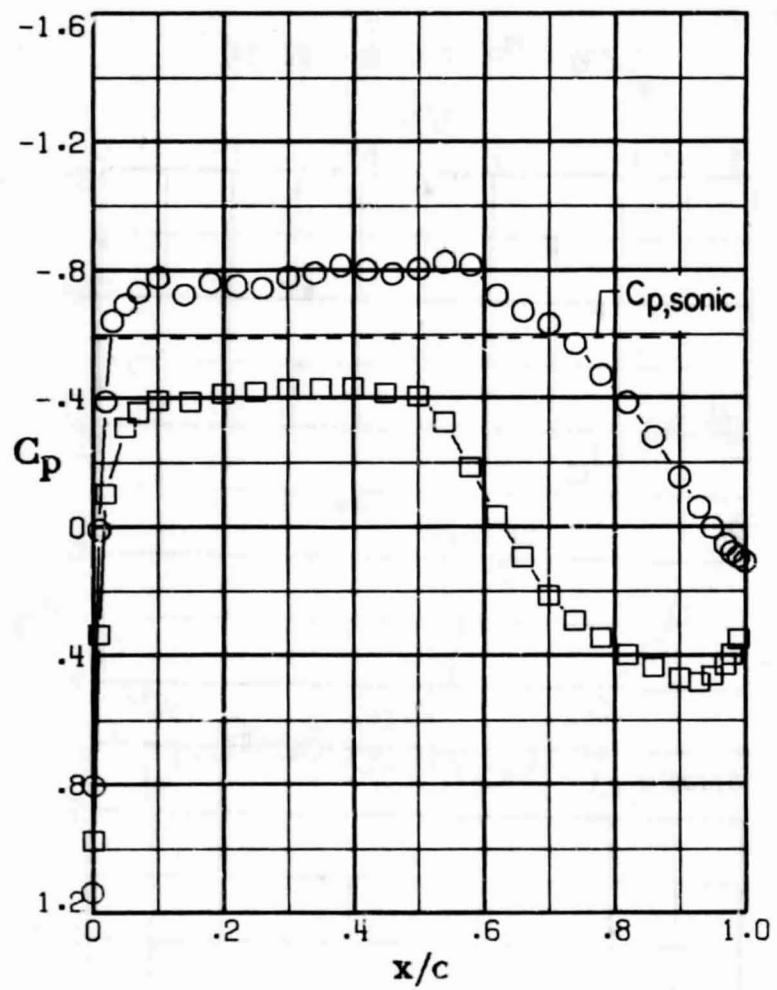


(a) $M = 0.75 ; c_n = 0.27.$

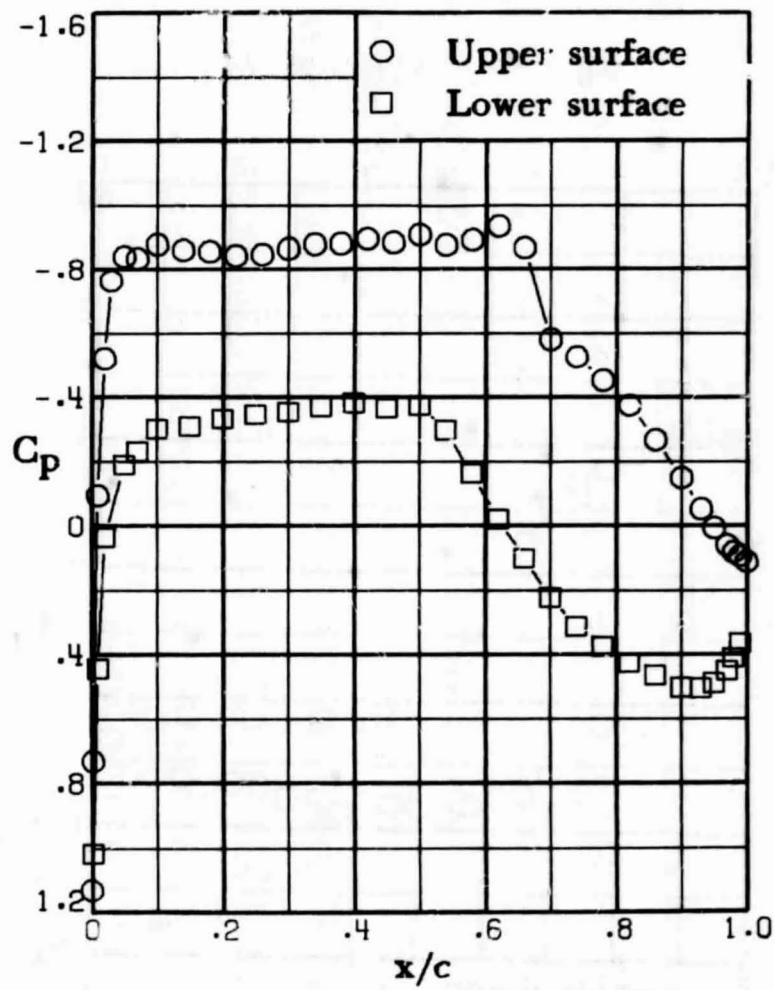


(b) $M = 0.75 ; c_n = 0.43.$

Figure 18.- Chordwise pressure distributions for 14-percent-thick supercritical airfoil. $M = 0.75$.



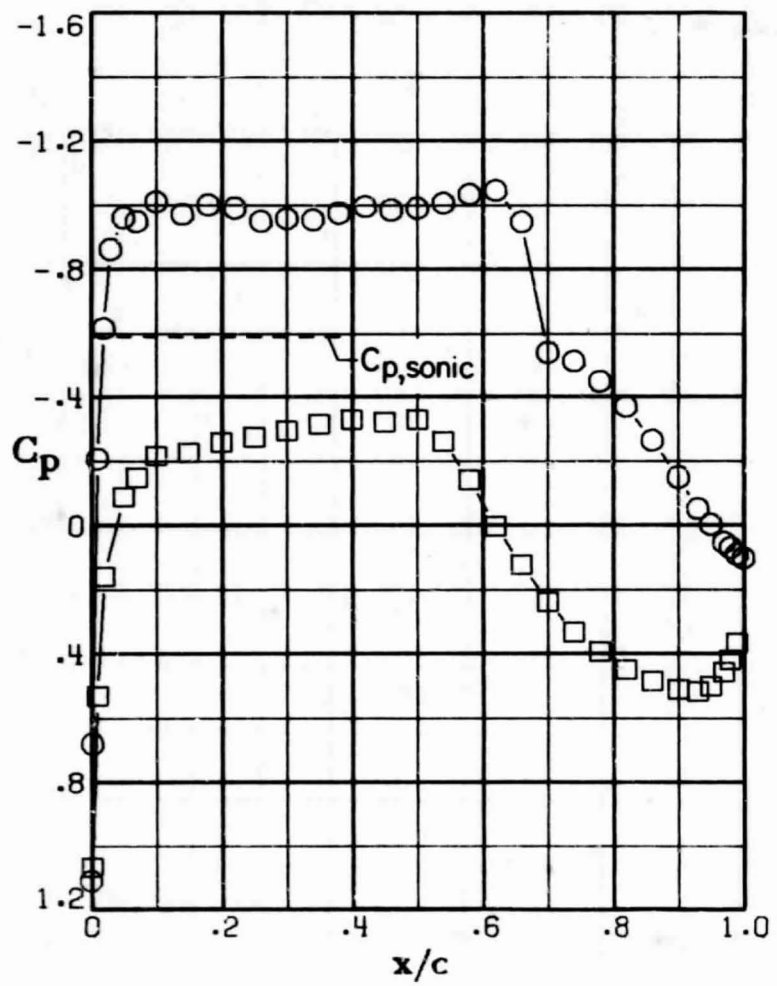
(c) $M = 0.75$; $c_n = 0.51$.



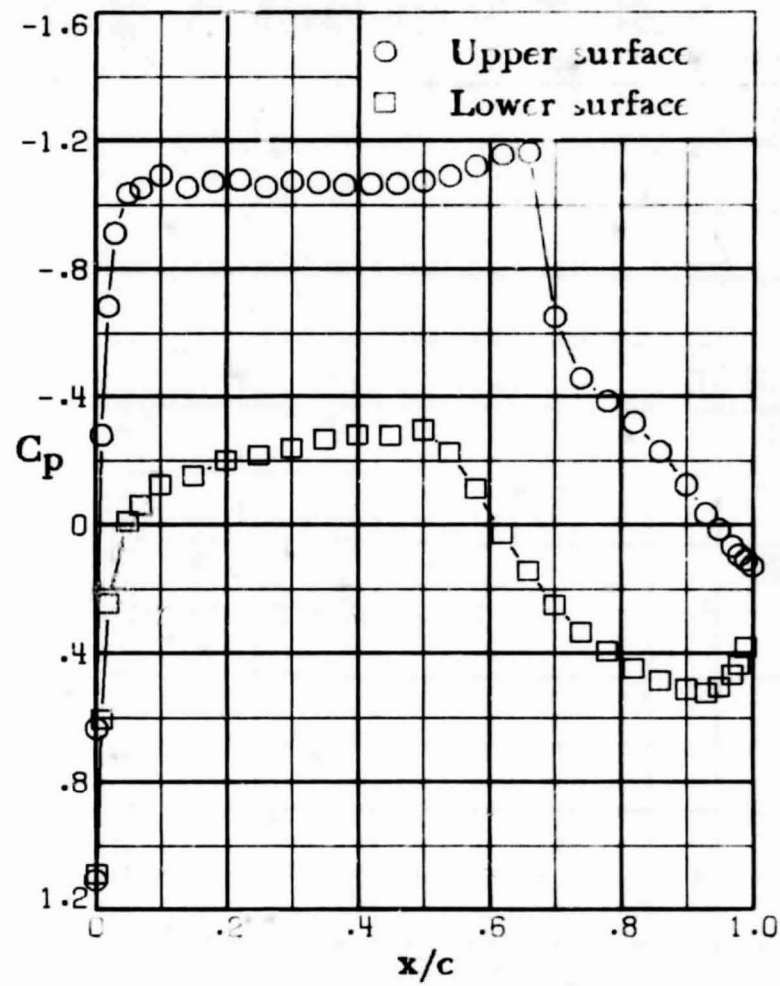
(d) $M = 0.75$; $c_n = 0.63$.

ORIGINAL PAGE IS
OF POOR
QUALITY

Figure 18. - Continued.



(e) $M = 0.75$; $c_n = 0.74$.

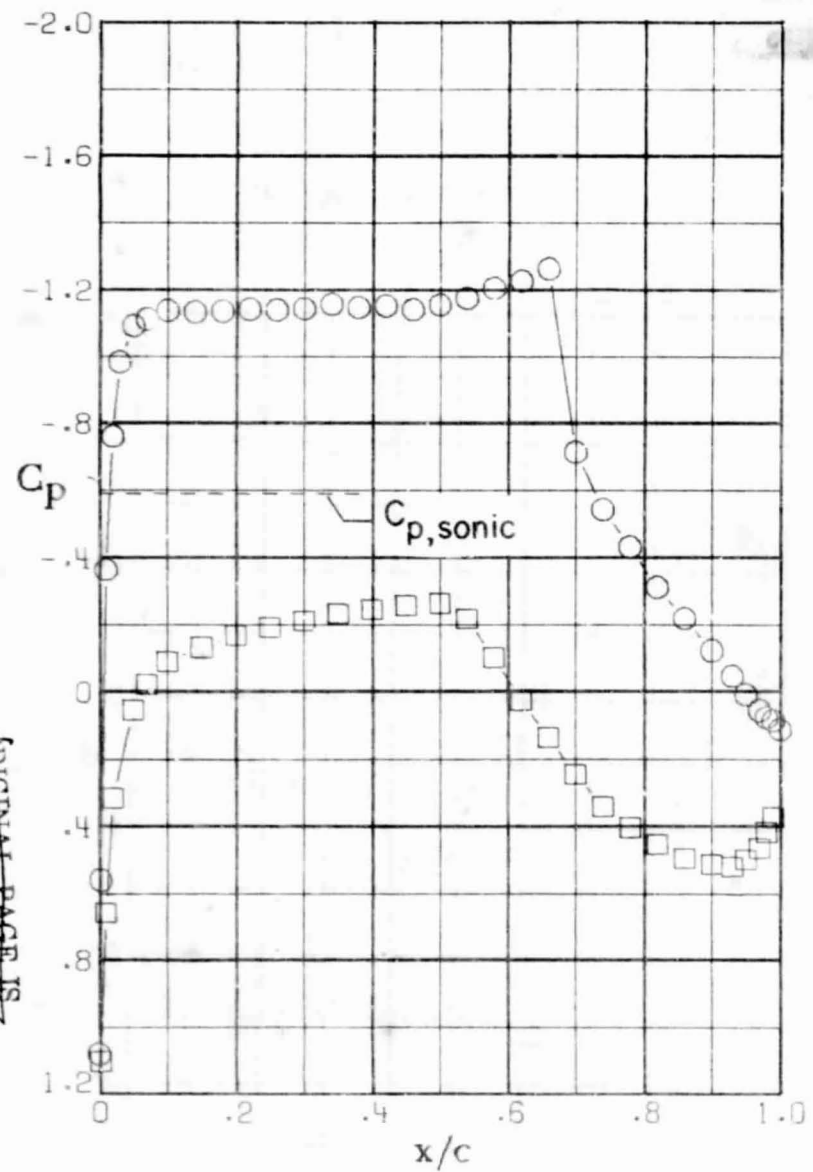


(f) $M = 0.75$; $c_n = 0.84$.

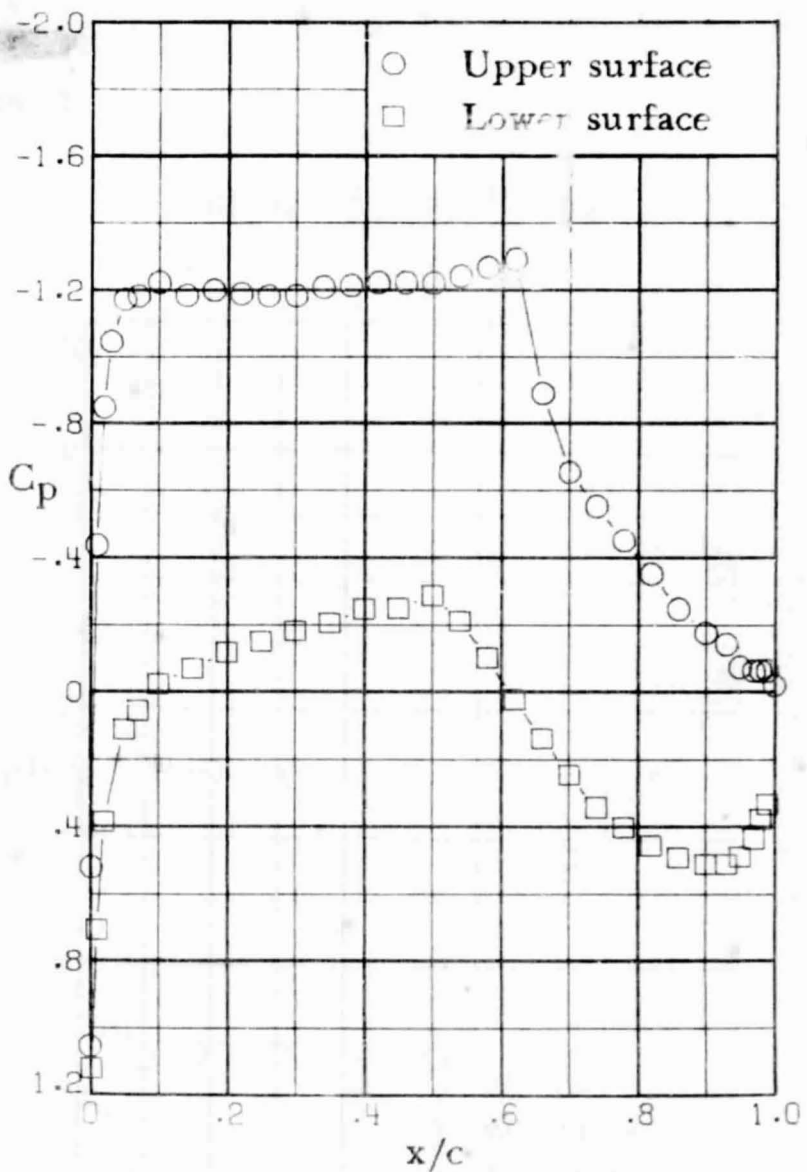
ORIGINAL PAGE IS
OF POOR
QUALITY

Figure 18.- Continued.

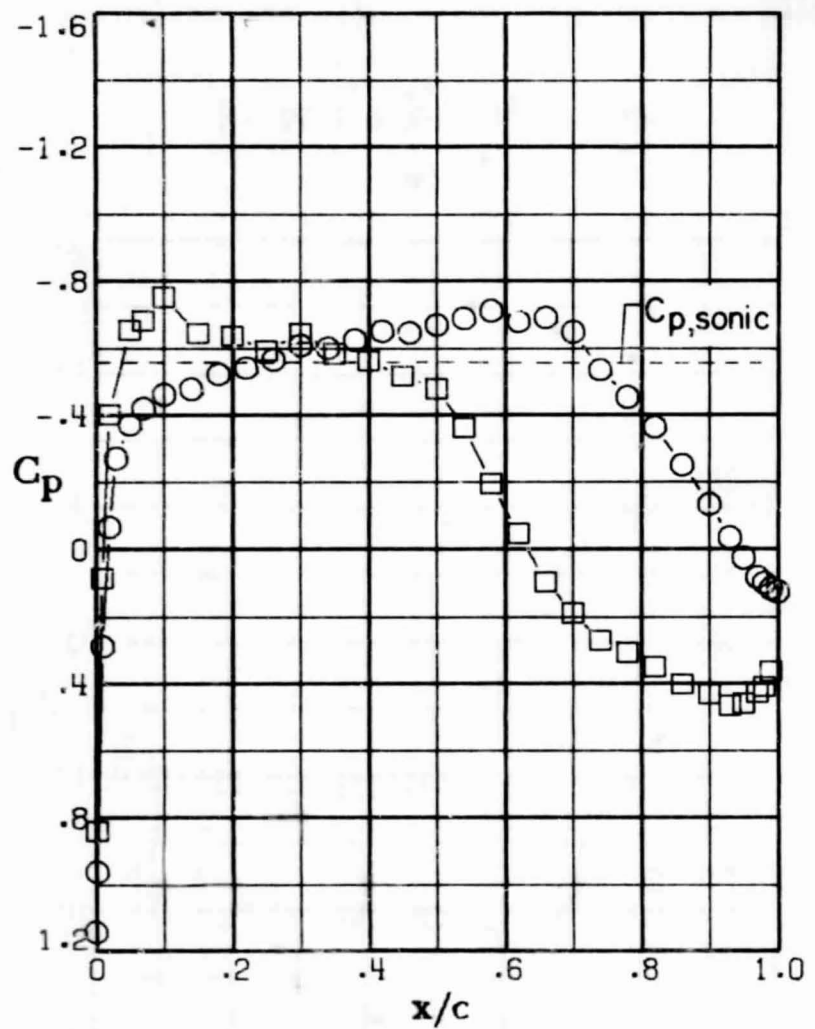
ORIGINAL PAGE IS
OF POOR QUALITY



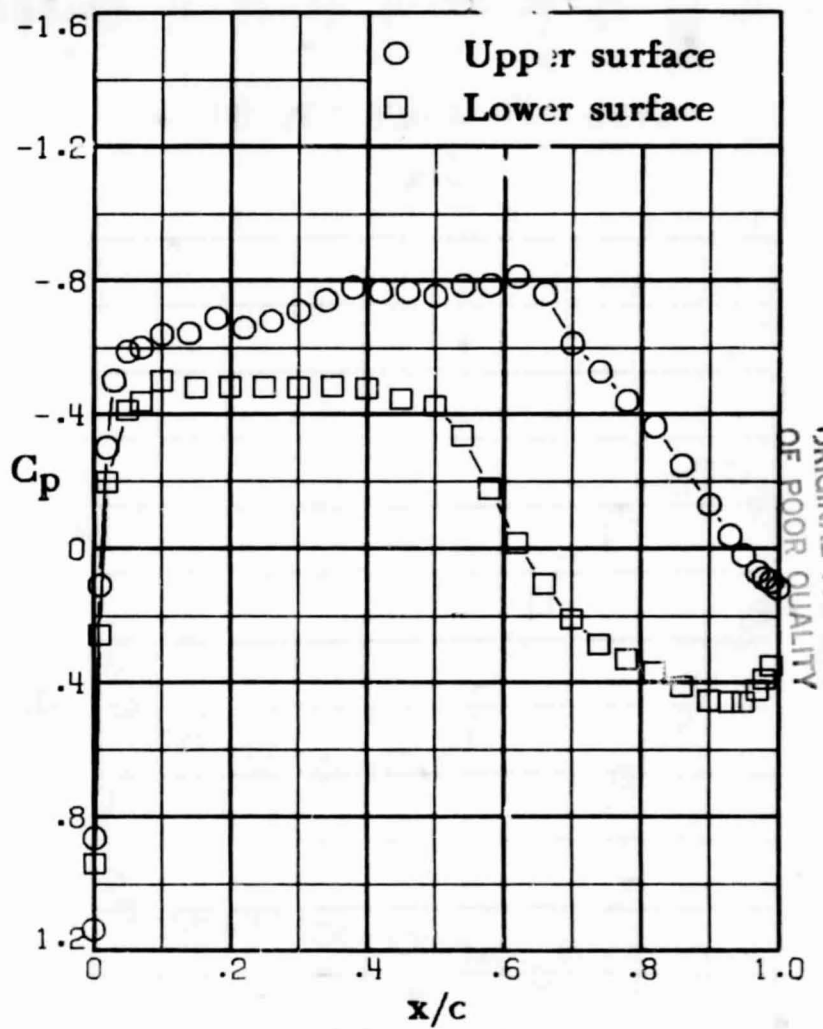
(g) $M = 0.75$; $c_n = 0.92$.



(h) $M = 0.75$; $c_n = 0.97$.

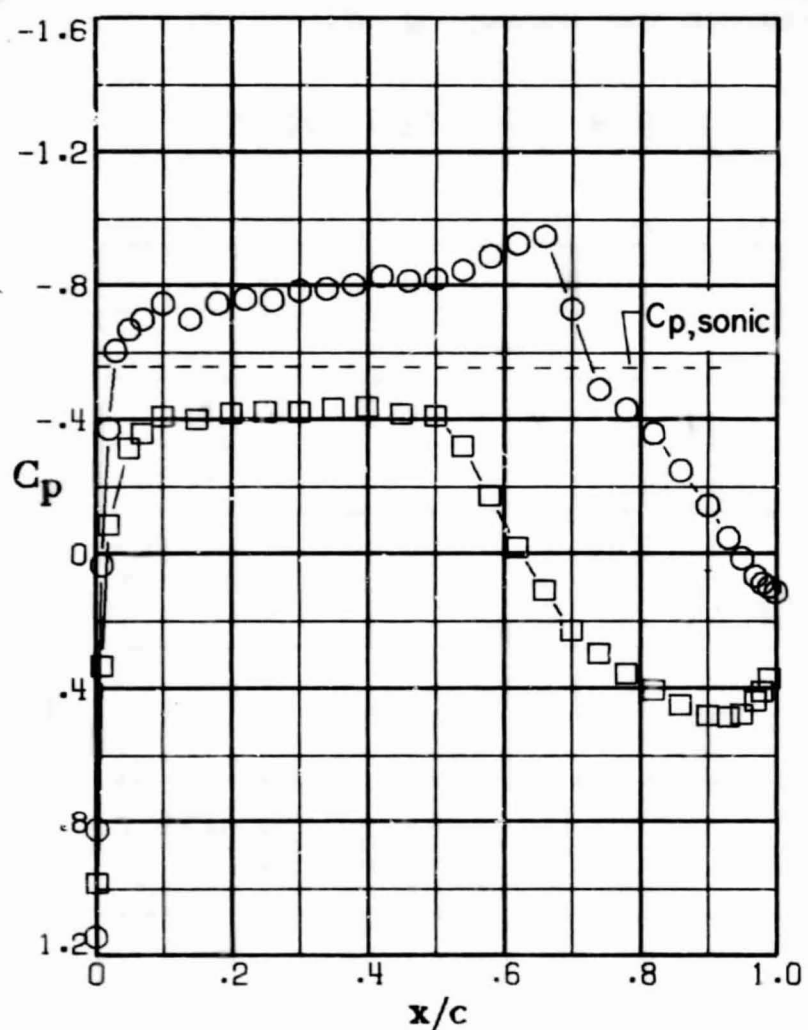


(a) $M = 0.76$; $c_n = 0.26$.

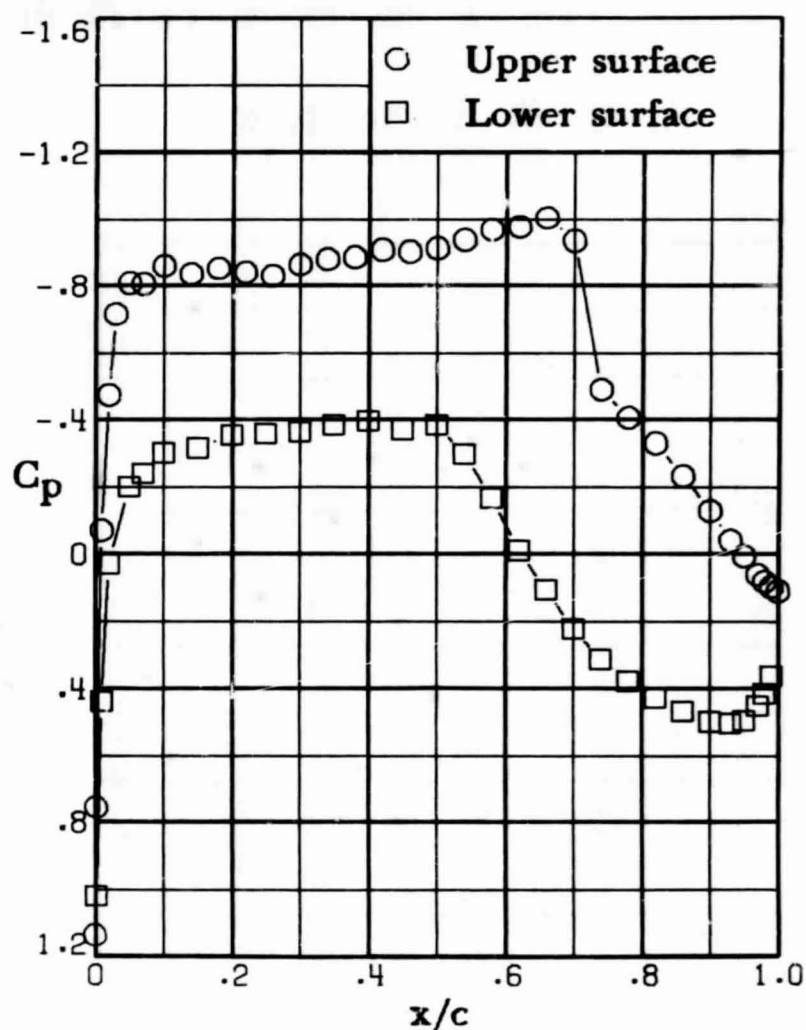


(b) $M = 0.76$; $c_n = 0.43$.

Figure 19.- Chordwise pressure distributions for 14-percent-thick supercritical airfoil. $M = 0.76$.



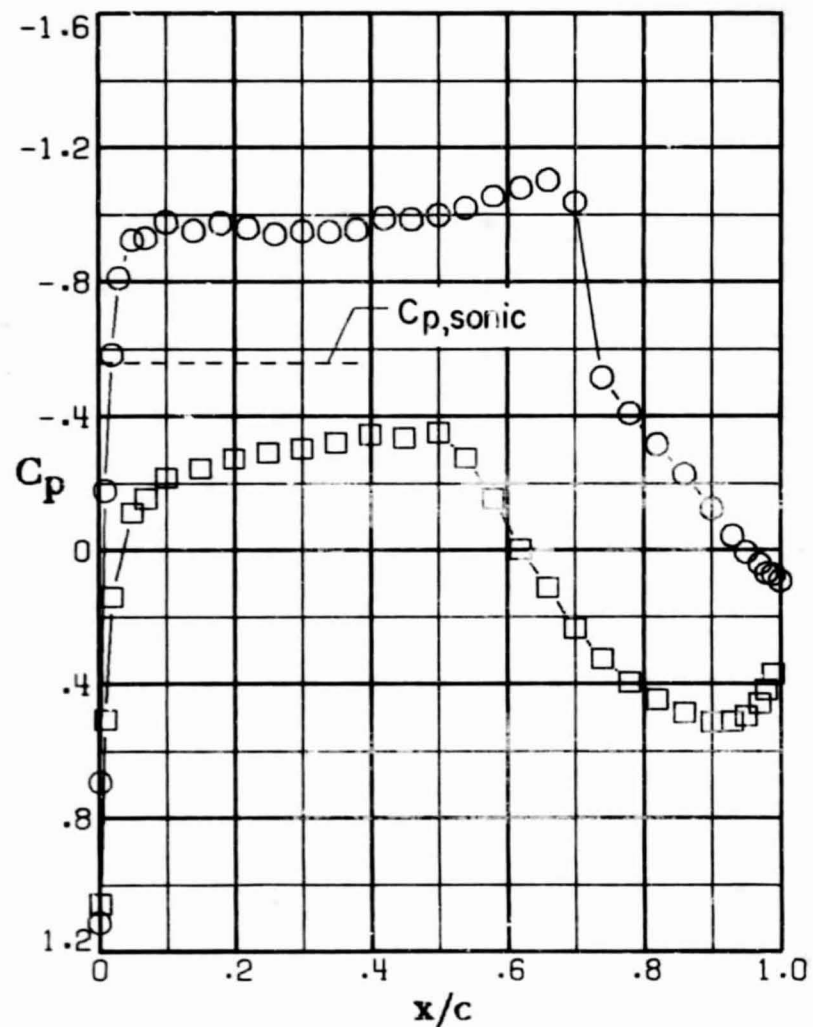
(c) $M = 0.76$; $c_n = 0.53$.



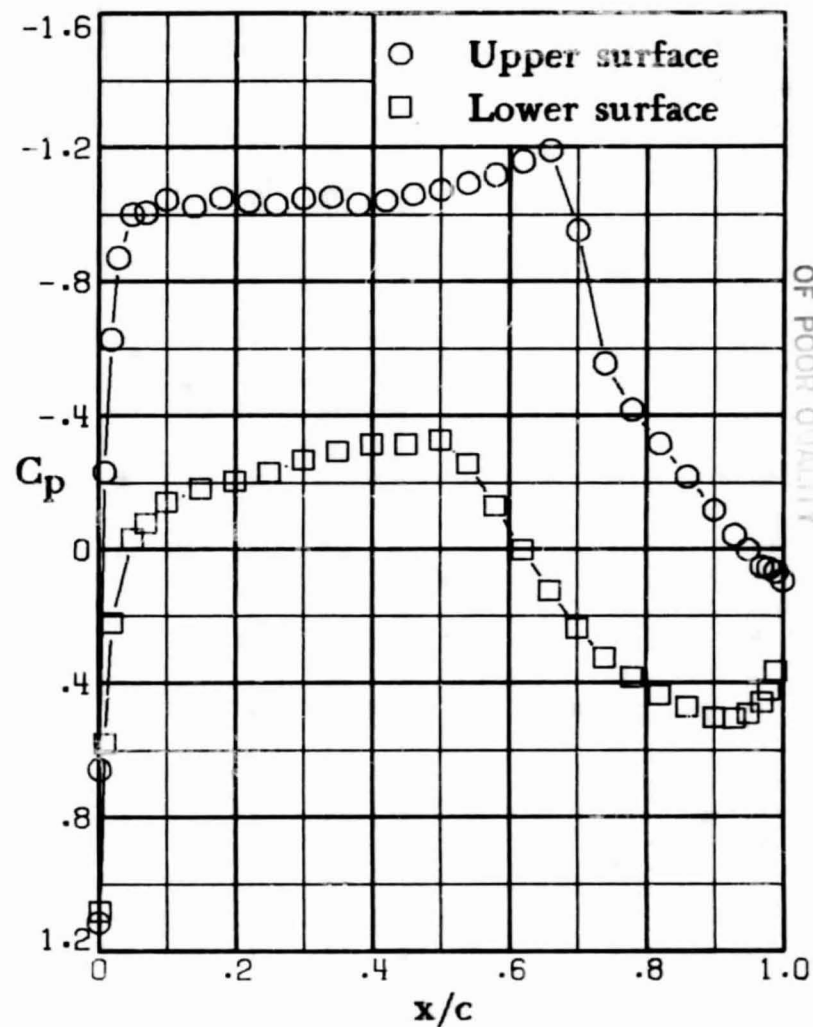
(d) $M = 0.76$; $c_n = 0.64$.

ORIGINAL PAGE IS
OF POOR
QUALITY

Figure 19. - Continued.



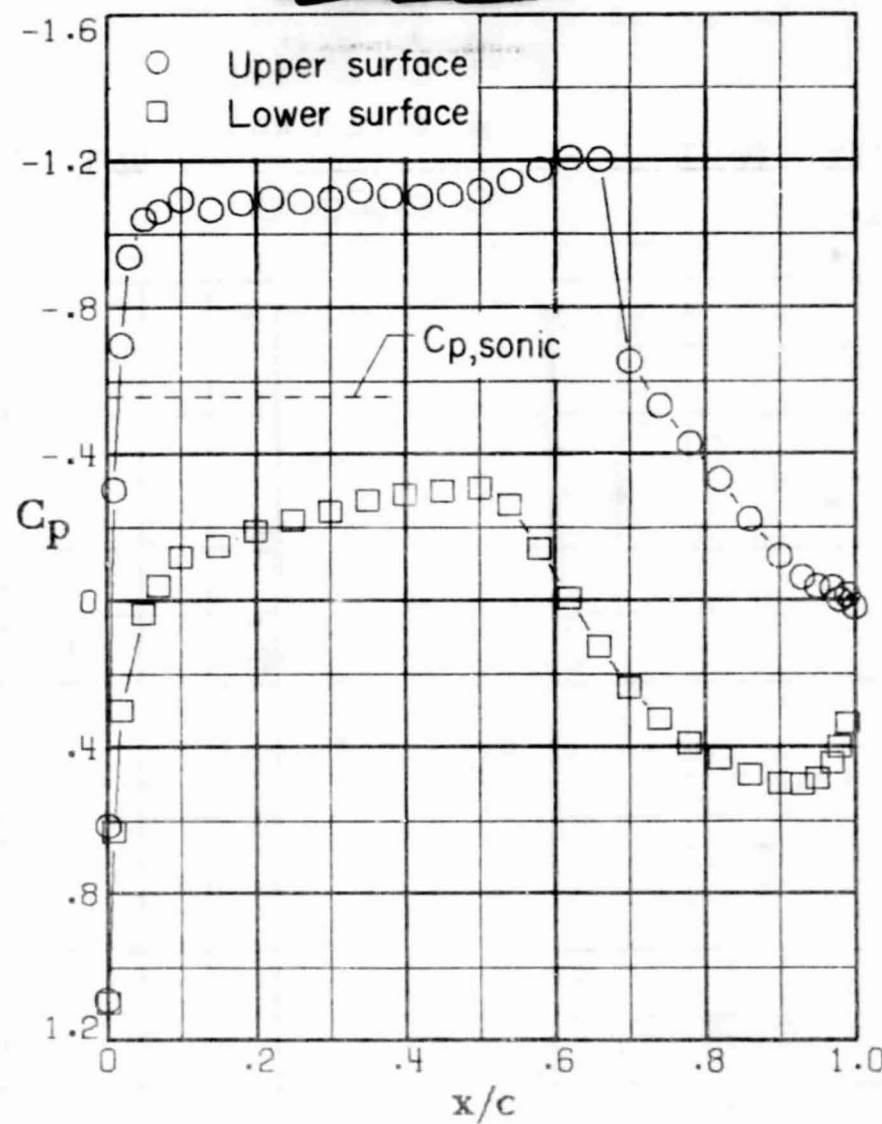
(e) $M = 0.76$; $c_n = 0.75$.



(f) $M = 0.76$; $c_n = 0.82$.

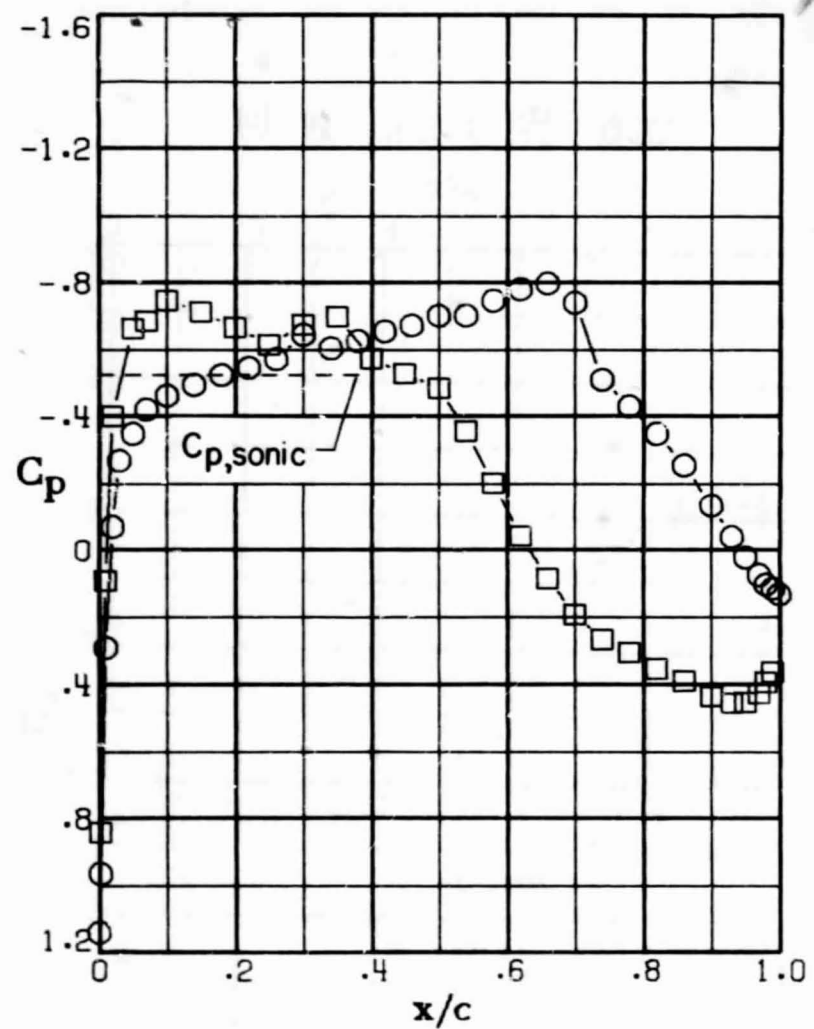
Figure 19. - Continued.

ORIGINAL PAGE IS
OF POOR QUALITY

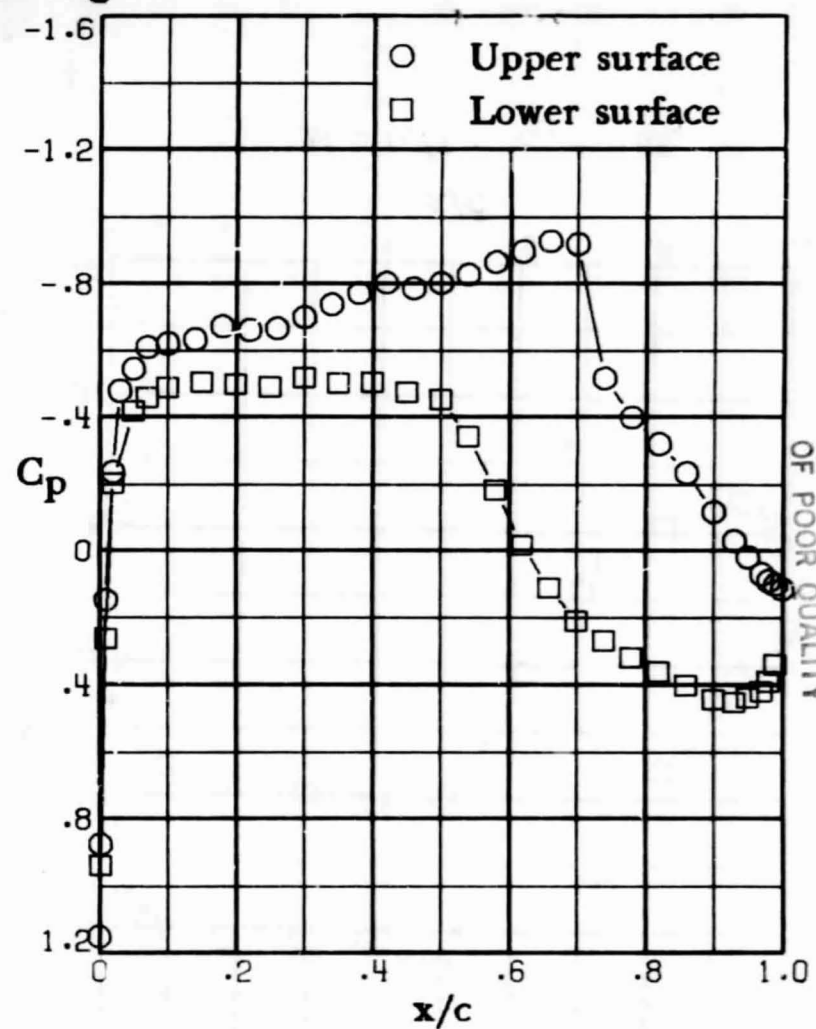


(g) $M = 0.76$; $c_n = 0.86$.

Figure 19. - Concluded.

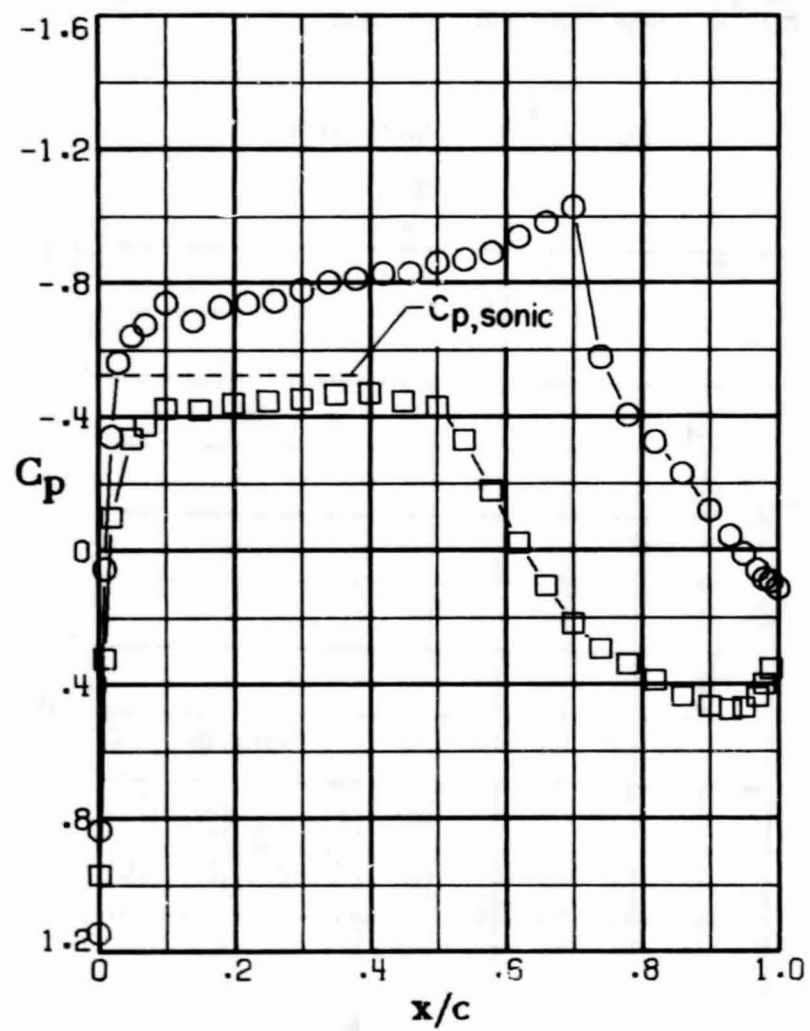


(a) $M = 0.77$; $c_n = 0.26$.

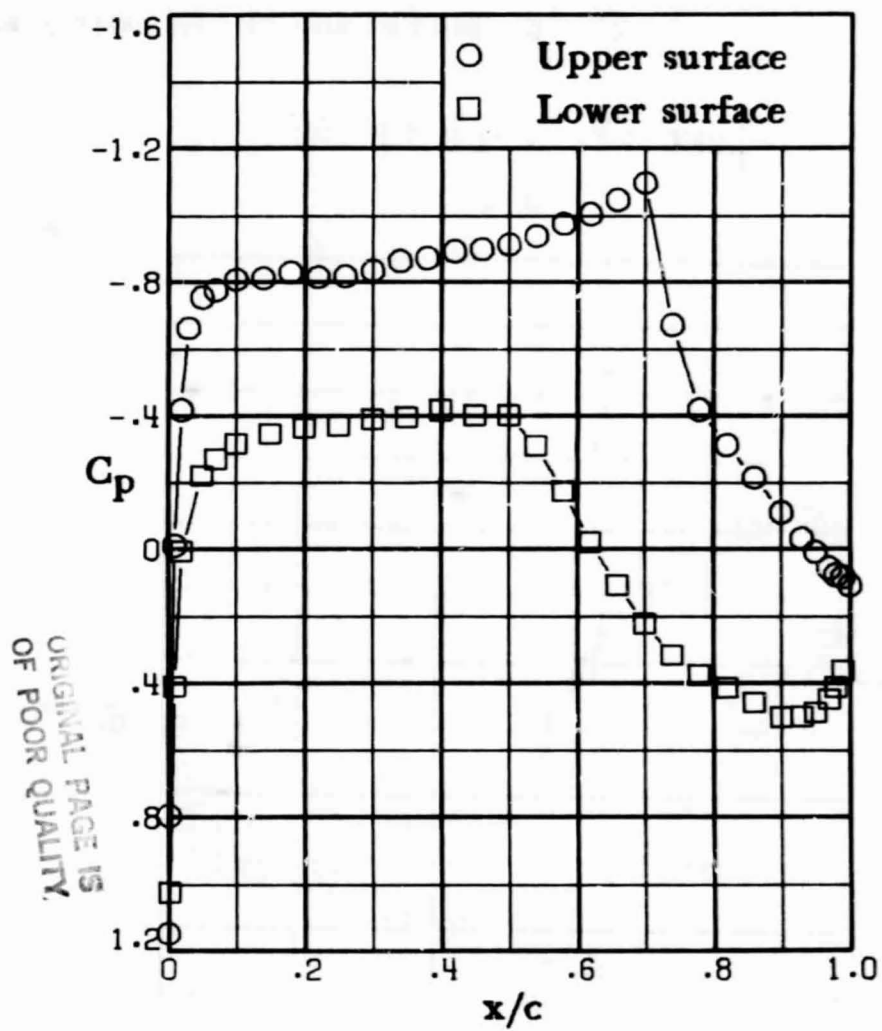


(b) $M = 0.77$; $c_n = 0.44$.

Figure 20.- Chordwise pressure distributions for 14-percent-thick supercritical airfoil. $M = 0.77$.



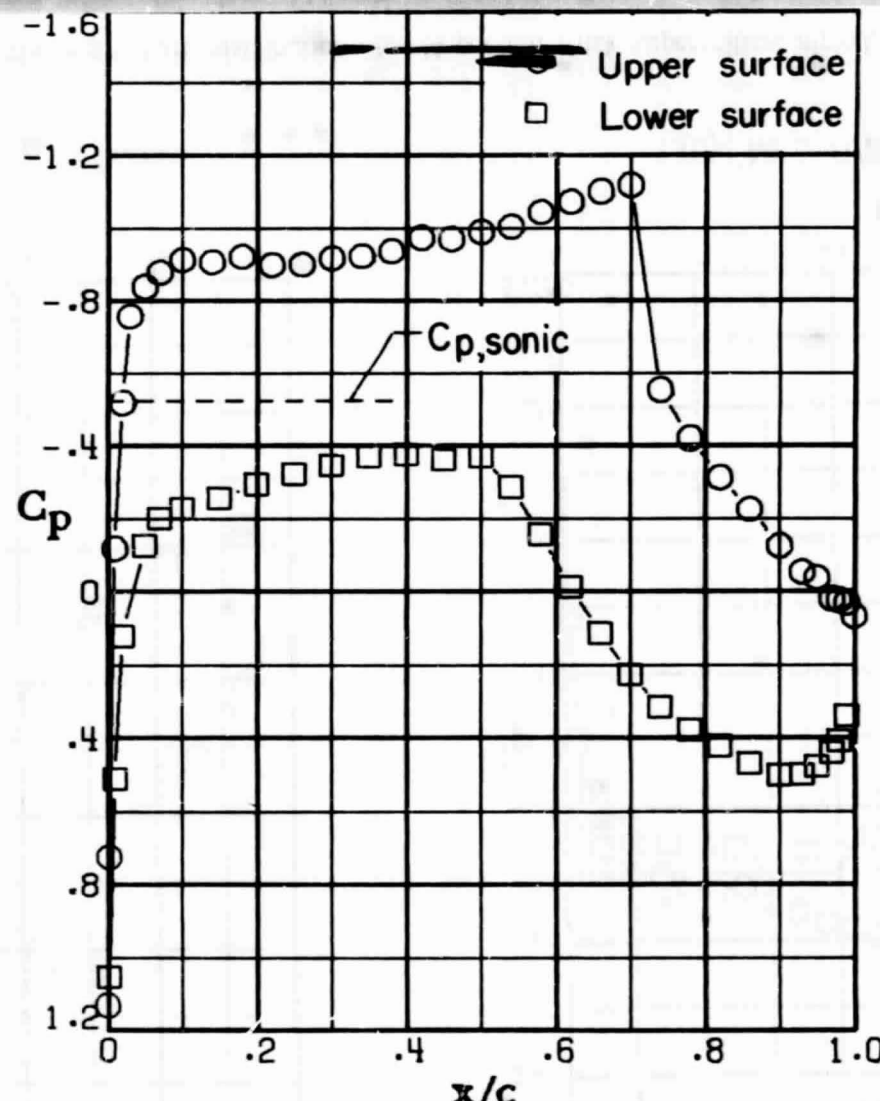
(c) $M = 0.77$; $c_n = 0.52$.



(d) $M = 0.77$; $c_n = 0.63$.

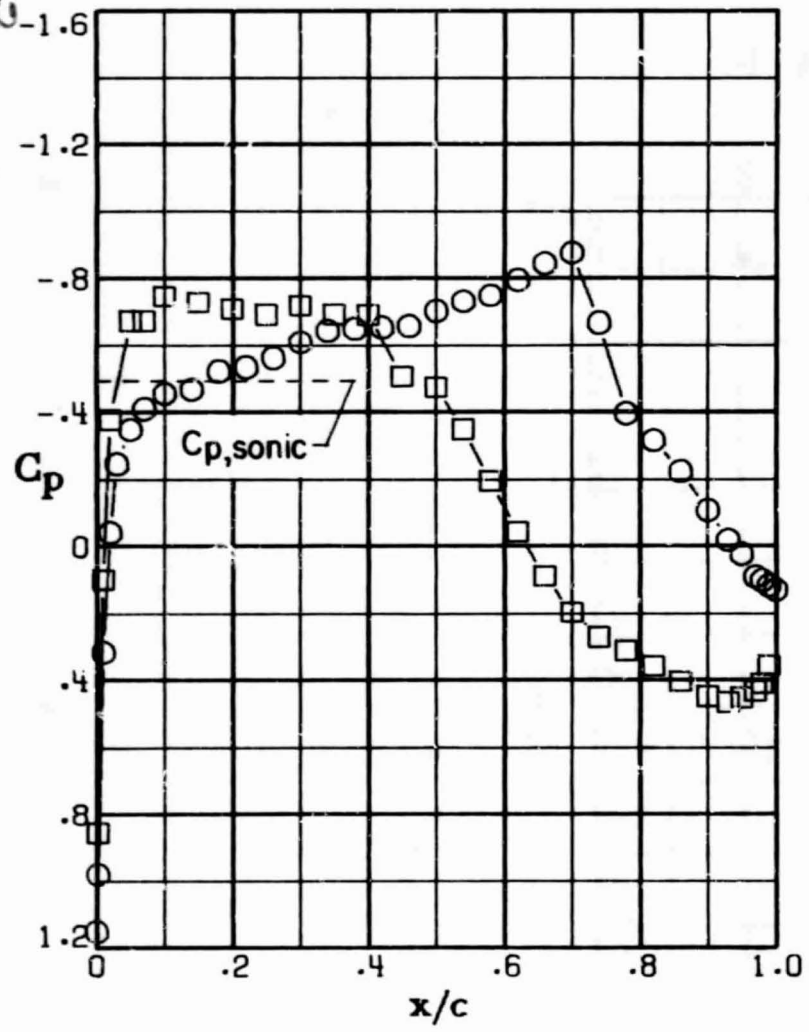
Figure 20. - Continued.

ORIGINAL PAGE IS
OF POOR QUALITY

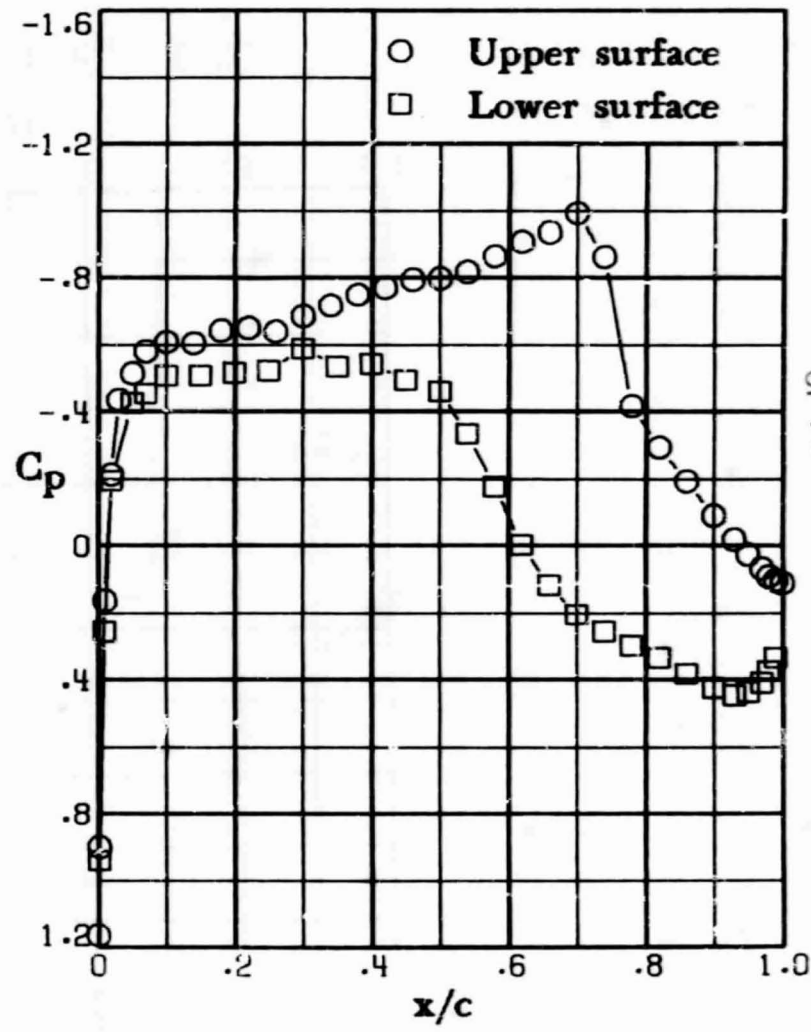


(e) $M = 0.77$; $c_n = 0.71$.

Figure 20. - Concluded.



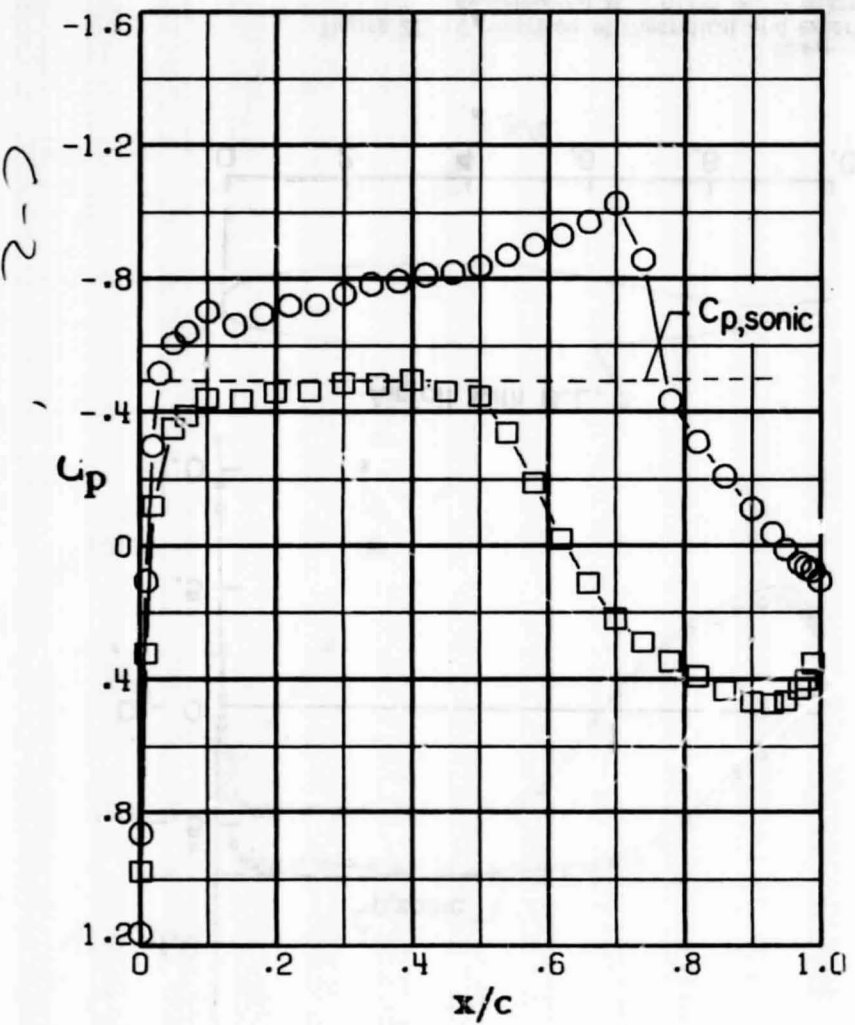
(a) $M = 0.78 ; c_n = 0.26.$



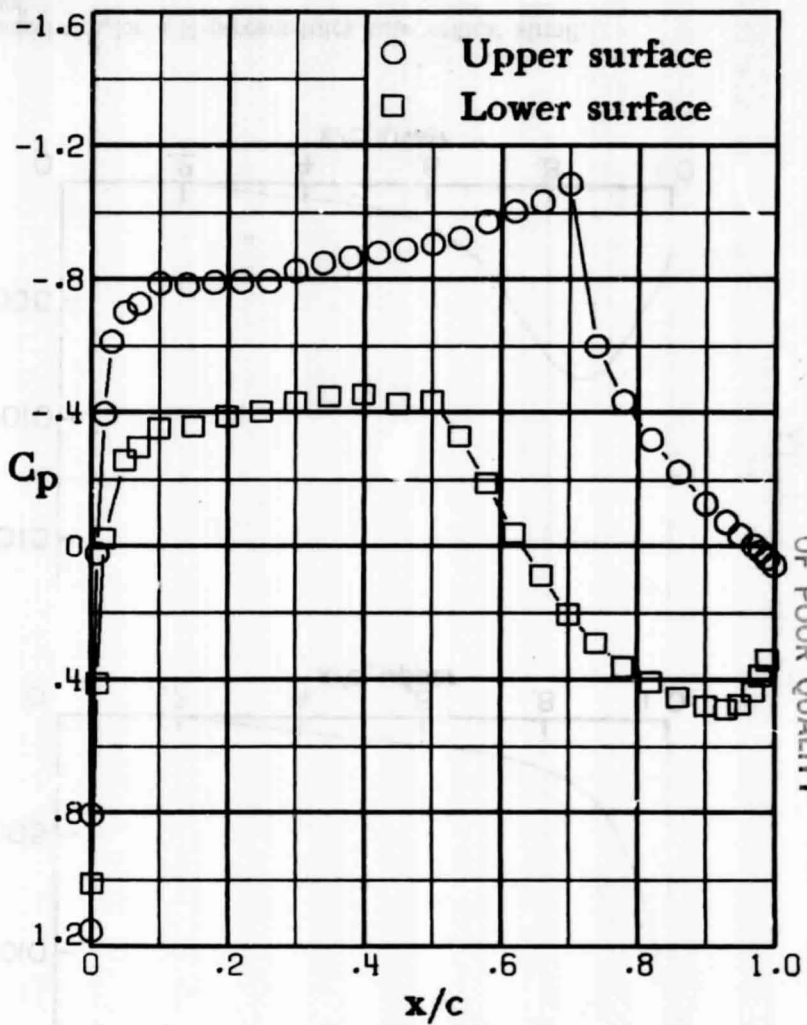
(b) $M = 0.78 ; c_n = 0.43.$

ORIGINAL PAGE IS
OF POOR
QUALITY

Figure 21. - Chordwise pressure distributions for 14-percent thick supercritical airfoil. $M = 0.78.$

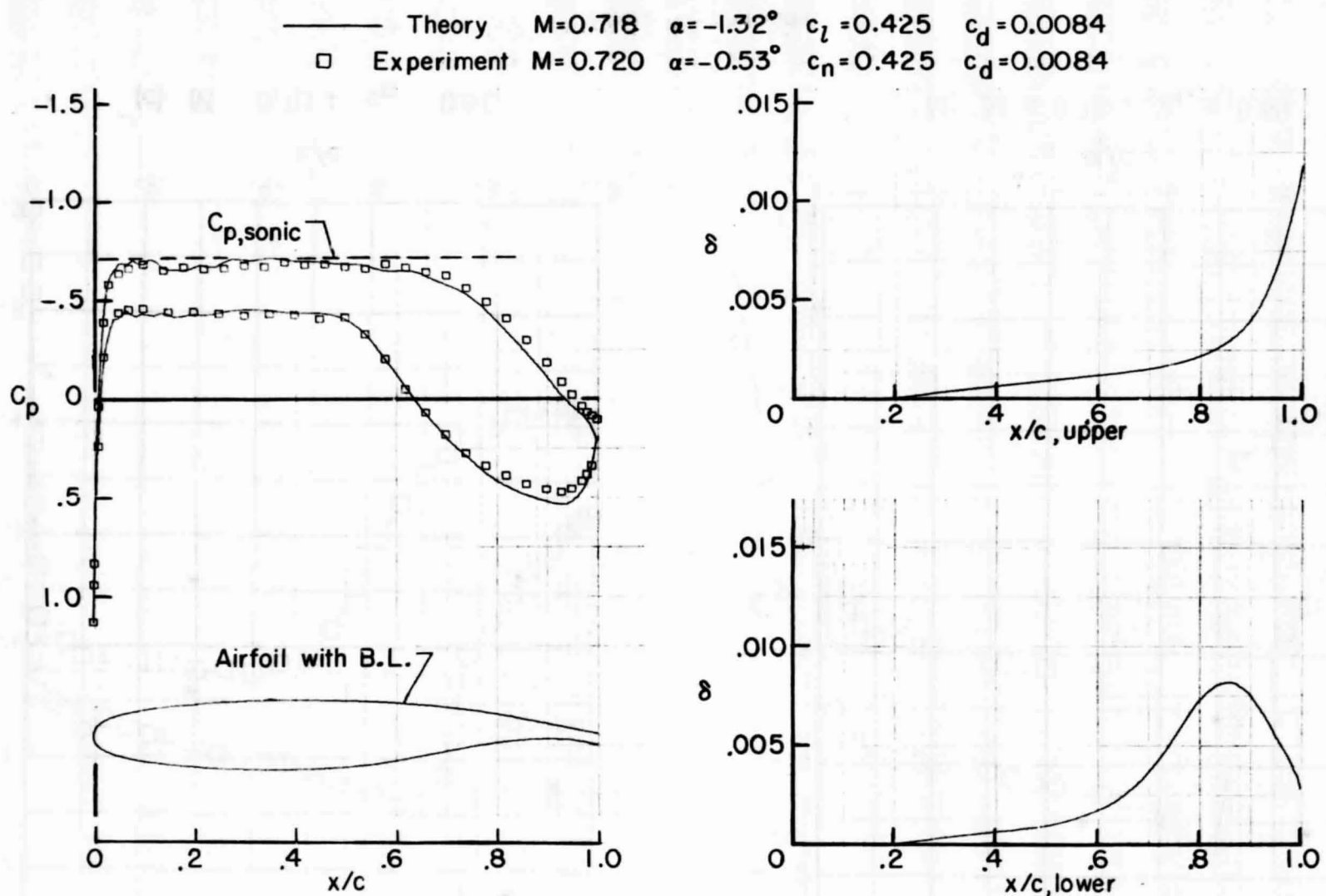


(c) $M = 0.78$; $c_n = 0.51$.



(d) $M = 0.78$; $c_n = 0.59$.

Figure 21. - Concluded.



ORIGINAL PAGE IS
OF POOR QUALITY

Figure 22.- Comparison of theoretical and experimental characteristics for a 14-percent-thick supercritical airfoil.
 Experimental $M = 0.720$; $c_n = 0.425$; $R = 7.4 \times 10^6$.

[REDACTED]

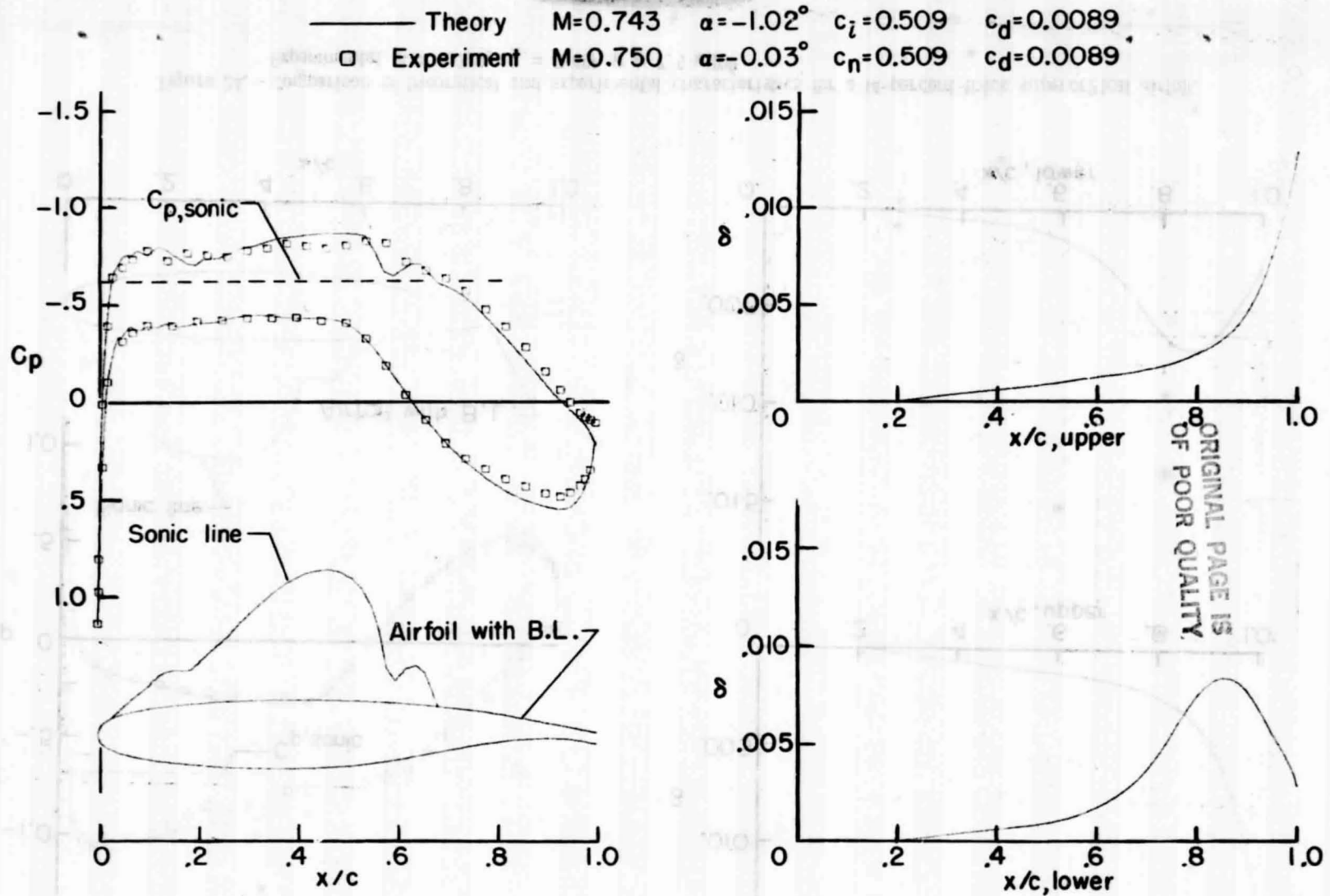


Figure 23.- Comparison of theoretical and experimental characteristics for a 14-percent-thick supercritical airfoil.
 Experimental $M = 0.750$; $c_l = 0.509$; $R = 7.6 \times 10^6$.

Theory $M=0.722$ $\alpha = -0.07^\circ$ $c_l = 0.691$ $c_d = 0.0088$
 Experiment $M=0.730$ $\alpha = 0.97^\circ$ $c_l = 0.691$ $c_d = 0.0086$

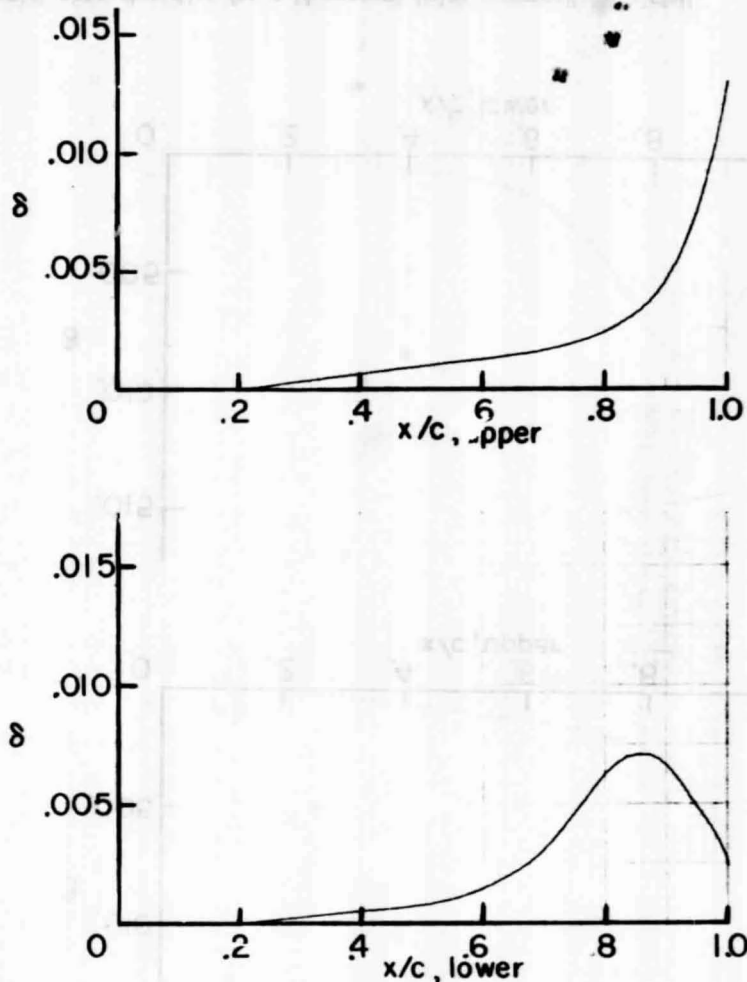
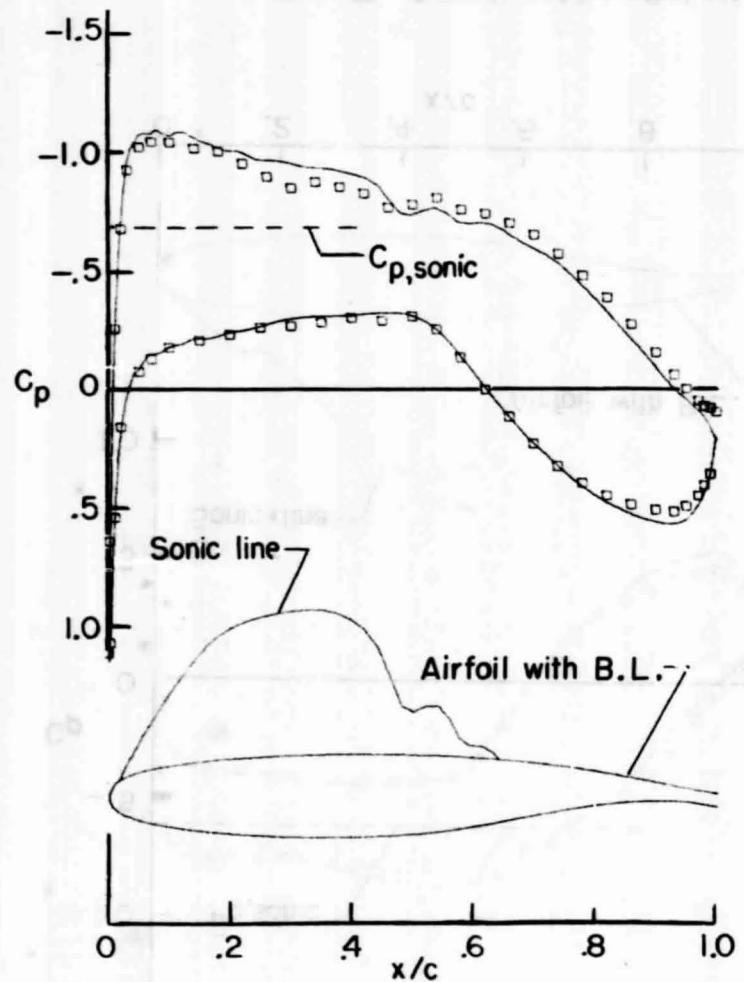


Figure 24. - Comparison of theoretical and experimental characteristics for a 14-percent-thick supercritical airfoil.
 Experimental $M = 0.730$; $c_l = 0.691$; $R = 7.5 \times 10^6$.

ORIGINAL PAGE IS
OF POOR QUALITY